Renewable and Sustainable Energy Reviews 226 (2026) 116318

Contents lists available at ScienceDirect

Renewable and Sustainable Energy Reviews

journal homepage: www.elsevier.com/locate/rser

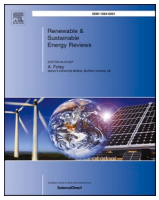

# Redox-active covalent organic frameworks for supercapacitors: A molecular-level design and integration approach

Mahmoud Younis [a,b], Ji.Wu Han [a], Hongta Yang [a], Ahmed F.M. EL-Mahdy [c], Rong.Ho Lee [a,d,*]

[a] Department of Chemical Engineering, National Chung Hsing University, Taichung, 402, Taiwan
[b] Chemistry Department, Faculty of Science, New Valley University, El-Kharja, 72511, Egypt
[c] Department of Materials and Optoelectronic Science, National Sun Yat-Sen University, Kaohsiung, 80424, Taiwan
[d] Department of Chemical Engineering and Materials Science, Yuan Ze University, Taoyuan City, 320, Taiwan

ARTICLE INFO

*Keywords:*
Covalent organic frameworks
Redox-active materials
Energy storage
Electrode materials
Supercapacitors

ABSTRACT

Supercapacitors (SCs) represent critical electrochemical energy storage technologies, yet breakthrough performance requires revolutionary electrode materials with precise molecular engineering. Developing electrodes with high capacitance is a direct and efficient approach to enhance the energy storage capability of supercapacitors. Organic materials, whose molecular structures can be diversely designed to achieve high pseudocapacitance through redox-active units in their backbone, serve as promising electrode candidates for supercapacitors. Covalent organic frameworks (COFs) offer unprecedented opportunities for atomic-level customization through structural tunability, exceptional porosity, and modular architecture. This review establishes the first systematic redox-center classification framework for COF-based SC materials, directly linking molecular structure to electrochemical performance. This review comprehensively categorize COF architectures based on redox-active centers: carbonyl/hydroxyl frameworks, heteroatom-engineered structures, and radical-stabilized systems. Subsequently, this review examines diverse COF-based electrodes including 2,6-diaminoanthraquinone, azodianiline, naphthalene, nitrogen-rich (pyridine, triazine, benzimidazole, triphenylamine), and thiol-based platforms. A distinctive contribution involves elucidating interfacial engineering strategies through systematic COF integration with carbon allotropes, metals, MXenes, and conductive polymers. This review establishes quantitative structure-performance relationships governing charge transfer mechanisms and capacitive behavior at engineered interfaces. Additionally, this review presents the first comprehensive analysis of COF carbonization pathways, revealing transformation mechanisms enabling tailored porosity and conductivity optimization. This work identifies critical technological challenges and presents innovative solutions for scalable synthesis, enhanced stability, and application-specific optimization. The molecular-level design framework and integration strategies establish a roadmap for next-generation COF-based energy storage systems, positioning these materials at the forefront of sustainable electrochemical technologies.

Abbreviation Table⊓⊓

| Abbreviation | Full Form |
|---|---|
| AC | Activated Carbon |
| AQ | Anthraquinone |
| ASCs | Asymmetric Supercapacitors |
| AZO | Azodianiline |
| BET | Brunauer-Emmett-Teller |
| CCF | Conductive Carbon Fibers |
| CMF | COF/MXene Film |

(*continued on next column*)

(*continued*)

| Abbreviation | Full Form |
|---|---|
| CNTs | Carbon Nanotubes |
| COFs | Covalent Organic Frameworks |
| CV | Cyclic Voltammetry |
| Da | Anthracene |
| DAAQ | 2,6-Diaminoanthraquinone |
| DAP | Diaminopyridine |
| DBT | 2,5-Dibromothiophene |

(*continued on next page*)

* Corresponding author. Department of Chemical Engineering, National Chung Hsing University, Taichung, 402, Taiwan.
*E-mail address:* rhl@dragon.nchu.edu.tw (Rong.Ho Lee).

https://doi.org/10.1016/j.rser.2025.116318
Received 10 February 2025; Received in revised form 1 September 2025; Accepted 16 September 2025
Available online 22 September 2025

(*continued*)

| Abbreviation | Full Form |
|---|---|
| ECs | Electrochemical Capacitors |
| EDLCs | Electrochemical Double-Layer Capacitors |
| EES | Electrochemical Energy Storage |
| g-$C_3N_4$ | Graphitic Carbon Nitride |
| GCD | Galvanostatic Charge/Discharge |
| GO | Graphene Oxide |
| IL-COFs | Ionic Liquid-loaded COFs |
| LIB | Lithium-Ion Battery |
| MA | Melamine |
| NDA | 1,5-Diaminonaphthalene |
| PANI | Polyaniline |
| POPs | Porous Organic Polymers |
| PPy | Polypyrrole |
| rGO | Reduced Graphene Oxide |
| SCs | Supercapacitors |
| SSC | Symmetric Supercapacitor |
| TCOF | Triazine-based Covalent Organic Framework |
| TFP | 1,3,5-Triformylphloroglucinol |
| TFPB | 1,3,5-Tris(p-formylphenyl)benzene |
| TFPA | Tris(4-formylphenyl)amine |

## 1. Introduction

The development of electrochemical energy storage (EES) has been crucial in addressing the global energy crisis [1,2]. As shown in (Fig. 1), batteries, fuel cells, and electrochemical capacitors (ECs) are the three main electrochemical energy conversion and storage systems [3]. Because of their special electrochemical qualities, ECs, commonly referred to as SCs, have garnered a lot of attention on a global scale. SCs are a useful intermediary between batteries and conventional capacitors [3,4]. SCs have a high specific power and energy density, as well as quick charge and discharge rates, reversible energy storage, and superior cycle performance [5].

SCs store electrical energy through two distinct mechanisms: faradaic and non-faradaic processes. The faradaic processes, also known as pseudocapacitance, result from electrode-bound reversible redox reactions. By contrast, the electrochemical double layer is linked to non-faradaic phenomena. At the electrode-electrolyte interface, ions are adsorbed to store charges in electrochemical double-layer capacitors (EDLCs). Pseudocapacitors, on the other hand, utilize reversible redox reactions occurring on the electrode surface, potentially generating higher capacitance than most EDLCs [1,6–12]. SCs, particularly EDLCs, offer 100–1000 times higher power density compared to batteries, albeit

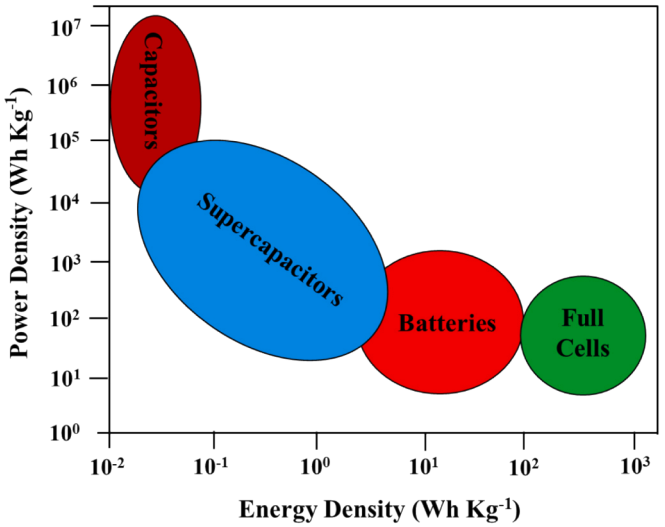


**Fig. 1.** Different energy storage devices.

with 3–30 times lower energy density [8]. SCs based on redox-active materials operate through dual charge storage mechanisms, combining electrical double-layer capacitance with pseudocapacitance derived from reversible redox reactions of the electrode materials. This hybrid mechanism results in significantly enhanced specific capacitance and energy density compared to conventional EDLCs [13]. In pseudocapacitive systems, rapid and reversible redox processes occur at the electrode surface, generating faradaic contributions through multiple pathways including surface redox reactions, electrosorption, and intercalation phenomena. These faradaic processes yield substantially higher capacitance values than those achievable through electrical double-layer formation alone. The integration of redox-active functionalities can be accomplished through covalent attachment or physical adsorption onto high-surface-area electrode substrates [14,15]. However, SCs also present several limitations: (i) Restricted porosity, which impedes mass transfer; (ii) changes in volume (swelling and shrinking) that occur during galvanostatic charge and discharge processes; (iii) structural characterization challenges that impede the comprehension of structure-function correlations with structures [16].

The performance of SCs is primarily driven by the properties of their electrode materials. Optimal electrodes require appropriate porosity, high specific surface area, strong atomic conductivity, and structural periodicity [3,9]. Given their high packing density and wide specific surface area, amorphous polymer materials with carbon-based architectures have been thoroughly studied as possible SC electrode materials. However, the absence of a controlled porous structure and pore size distribution in these materials often leads to slow ion diffusion and undesired capacity loss during rapid charge-discharge processes [17].

Recently, research has focused on developing organic materials suitable for energy storage applications, leading to the creation of porous organic polymers (POPs). These materials have shown great promise in energy storage due to their exceptional surface area, thermal stability, chemical resistance, and customizable structure and porosity [7]. A type of crystalline POPs known as COFs is made up of organic building blocks joined by powerful covalent bonds [18–20]. COFs offer distinct advantages, such as low density, well-organized structures, high specific surface area, excellent crystallinity, strong conjugation, and ease of functionalization and customization [9,21]. The inherent structural regularity and porosity of COFs facilitate efficient ion transport [22], while their tunable chemistry enables precise control over electronic properties and redox activities. Despite these promising attributes, several challenges remain in translating the theoretical potential of COFs into practical high-performance SC devices.

Crystalline redox-active COFs exhibit distinctive physicochemical properties that render them highly promising candidates for SC device applications. These materials possess several advantageous characteristics: (i) Redox-active COFs are crystalline polymers featuring extended, rigid skeletal architectures stabilized by robust covalent bonding networks. This structural rigidity enables framework preservation under demanding operational conditions while maintaining exceptional electrochemical stability across diverse electrolyte systems. (ii) The ordered, open channel architecture inherent to redox-active COFs promotes efficient electrolyte ion adsorption and transport kinetics. (iii) The modular nature of COF synthesis permits facile incorporation of various redox-active functional groups into the framework skeleton, with active site density readily tunable through strategic pore-wall engineering approaches [23,24]. (iv) Two-dimensional redox-active COFs demonstrate excellent processability for thin-film growth at diverse interfaces [25], thereby facilitating seamless integration into electrochemical device architectures.

While numerous reviews have addressed various aspects of SC technology and materials and others have broadly examined COFs for energy applications [26–28], existing literature lacks a systematic classification approach based on redox centers that connect molecular structure to device performance. Previous reviews have typically categorized COF materials by synthetic methods or general applications,

without establishing clear structure-property-performance relationships at the molecular level. Furthermore, the critical interface engineering between COFs and complementary materials (carbon, metals, MXenes, and polymers) has received insufficient attention, despite its profound impact on charge transfer and storage properties. This review uniquely addresses these critical gaps by providing: 1) A comprehensive redox-center based classification system for COF materials in SC. 2) Molecular-level design principles that directly connect functional moieties to device performance. 3) Systematic analysis of various COF-based electrodes, including 2,6-diaminoanthraquinone (DAAQ), azodianiline (AZO), naphthalene, and nitrogen-rich COFs (e.g., pyridine, triazine, benzimidazole, and triphenylamine-based frameworks), as well as thiol-based COFs. 4) Unprecedented insights into integration mechanisms between COFs and complementary materials, with detailed examination of interface engineering for enhanced charge transfer and storage properties. 5) Specific transformation pathways for COF carbonization and their impact on SC performance. An overview of this review is shown in (Fig. 2).

## 2. Methodology

This narrative review aims to provide a comprehensive overview of recent advancements in COFs for SC applications, focusing on their classification, electrode materials, and future research directions. To ensure a thorough and systematic synthesis of the literature, relevant studies were identified through a targeted search of peer-reviewed publications in databases including Scopus, Web of Science, and Google Scholar. The search was conducted using a combination of keywords such as "covalent organic frameworks," "supercapacitors," "electrode materials," "redox-active COFs," "pseudocapacitance," and "energy storage," along with their relevant synonyms and Boolean operators (e.g., "COF and supercapacitor"). The search was limited to articles published in English between January 2010 and March 2025 to capture recent developments in the field.

Studies were included if they focused on the design, synthesis, or electrochemical performance of COF-based materials for SCs, including pure COFs, COF composites, and carbonized COFs. Exclusion criteria included non-peer-reviewed sources, review articles (to avoid overlap), and studies not directly related to SC applications. Additional relevant studies were identified by manually reviewing the reference lists of key articles to ensure comprehensive coverage of the topic. The selected literature was organized and synthesized based on key themes, including the classification of COFs by redox-active centers (e.g., carbonyl/hydroxyl, heterostructures, free radicals), types of COF-based electrodes (e.g., DAAQ, AZO, naphthalene, nitrogen-rich, and thiol-based COFs), and COF composites (e.g., with carbon, metals, MXenes, and polymers). The synthesis process involved a qualitative analysis of electrochemical performance metrics, such as specific capacitance, cycling stability, and energy/power density, to highlight structure-performance relationships. This approach enabled a structured discussion of COF-based materials, their challenges, and opportunities for future development in SC applications.

## 3. Classification of the COF materials for SCs

The design and synthesis of efficient electrode materials are crucial for achieving optimal electrochemical performance in practical applications. COFs incorporating redox moieties have been developed to increase specific capacitance compared to their counterparts with similar, but non-redox-active, COFs [29]. Recent findings have revealed a significant correlation between COF structure and SC performance [30]. (Fig. 3), presents a comprehensive collection of the most frequently utilized monomers in COF synthesis for SC applications, highlighting the structural diversity employed to achieve enhanced electrochemical performance. These monomers serve as fundamental building blocks, featuring various amine-functionalized structures including simple aromatic diamines, extended π-conjugated systems, and heteroatom-rich frameworks. COFs containing redox-active moieties have demonstrated improved electrochemical performance for SC applications. Redox-active moieties have been incorporated into COF skeletons by (i) using redox-active building blocks for COF construction [31], as exemplified by monomers containing electroactive groups such as carbonyl, hydroxyl, or heterocyclic units shown in (Fig. 3), and (ii) employing covalent bonding to post-modify COF scaffolds, thereby adding redox-active sites to their channel walls [29,30]. Based on the chemical structure of their redox moieties, redox-active COFs can be divided into three groups, as far as we know: carbonyl/hydroxyl type, heterostructure-based type, and free radical type.

### 3.1. Carbonyl/hydroxyl as redox-active centers

In EES systems, the carbonyl group plays a crucial role in facilitating

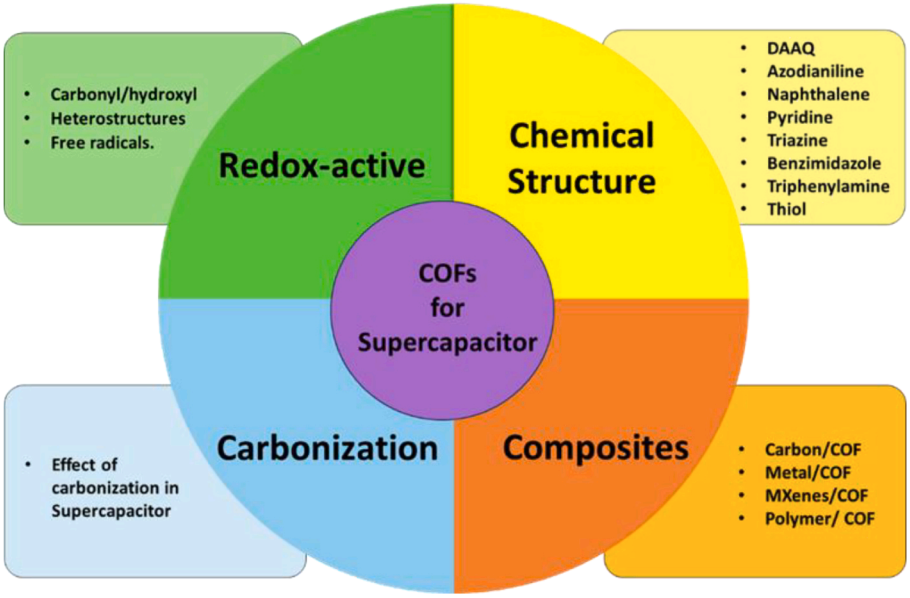


**Fig. 2.** Review structure and methodology overview.

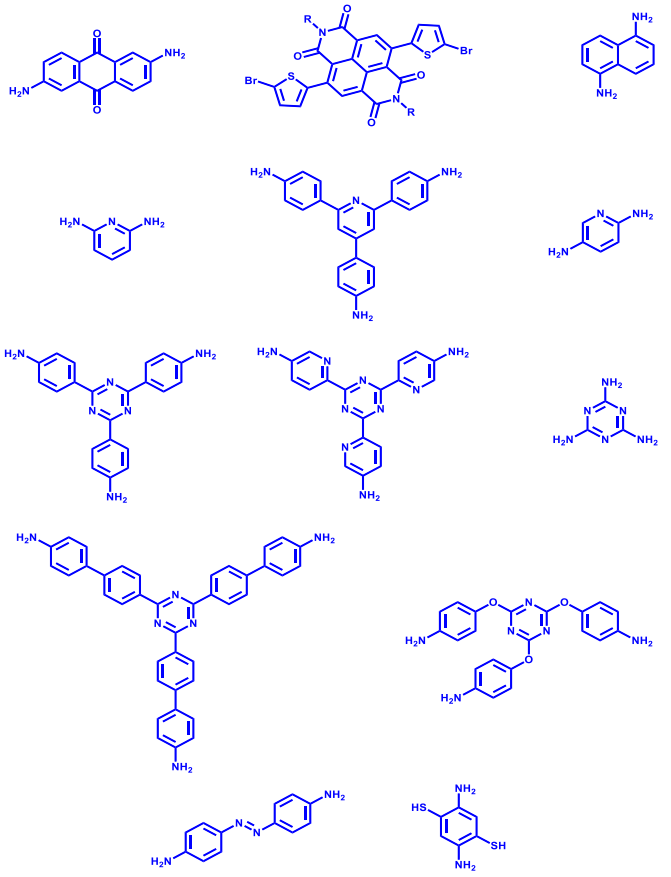

**Fig. 3.** Representative building blocks used in the construction of COF-based SC materials.

electron and proton transfer reactions. Simultaneously, hydrogen-bond interactions further enhance these electron/proton transfer processes [29]. To increase pseudocapacitive contribution, the Dichtel group introduced the anthraquinone (AQ) unit as an active site and, in 2013, developed β-ketoenamine-linked 2D COFs (DAAQ-TFP COF) as electrode materials for SCs for the first time. Compared to its AQ-free counterpart (DAB-TFP COF), DAAQ-TFP COF demonstrated a significantly higher specific capacitance [29]. Halder et al. reported a redox-active, chemically stable COF as a self-standing SC electrode material. The interlayer C—H···N hydrogen bonding, along with the adjacent $-OCH_3$ functionality, provides steric and hydrophobic protection to the imine (C=N) bonds, resulting in exceptional chemical stability. Moreover, this material exhibited an exceptionally high areal capacitance of 1600 mF $cm^{-2}$. Due to its high porosity and redox transitions between quinone and hydroquinone, it was hypothesized that energy storage occurred through both electric EDLC and pseudocapacitive mechanisms [30]. Catherine R. DeBlase and coworkers reported the fabrication of crystalline, oriented thin films of a redox-active two-dimensional COF deposited on gold working electrodes, with film thickness systematically controlled through variation of initial monomer concentrations. Electrochemical accessibility studies revealed that 80–99 % of the AQ redox-active groups remained accessible in films with thicknesses below 200 nm, representing an order-of-magnitude enhancement compared to the same COF material prepared as randomly oriented microcrystalline powder. Consequently, electrodes functionalized with these oriented COF thin films demonstrated a 400 % increase in areal capacitance relative to electrodes modified with randomly oriented COF powder, highlighting the critical importance of structural orientation and film morphology in optimizing electrochemical performance. This work demonstrates that controlled film deposition and orientation significantly enhances the utilization efficiency of redox-active sites, providing a promising strategy for improving the practical performance of COF-based electrode [32]. In 2017, the Banerjee research group reported the synthesis and electrochemical evaluation of two hydroxyl-functionalized COFs, TpPa-$(OH)_2$ and TpBD-$(OH)_2$, constructed from 1,3,5-triformylphloroglucinol (TFP) with 2,5-dihydroxy-1,4-phenyldiamine [Pa-$(OH)_2$] and 3,3′-dihydroxybenzidine [BD-$(OH)_2$], respectively, both incorporating redox-active hydroxyl functionalities. The TpPa-$(OH)_2$ framework demonstrated superior electrochemical performance, with p-benzoquinone functional groups exhibiting reversible redox behavior and achieving a maximum specific capacitance of 416 F $g^{-1}$ at 0.5 A $g^{-1}$ under three-electrode configuration while maintaining 66 % capacitance retention after 10,000 electrochemical cycles. The exceptional specific capacitance was mechanistically attributed to reversible proton-coupled electron transfer processes ($2H^+/2e^-$) involving hydroquinone/benzoquinone ($H_2Q/Q$) redox couples, with approximately 43 % of $H_2Q$ redox-active sites remaining electrochemically accessible [33].

Miao Li and coworkers systematically investigated orthoquinone motifs in COF-based energy storage by synthesizing three redox-active frameworks (1 KT-Tp, 2 KT-Tp, and 4 KT-Tp COFs) with varying carbonyl group densities through solvothermal condensation of 2,4,6-triformylphloroglucinol with different redox-active linkers containing one, two, and four carbonyl groups, respectively [23]. Using 1 M aqueous $H_2SO_4$ electrolyte, the 2 KT-Tp and 4 KT-Tp COF electrodes delivered exceptional gravimetric capacitances of 256 and 583 F $g^{-1}$ at 0.2 A $g^{-1}$, significantly surpassing 1 KT-Tp COF (61 F $g^{-1}$), while control COFs lacking orthoquinone structures showed negligible capacitances (20–25 F $g^{-1}$). Long-term stability tests revealed excellent cycling durability with 92–96 % capacitance retention after 20,000 cycles at 5 A $g^{-1}$. These results demonstrate that orthoquinone moieties provide high-density redox-active sites and enable cooperative participation of adjacent carbonyl groups in redox processes, establishing the strategic incorporation of orthoquinone structures as a promising approach for designing high-performance organic electrode materials.

### 3.2. *Heterostructures as redox-active centers*

The incorporation of heterostructures containing lone-pair electrons into the carbon skeleton can modulate the electronic structure, thereby enhancing the supercapacitive properties [31]. Heterostructure groups, such as pyridine, thiophene, porphyrin, and triazine, are recognized as effective redox-active sites. In 2016, Khattak et al. developed a redox-active pyridine-based COF via solvothermal condensation of diaminopyridine (DAP) and TFP, achieving a specific capacitance of 102 F $g^{-1}$. The resulting TaPa-Py COF demonstrated a combination of pseudocapacitance and EDLC, whereas the reference COF, constructed from diaminobenzene and TFP, exhibited only EDLC [34]. Li et al. designed and synthesized a two-dimensional triazinyl COF material, named DBT-MA-COF, with a specific capacitance of 407 F $g^{-1}$. This material was synthesized through a C–N coupling reaction using 2,5-dibromothiophene (DBT) and melamine (MA) as monomers. The structure of DBT-MA-COF features both triazine and thiophene units, resulting in channels with high heteroatom content. When used as an electrode material for SCs, this configuration facilitates the rapid transport of electrolyte ions within the COF channels. Additionally, the triazine units exhibit redox activity, serving as energy storage sites for pseudocapacitance [35]. Furthermore, Bhattacharya et al. reported a porphyrin-tetraphenyl ethylene-based COF (PT-COF) linked by imine bonds (−C=N), forming a square lattice (sql). This material displayed a high specific capacitance of 1443 F $g^{-1}$ at a current density of 1 A $g^{-1}$ in 0.5 M $H_2SO_4$. Its high redox activity is attributed to the presence of pyrrolic moieties [12].

In 2023, Haijun Peng et al., reported the development of donor–acceptor carbon-linked conjugated polymers (DA-CCPs) as cathode materials for aqueous zinc hybrid supercapacitors. The researchers

synthesized two DA-CCPs through Knoevenagel polymerization between the electron-accepting building block 2,2′,2″-(benzene-1,3,5-triyl)triacetonitrile and electron-donating aldehydes, specifically 2,5-thiophene dicarboxaldehyde and [2,2′-bithiophene]-5,5′-dicarboxaldehyde, yielding DA-CCP-1 and DA-CCP-2, respectively [36]. DA-CCP-2, featuring an additional thiophene unit in its polymeric backbone, demonstrated superior electrochemical performance compared to DA-CCP-1 and exceeded the performance metrics of previously reported cathode materials for aqueous $Zn^{2+}$ energy storage systems. The DA-CCP-1 and DA-CCP-2 based electrodes achieved exceptional energy densities of 80.6 and 196.3 W h $kg^{-1}$, respectively, highlighting the effectiveness of donor–acceptor architectural design in enhancing the electrochemical properties of carbon-linked conjugated polymer cathodes for advanced aqueous energy storage applications.

### 3.3. Free radicals as redox-active centers

Organic free radicals, characterized by unpaired electrons, exhibit unique redox capabilities. The first radical-containing COF was synthesized by Xu et al., in 2015 [37], demonstrating that TEMPO-functionalized COFs possess high capacitance and excellent rate capability for capacitive energy storage. The TEMPO units, covalently attached to the COF pore walls, undergo rapid and reversible one-electron redox reactions, enabling efficient charge storage and release. Similarly, Xu et al. developed 2D COFs containing carbon-oxygen radicals (COR-Tf-DHzDM-COFs) as dendrite-free alkali metal anodes [38]. Bebin Ambrose and coworkers reported the synthesis of two distinct viologen-based covalent organic polymers with controlled morphologies: COP-1 exhibiting hollow sphere architecture and COP-2 displaying hollow tube morphology, both prepared via the Zincke reaction through strategic modulation of solvent polarity. The inherent structural stability and extended π-conjugation of these materials effectively addressed critical limitations commonly observed in conventional polymer electrodes, including inhomogeneous aggregation arising from structural defects, restacking phenomena during repeated electrochemical cycling, and inadequate inter-chain connectivity during assembly processes. When evaluated as electrode materials in three-electrode supercapacitor configuration using 1 M $H_2SO_4$ as the aqueous electrolyte, COP-2 demonstrated exceptional electrochemical performance, achieving a specific capacitance of 604 F $g^{-1}$ at 2 A $g^{-1}$ current density in three-electrode studies and 404 F $g^{-1}$ at 0.5 A $g^{-1}$ in full-cell investigations. Remarkably, COP-2 exhibited outstanding long-term stability with 100 % capacitance retention after 50,000 electrochemical cycles, demonstrating the superior durability and practical viability of viologen-based covalent organic polymers for advanced supercapacitor applications [39]. These radicals, with their high redox reactivity, significantly improved charge storage capacity. The ordered structure and high surface area of COFs provide an ideal platform for these redox-active units, facilitating fast ion transport and easy access to active sites. However, a critical challenge in this field is achieving a balance between redox activity and framework stability. While increased radical reactivity enhances charge storage performance, it can also compromise the structural integrity of the COF skeleton. Striking an optimal balance between redox activity and structural stability is essential to unlocking the full potential of radical-containing COFs for next-generation energy storage devices, particularly in achieving high energy density, superior rate capability, and long-term cycling stability.

Comparative performance analysis across these three COF categories reveals distinct advantages and application-specific trends. Heterostructure-based COFs consistently demonstrate the highest specific capacitance values, with optimized systems such as PT-COF achieving capacitances exceeding 1000 F $g^{-1}$. This exceptional performance is attributed to the synergistic integration of multiple redox-active sites with efficient electrolyte ion transport pathways. Porphyrin- and triazine-based frameworks exemplify this approach, exhibiting enhanced pseudocapacitive contributions derived from their electron-rich heteroatomic architectures, as validated through in-situ electrochemical impedance spectroscopy investigations. Free radical-functionalized COFs, exemplified by TEMPO-containing systems, demonstrate exceptional rate capability and rapid redox kinetics, achieving specific capacitances up to 800 F $g^{-1}$. However, these materials face significant challenges regarding long-term operational stability due to radical-induced framework degradation processes, limiting their practical implementation despite superior kinetic performance. Carbonyl/hydroxyl-functionalized COFs, such as DAAQ-TFP COF, typically exhibit moderate specific capacitance values in the range of 400–600 F $g^{-1}$ but demonstrate exceptional chemical stability and cycling durability, positioning them as optimal candidates for long-term operational applications. Computational investigations have elucidated the critical role of hydrogen-bonding interactions in stabilizing carbonyl-based frameworks, thereby enhancing electron/proton transfer efficiency.

These performance trends reveal inherent trade-offs between specific capacitance, rate capability, and operational stability, providing essential guidance for the rational design of COF-based supercapacitors tailored to specific application requirements. The selection of appropriate COF architectures must consider the relative importance of energy density, power density, and cycle life for the intended application. Advanced COF-based supercapacitor development requires focused investigation in several critical areas. Optimization of hierarchical pore architectures to maximize electrolyte ion accessibility represents a primary objective. Development of hybrid COF composites incorporating carbon-based materials offers opportunities to synergistically combine pseudocapacitive and electric double-layer capacitance mechanisms. Additionally, addressing stability limitations in free radical COFs through advanced synthetic methodologies, including covalent cross-linking strategies and steric protection approaches, remains essential for their practical implementation. The systematic pursuit of these research directions will enable the development of next-generation COF-based supercapacitor materials with optimized performance characteristics tailored to specific energy storage applications.

## 4. COF material-based electrodes for SCs

Drawing from the classification of redox-active COFs into carbonyl/hydroxyl, heterostructure-based, and free radical types outlined in the last section, this section builds on their structural diversity to explore their role as SC electrodes. This foundation enables a detailed analysis of how their design influences performance, bridging the chemical structure insights from the previous chapter with practical electrochemical applications. The structural characteristics of COFs, such as pore size and distribution, specific surface area, degree of conjugation, and surface functionalization, influence their electrochemical performance. Three main factors can be used to characterize the structure-performance characteristics of COF-based electrode materials in SC applications: (i) Strong skeletons and covalent bonds provide COFs exceptional chemical, thermal, and electrochemical stability. This improves cyclability by efficiently suppressing structural alterations brought on by ion deintercalation during the charge–discharge process. (ii) High specific surface area combined with well-organized, open channels promote electron/proton transport between COF electrodes and electrolytes, enhancing rate performance and power density. (iii) Sufficient and well-planned building blocks guarantee that the COF platform exhibits considerable promise as SC electrodes.

### 4.1. Di-aminoanthraquinone-based COFs for SCs

The poor chemical and oxidative stability of well-established links, including boroxines and boronate esters, restricts the applicability of many COFs. Consequently, no 2D COF had previously demonstrated reversible redox behavior. DeBlase et al. addressed this limitation by

incorporating redox-active DAAQ moieties into a 2D COF connected by β-ketoenamine linkages. The DAAQ-TFP COF is the first to exhibit well-defined, rapid redox processes, demonstrating higher capacitance than analogous non-redox-active COFs, even after 5000 charge-discharge cycles [29].

In a 2015 study, DeBlase et al. significantly improved the charge storage capacity of DAAQ-TFP COF from 0.4 to 3.0 mF $cm^{-2}$ by controlling the film thickness through adjustments to the initial monomer concentration [32]. For films thinner than 200 nm, 80–99 % of the AQ groups became electrochemically accessible, greatly outperforming the randomly oriented microcrystalline COF powder. As shown in (Fig. 4), the capacitance (scaled to electrode area) of oriented COF films was 400 % higher than that of electrodes functionalized with randomly oriented COF powder.

In 2018, Halder et al. reported that TpOMe-DAQ exhibited remarkable chemical stability under extreme conditions, including exposure to strong acids (18 M $H_2SO_4$ and 12 M HCl) and strong bases (9 M NaOH) [30]. This stability was attributed to interlayer C–H···N hydrogen bonding between the methoxy C–H group and the imine nitrogen atom of adjacent layers, with bond geometries of [D = 3.26 Å, d = 2.17 Å, θ = 168.2°] and [D = 3.16 Å, d = 2.07 Å, θ = 165.8°]. Additionally, TpOMe-DAQ COF could be fabricated into uniform and continuous thin sheets on a centimeter scale, maintaining a thickness of approximately 200 μm. These properties enabled the use of these COF thin sheets as free-standing SC electrodes, employing concentrated aqueous $H_2SO_4$ (2 M and 3 M) as the electrolyte. In three-electrode configurations with 3 M aqueous $H_2SO_4$, the COF thin sheets demonstrated an exceptionally high areal capacitance of 1600 mF $cm^{-2}$, corresponding to a gravimetric capacitance of 169 F $g^{-1}$ [30].

Modern electronics require flexible SCs with lightweight electrodes that possess large surface areas, finely integrated redox moieties, and mechanical properties that are strong, flexible, and free-standing. The incorporation of π-electron-rich anthracene (Da) linkers enhances non-covalent interactions between crystallites, thereby improving the mechanical properties of free-standing thin sheets. Khayum et al. reported the in-situ incorporation of redox-active AQ and π-electron-rich Da linkers into a β-ketoenamine-linked COF in varying ratios (1:2, 1:1, and 2:1, referred to as Dq1Da2Tp, Dq1Da1Tp, and Dq2Da1Tp, respectively) using a solid-state molecular mixing procedure (Fig. 5) [40]. These COFs were successfully fabricated into highly desirable thin, free-standing sheets with thicknesses ranging from 25 to 100 μm. Among the synthesized materials, the Dq1Da1Tp COF thin sheet demonstrated superior mechanical strength, with a 5 % breaking strain, and a specific capacitance of 111 F $g^{-1}$. The precise integration of AQ moieties within the COF structure imparted redox activity to the thin sheet, enhancing its potential for SC applications [40].

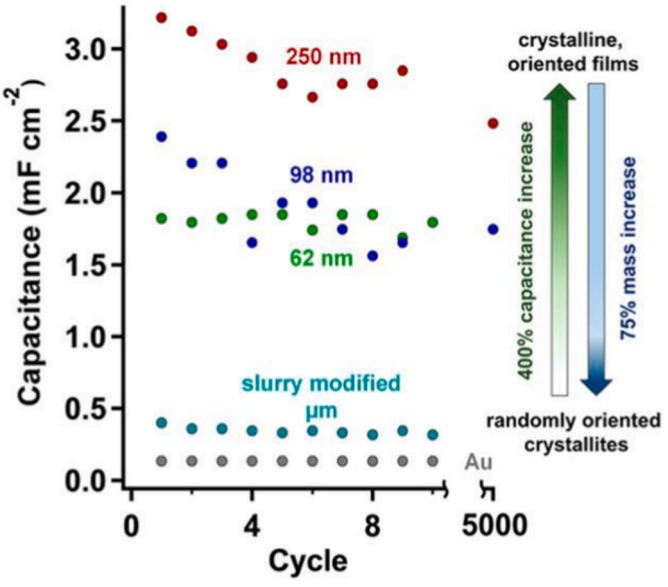


**Fig. 4.** Capacitance comparison of DAAQ-TFP COF thin films of varying thicknesses with reference electrodes. Reproduced with permission from Ref. [32]. Copyright 2015, American Chemical Society.

Four DAAQ-based COFs for SCs are compared in Table 1 based on their capacitance properties: DAAQ-TFP COF, DAAQ-TFP, TpOMe-DAQ, and Dq1Da1Tp COF. The specific capacitances of the materials vary widely, with TpOMe-DAQ displaying an extraordinarily high value of 1600 mF $cm^{-2}$. Under various situations, current densities and capacitance retention are recorded, with cycle counts ranging from 5000 to 50,000. While TpOMe-DAQ retains 65 % capacity over 50,000 cycles, DAAQ-TFP exhibits the greatest retention at 93 % after 5000 cycles, suggesting a trade-off between high capacitance and long-term stability. The various performance indicators demonstrate how DAAQ-based COFs can be customized to meet certain SC needs.

Notwithstanding the demonstrated electrochemical efficacy of DAAQ-based COF, substantial research lacunae persist. The mechanistic delineation between pseudocapacitive and EDLC contributions remains inadequately characterized, with limited operando spectroscopic investigations of AQ redox mechanisms. Scalability challenges in thin-sheet fabrication and insufficient electrolyte composition studies further impede practical implementation. The field exhibits significant discrepancies in reported specific capacitances (1600 mF $cm^{-2}$ for TpOMe-DAQ vs. 3.0 mF $cm^{-2}$ for DAAQ-TFP), potentially attributable to synthetic heterogeneities, morphological variations, and inconsistent electrochemical protocols. The observed trade-off between capacitance and stability (TpOMe-DAQ: 65 % retention after 50,000 cycles vs. DAAQ-TFP: 93 % after 5000 cycles) suggests unresolved material design inconsistencies.

### 4.2. *Azodianiline-based COFs for SCs*

The presence of conjugated double bonds and heteroatomic nitrogen in AZO-based COFs supports their potential application in SCs and facilitates their use as electrodes. These structural features contribute to enhanced electrical conductivity and charge storage capabilities. However, the current body of knowledge regarding AZO-based COFs is limited, particularly in terms of their adaptability and EES properties. This gap in understanding presents an opportunity for further research to elucidate the structure-property relationships and optimize the performance of AZO-based COFs in energy storage applications [7,41] Ahmadi et al. successfully synthesized two distinct AZO-based COFs utilizing different precursors: tris(4-formylphenyl)amine (TFPA) and 1,3,5-tris(p-formylphenyl)benzene (TFPB) [7]. Brunauer-Emmett-Teller (BET) analysis revealed specific surface areas of 987 $m^2$ $g^{-1}$ and 425 $m^2$ $g^{-1}$ for TFPB-AZO-COF and TFPA-AZO-COF, respectively. Electrochemical characterization demonstrated that TFPB-AZO-COF exhibited superior performance with a specific capacity of 450 F $g^{-1}$, an energy density of 24.6 W h $kg^{-1}$, and a power density of 8500 W $kg^{-1}$, while TFPA-AZO-COF showed values of 160 F $g^{-1}$, 9.8 W h $kg^{-1}$, and 8600 W $kg^{-1}$, respectively. The electrochemical behavior of TFPB-AZO-COF was further investigated using a three-electrode configuration (Fig. 6). Cyclic voltammetry (CV) curves (Fig. 6a) revealed enhanced pseudocapacitive behavior at elevated scan rates, with peak shifting indicative of quasi-reversible faradaic reactions. Galvanostatic charge/discharge (GCD) profiles (Fig. 6b) exhibited near-linear behavior, confirming the pseudocapacitive charge storage mechanism. The specific capacitance (Fig. 6c) showed a decrease with increasing current density while maintaining 53 % retention after a tenfold increase, demonstrating excellent rate capability. Electrochemical impedance spectroscopy (EIS) analysis, presented as a Nyquist plot (Fig. 6d), revealed a low charge transfer resistance of 1.85 Ω, indicating efficient charge transfer kinetics and high conductivity of the TFPB-AZO-COF material [7].

The nascent literature on AZO-based COFs presents significant

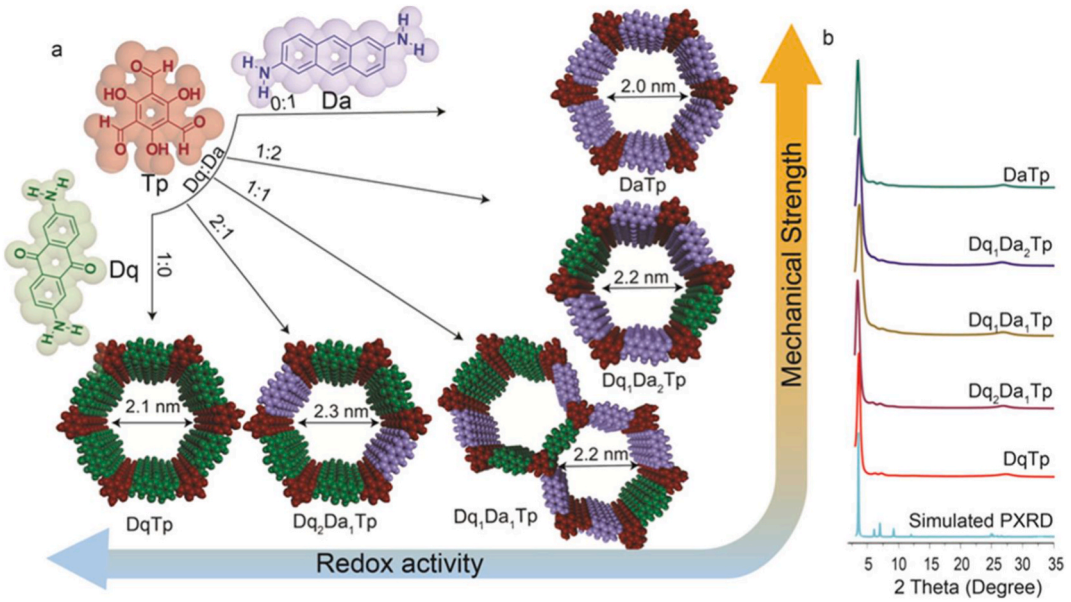


**Fig. 5.** Synthesis scheme and PXRD patterns of Dq/Da/Tp-based COF thin sheets. Reproduced with permission from Ref. [40]. Copyright 2018, American Chemical Society.

**Table 1**
Capacitance properties of DAAQ-based COFs for SCs.

| Materials | Redox group | Electrolyte | Potential window | Specific capacitance | Current density | Capacitance retention | Ref |
|---|---|---|---|---|---|---|---|
| DAAQ-TFP COF | Anthraquninone | 1 M H2SO4 | −0.3 to 0.3 V | 0.4 mF $cm^{-2}$ | 0.1 A $g^{-1}$ | >80 % after 5000 cycles. | [29] |
| DAAQ-TFP | Anthraquninone | 0.1 M TBAPF6 | −1.7 to 1.1 V | 3.0 mF $cm^{-2}$ | 150 μA $cm^{-2}$ | 93 % after 5000 cycles | [32] |
| TpOMe-DAQ | Anthraquninone | 3 M $H_2SO_4$ | −0.50 to 0.50 V | 1600.0 mF $cm^{-2}$ | 5.0 mA $cm^{-2}$ | 65 % after 50,000 cycles | [30] |
| Dq1Da1Tp COF | Anthraquninone | 1 M $H_2SO_4$ | 0.2 to 0.4 V | 111 $Fg^{-1}$ | 1.56 mA $cm^{-2}$ | 78 % after 7000 cycles. | [40] |

knowledge lacunae that impede comprehensive elucidation of structure-property correlations, particularly regarding nitrogen heteroatom contributions to pseudocapacitive behavior. The pronounced disparities in specific surface areas (987 $m^2$ $g^{-1}$ for TFPB-AZO-COF versus 425 $m^2$ $g^{-1}$ for TFPA-AZO-COF) and their mechanistic implications for electrochemical performance remain inadequately investigated, while long-term stability assessments beyond preliminary characterizations are conspicuously absent. The substantial performance divergence between TFPB-AZO-COF (450 F $g^{-1}$) and TFPA-AZO-COF (160 F $g^{-1}$) introduces methodological uncertainties potentially attributable to precursor chemistry variations, pore architectural differences, or experimental protocol inconsistencies. The reproducibility of reported high power densities (8500 W $kg^{-1}$ for TFPB-AZO-COF) across diverse electrolyte systems and device configurations remains unvalidated. Furthermore, the predominant charge storage mechanism in AZO-based COFs remains contentious, with conflicting interpretations emphasizing either pseudocapacitive or EDLC contributions.

### 4.3. Naphthalene-based COFs for SCs

The advanced applications of COFs as electrode materials rely on three key factors: their high surface area, extended π-electronic conjugation, and the presence of active redox sites. These structural and electronic properties collectively enhance the potential of COFs for improved performance in EES and conversion devices [42]. Das et al. reported the synthesis of a porous, extended π-conjugated network, TFP-NDA-COF, via solvothermal Schiff base condensation of 1,5-diaminonaphthalene (NDA) and TFP [43]. Electrochemical characterization revealed that TFP-NDA-COF exhibited excellent energy storage capabilities, achieving a specific capacitance of 379 F $g^{-1}$ at a scan rate of 2 mV $s^{-1}$ and 348 F $g^{-1}$ at a current density of 0.5 A $g^{-1}$. Moreover, the material demonstrated notable cycling stability, retaining 75 % of its initial specific capacitance after 8000 charge-discharge cycles [43]. Ruidas et al. investigated TFPh-NDA and TFR-NDA, two π-conjugated COFs (IC-COFs), and assessed their potential as electrode materials for ASCs [44]. These IC-COFs exhibited excellent crystallinity, large surface areas, and bimodal porosity. The electrodes based on TFPh-NDA and TFR-NDA demonstrated remarkable redox-active behavior, with gravimetric capacitances of 583 F $g^{-1}$ and 362 F $g^{-1}$, respectively, in a three-electrode setup. Asymmetric supercapacitors (ASCs) were fabricated using TFPh-NDA COF and activated carbon (AC), featuring a broad operating voltage window of 2.5 V (−1.0 to 1.5 V). These ASCs exhibited exceptional cycling stability, retaining 98 % of their initial capacitance after 10,000 CV cycles. They also achieved a maximum specific capacitance of 323.25 F $g^{-1}$ at 1 mV $s^{-1}$ and a maximum energy density of 280.58 W h $kg^{-1}$ at a power density of 404.06 W $kg^{-1}$ [44].

Weng et al. reported the synthesis of a conjugated microporous polymer (designated as NDTT) with structural characteristics analogous to COFs [45]. The polymer was synthesized via Stille coupling polymerization, incorporating triazine and thiophene-substituted naphthalene diimides to form a single-bond directly linked network with satisfactory crystallinity. A comprehensive analysis of the electrochemical properties of NDTT-based electrodes was conducted (Fig. 7) [45]. CV measurements (Fig. 7a) revealed distinct redox peaks at various scan rates, indicating a reversible, diffusion-controlled redox mechanism. The pseudocapacitive nature of the charge storage mechanism was further confirmed by the symmetric charge-discharge plateaus observed in the galvanostatic charge-discharge (GCD) profiles (Fig. 7b). Performance studies showed a high specific capacitance of 425.3 F $g^{-1}$ at a current density of 0.2 A $g^{-1}$ (Fig. 7c). Notably, the material retained 80.2 % of its initial capacitance at high current densities after 2000 cycles (Fig. 7d), demonstrating excellent electrochemical reversibility

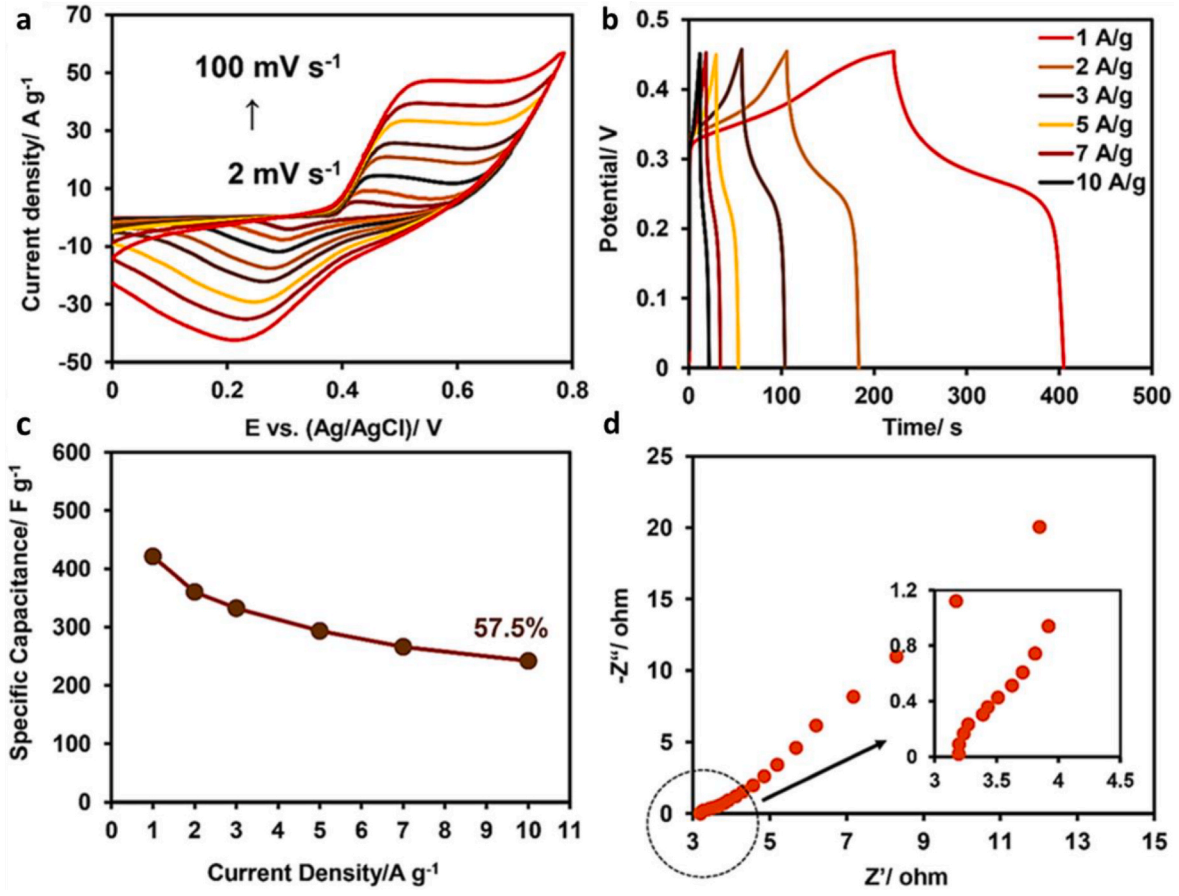


**Fig. 6.** TFPB-AZO-COF electrochemical performance: CV (a), GCD (b), capacitance (c), and EIS analysis (d). Reproduced with permission from Ref. [7]. Copyright 2023, Elsevier.

and cycling stability [45].

For SCs, Table 2 summarizes the capacitance properties of naphthalene-based COFs, comparing TFP-NDA-COF, TFPh-NDA, and NDTT. The table highlights the specific capacitance, current density, and capacitance retention for each COF material after multiple charge-discharge cycles. These naphthalene-based COFs exhibit a wide range of specific capacitances for charge storage, from 379 F $g^{-1}$ (TFP-NDA-COF) to 583 F $g^{-1}$ (TFPh-NDA). The cycle counts for all materials range between 2000 and 10,000, with their respective capacitance retention also provided. TFPh-NDA demonstrates exceptional stability, retaining 100 % of its capacitance after 10,000 cycles. NDTT and TFP-NDA-COF retain 80.2 % and 75 % of their initial capacitance, respectively, after 8000 cycles. Among the materials, TFPh-NDA stands out with the highest specific capacitance (583 F $g^{-1}$) and the best retention rate, combining superior charge storage performance and stability.

Contemporary investigations of naphthalene-based COF exhibit fundamental deficiencies in elucidating π-conjugation contributions to charge transport phenomena, thereby constraining mechanistic understanding of electrochemical performance enhancement. While bimodal porosity in materials such as TFPh-NDA and TFR-NDA has been qualitatively acknowledged, quantitative correlations between pore architecture and ion diffusion kinetics remain underdeveloped, impeding rational optimization strategies. Solvothermal synthesis scalability presents formidable implementation barriers, and two-electrode system evaluations are substantially underrepresented relative to three-electrode configurations. The remarkable specific capacitance disparity between TFPh-NDA (583 F $g^{-1}$) and TFP-NDA-COF (379 F $g^{-1}$) introduces methodological uncertainties potentially attributable to electrode preparation inconsistencies or experimental protocol variations. The reported 100 % capacitance retention for TFPh-NDA following 10,000 cycles represents an anomalous performance metric requiring independent validation, particularly given typical retention rates of 75–80 % for comparable materials. The mechanistic debate regarding naphthalene's redox activity versus structural porosity contributions to capacitive behavior remains unresolved, lacking definitive consensus. Future investigations should integrate advanced electrochemical diagnostics and computational modeling to quantitatively delineate π-conjugation and porosity effects, validate exceptional stability claims through independent corroboration, and explore scalable mechanochemical synthesis alternatives to enhance translational potential.

### 4.4. Nitrogen-rich COFs for SCs

The incorporation of heteroatoms into the two-dimensional structure of COFs can significantly enhance ion transfer through their porous channels. The structural integrity and rigidity of COF materials arise from the periodic covalent bonding between light elements (such as C, O, B, and N) that form their individual building blocks. This combination of heteroatom incorporation and structural stability contributes to the unique porous architecture of COFs, characterized by its robustness and potential for facilitating ion transport. These properties position COFs as highly promising materials for energy storage applications and other fields requiring controlled ion mobility within a stable, porous framework [31,43].

#### 4.4.1. Pyridine-based COFs for SCs

Nitrogen-containing functional groups, such as phenazine, triazine, and pyridine, serve as efficient redox-active sites in COFs. Khattak et al. successfully synthesized a redox-active pyridine-based COF via

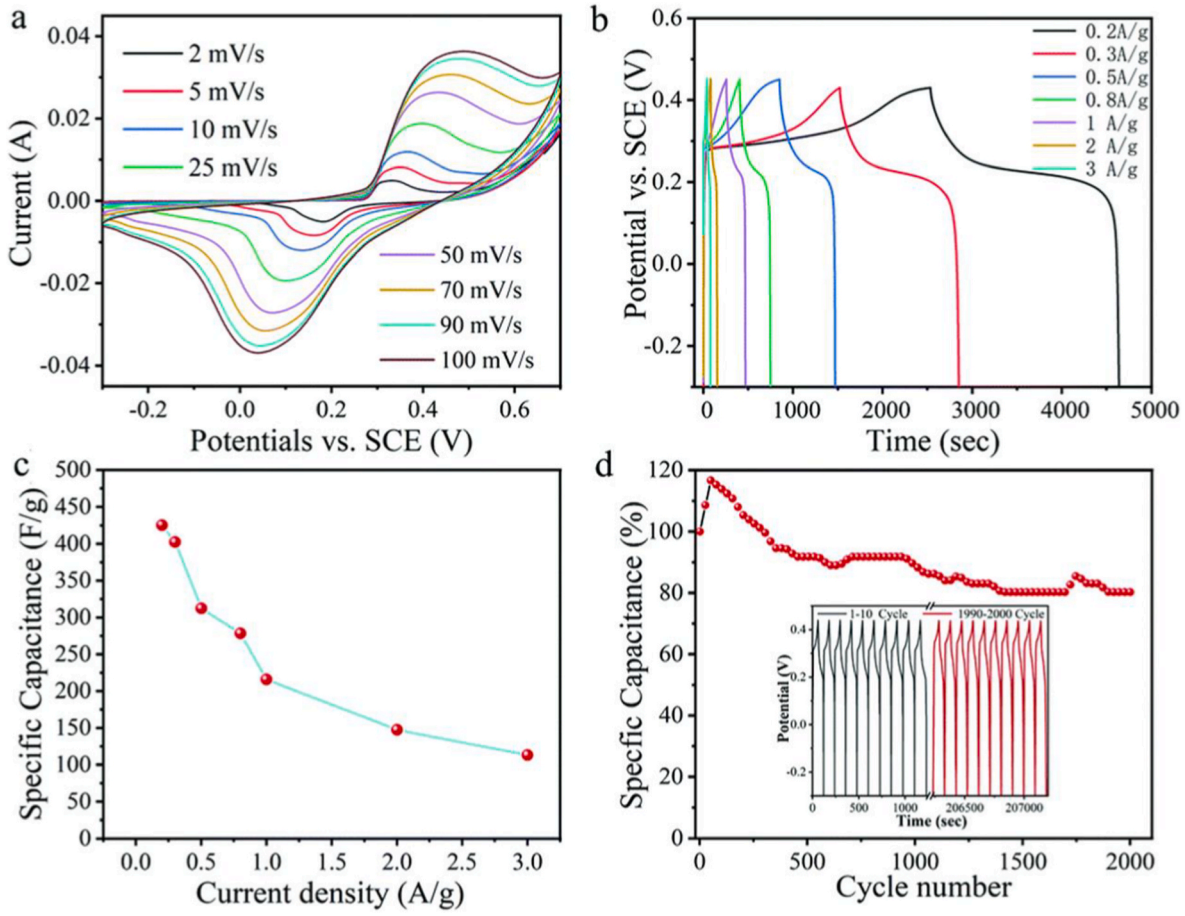


**Fig. 7.** NDTT electrode: CV (a), GCD (b), capacitance (c), and cycling stability in KOH electrolyte (d). Reproduced with permission from Ref. [45]. Copyright 2022, Royal Society of Chemistry.

**Table 2**
Capacitance properties of naphthalin-based COFs for SCs.

| Materials | Redox group | Electrolyte | Potential window | Specific capacitance | Current density | Capacitance retention | Ref |
|---|---|---|---|---|---|---|---|
| TFP-NDA-COF | naphthalene | 1 M $H_2SO_4$ | 0 to 0.8 V | 379 F $g^{-1}$ | 2 mV $s^{-1}$ | 75 % after 8000 cycles | [43] |
| TFPh-NDA | naphthalene | 1 M $H_2SO_4$ | −0.2 to 0.8 V | 583 F $g^{-1}$ | 1 mV $s^{-1}$ | 100 % after 10,000 cycles | [44] |
| NDTT | Naphthalene Diimide | 1 M KOH | −0.3 to 0.7 V | 425.3 F $g^{-1}$ | 0.2 A $g^{-1}$ | 80.2 % after 2000 cycles | [45] |

solvothermal condensation of DAP and triformylphloroglucinol (TFP) [34]. Electrochemical analysis of the synthesized TaPa-Py COF demonstrated reversible redox reactions associated with the pyridine moieties, manifesting distinctive faradaic capacitive behavior. The incorporation of these redox-active units resulted in enhanced specific capacitance compared to both the constituent electroactive monomer and a control COF lacking redox-active functionalities. Notably, the TaPa-Py COF--based device exhibited remarkable electrochemical stability, maintaining 92 % of its initial capacitance after 6000 charge-discharge cycles [34].

EL-Mahdy et al. reported the synthesis of β-ketoenamine-linked COFs using solvothermal Schiff-base [3 + 3] polycondensation reactions between TFP and 4,4′,4′′-(pyridine-2,4,6-triyl)trianiline [31]. The crystallinity of the resulting COFs was found to be influenced by the planarity of the tris(aminophenyl) linker: greater planarity reduced the π-interlayer distances between the 2D COF sheets while increasing the d100 value. The synthesized TFP-COFs exhibited remarkable crystallinity and high BET specific surface areas of up to 686 $m^2$ $g^{-1}$. Electrochemical analysis revealed superior specific capacitances of up to 291.1 F $g^{-1}$, highlighting the potential of these materials for energy storage applications [31].

Biradar et al. synthesized a three-dimensional (3D) COF, designated as PFM-COF1, using tris(4-formylphenyl) phosphate and 2,6-diaminopyridine [11]. The incorporation of a phosphonate-rich subunit was intended to impart flame retardancy, enhancing the potential for safer SC electrode applications. The no21nflammable PFM-COF1 demonstrated impressive electrochemical performance, achieving specific capacitances of 394.28 F $g^{-1}$ and 158 F $g^{-1}$ at a current density of 0.5 A $g^{-1}$ in three-electrode and symmetric two-electrode SC devices, respectively. Additionally, PFM-COF1 delivered a high power density of 1077.72 W $kg^{-1}$ at 0.5 A $g^{-1}$ and an energy density of approximately 28.44 Wh $kg^{-1}$. The material exhibited good cycling stability, retaining 81 % of its initial capacitance over 2000 cycles. While the COF featured a single pyridyl group per monomer, increasing the concentration of pyridyl groups within the framework presents an intriguing opportunity for further enhancing its capacitance, though this is not guaranteed [11].

Haldar et al. synthesized three COFs with pyridyl-lined micropores, systematically varying the concentration of hydroxyl groups within their structures [46]. These COFs were constructed using trialdehydes derived from phenol, resorcinol, and phloroglucinol, resulting in SERP-COF10 (1-OH), IISERP-COF11 (2-OH), and IISERP-COF12 (3-OH), respectively. The homogeneous micropores (5–10 Å) contributed to substantial

surface areas, with SERP-COF10 (1-OH) exhibiting the best electrochemical performance among the COF-derived solid-state capacitors. SERP-COF10 demonstrated an impressive specific capacitance of 546 F $g^{-1}$ at a current density of 500 mA $g^{-1}$ and an areal capacitance of approximately 92 mF $cm^{-2}$ at 0.5 mA $cm^{-2}$ under acidic electrolyte conditions. This performance corresponded to a high-power density of 98 μW $cm^{-2}$ at 0.5 mA $cm^{-2}$. The electrochemical performance of these pyridine-rich COFs as solid-state SCs was thoroughly investigated (Fig. 8). The device was fabricated by coating the COF onto carbon cloth (Fig. 8a). GCD profiles revealed rapid charge-discharge kinetics with minimal energy loss (Fig. 8c), while CV tests displayed rectangular-shaped curves for all three COFs, indicating optimal electric double-layer capacitance behavior (Fig. 8b). Among the synthesized COFs, IISERP-COF10 achieved the highest areal capacitance of 2 mA $cm^{-2}$ (Fig. 8d) [46].

While nitrogen heteroatoms, particularly pyridine moieties, are recognized for their redox enhancement capabilities, comprehensive mechanistic elucidation of electron transfer kinetics remains deficient, constraining optimization of charge storage phenomena. The influence of hydroxyl group concentration variations on capacitive behavior necessitates systematic investigation across diverse electrolyte systems to establish universally applicable structure-property relationships. The scalability and economic viability of pyridine-based COF synthesis present substantial impediments to industrial implementation. The extensive range of reported specific capacitances (102–546 F $g^{-1}$) introduces significant methodological uncertainties potentially attributable to variations in pore architecture, crystallinity, or electrode configuration protocols. The pronounced performance disparity between IISERP-COF10 (546 F $g^{-1}$) and TaPa-Py (102 F $g^{-1}$) exemplifies these inconsistencies, questioning the influence of structural parameters versus experimental methodologies. The mechanistic debate regarding faradaic versus non-faradaic contributions in nitrogen-enriched COFs remains contentious, with conflicting interpretations emphasizing either pseudocapacitive or EDLC mechanisms. Future investigations should integrate advanced in situ characterization techniques, including solid-state NMR spectroscopy and synchrotron X-ray diffraction, to definitively elucidate nitrogen's redox functionality, coupled with standardized electrochemical protocols and scalable synthetic methodologies to reconcile performance discrepancies and advance practical implementation.

#### 4.4.2. *Triazine-based COFs for SCs*

Recent research has identified triazine as a redox-active center in COFs. Triazine-based organic moieties have garnered significant attention in COF synthesis due to their cost-effectiveness and high nitrogen content, which enhances their reactivity. The multiple nitrogen groups in triazine structures make them particularly appealing for the development of COFs with superior electrochemical properties. This combination of affordability and electrochemical activity has driven the widespread use of triazine-based precursors in COF design, particularly

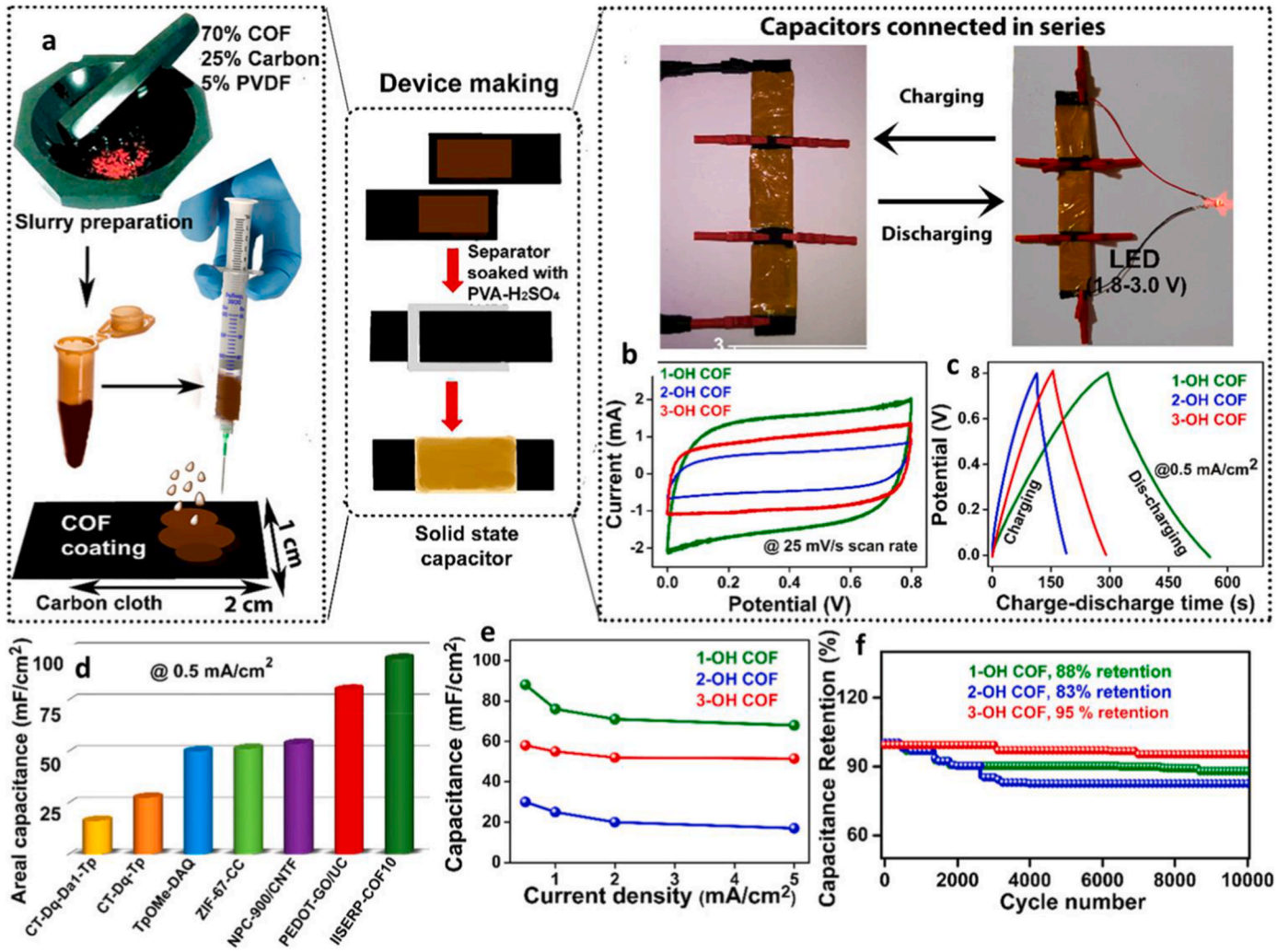


**Fig. 8.** COF-based solid-state SCs: device fabrication (a), CV (b), GCD (c), capacitance (d, e), and stability (f). Reproduced with permission from Ref. [46] Copyright 2022, Royal Society of Chemistry.

for energy storage and conversion applications. Incorporating triazine units into COFs allows for tuning redox properties and improving charge storage capabilities, positioning them as promising candidates for next-generation energy storage materials [6].

Kumar et al. synthesized four distinct porous COFs through the polycondensation of a heteroatom-rich, flexible triazine-based trialdehyde linker, 2,4,6-tris(4-formylphenoxy)-1,3,5-triazine (TPT-CHO), with four different triamine linkers [47]. These materials were designated IITR-COF-1, IITR-COF-2, IITR-COF-3, and IITR-COF-4. Among them, IITR-COF-1 exhibited outstanding electrochemical performance, with a high specific capacitance of 182.6 F $g^{-1}$, along with energy and power densities of 101.5 Wh $kg^{-1}$ and 298.3 W $kg^{-1}$, respectively, at a current density of 0.3 A $g^{-1}$ in a 0.5 M $K_2SO_4$ aqueous electrolyte. In a Symmetric Supercapacitor (SSC) configuration (IITR-CO-F-1//IITR-COF-1), comprehensive electrochemical characterization (Fig. 9), showed superior performance: Nyquist plots revealed the lowest impedance and highest conductivity (Fig. 9a–a′), while CV and GCD tests demonstrated ideal capacitive behavior (Fig. 9b and c). The device achieved an energy density of 17.0 Wh $kg^{-1}$ and a power density of 119.3 W $kg^{-1}$ (Fig. 9d), with an impressive specific capacitance of 30.5 F $g^{-1}$ at a current density of 0.12 A $g^{-1}$ (Fig. 9e). Remarkably, IITR-COF-1 exhibited exceptional cycling stability, maintaining 111.3 % of its initial specific capacitance after 10,000 charge-discharge cycles (Fig. 9g and h), suggesting potential capacity enhancement during cycling. It also demonstrated practical applicability by successfully powering both white and red LEDs (Fig. 9i–i‴) [47].

Xue et al. reported the synthesis of a microporous phosphazene-triazinyl-based COF, designated HM-COF, through a straightforward polymerization reaction between hexachlorocyclotriphosphazene and MA [21]. The resulting HM-COF exhibited a BET specific surface area of 305.7 $m^2$ $g^{-1}$ and a pore size of 12.6 Å. Electrochemical characterization demonstrated the material's promising performance as a SC electrode: CV measurements revealed well-defined redox peaks, indicative of reversible faradaic reactions, while GCD analysis showed a maximum specific capacitance of 145 F $g^{-1}$ at a current density of 0.5 A $g^{-1}$. HM-COF exhibited good rate capability, retaining 48.3 % of its capacitance when the current density increased 20-fold to 10 A $g^{-1}$, and demonstrated exceptional cycling stability, maintaining 84.6 % of its initial capacitance after 30,000 charge-discharge cycles at a current density of 2.0 A $g^{-1}$ [21].

Yang et al. synthesized two hydroxy-functionalized COFs—TAPT-2,3-NA$(OH)_2$ and TAPT-2,6-NA$(OH)_2$—using Schiff-base [3 + 2] polycondensation reactions [48]. These COFs were prepared by reacting 1,3,5-tris-(4-aminophenyl)triazine (TAPT-3$NH_2$) with 2,

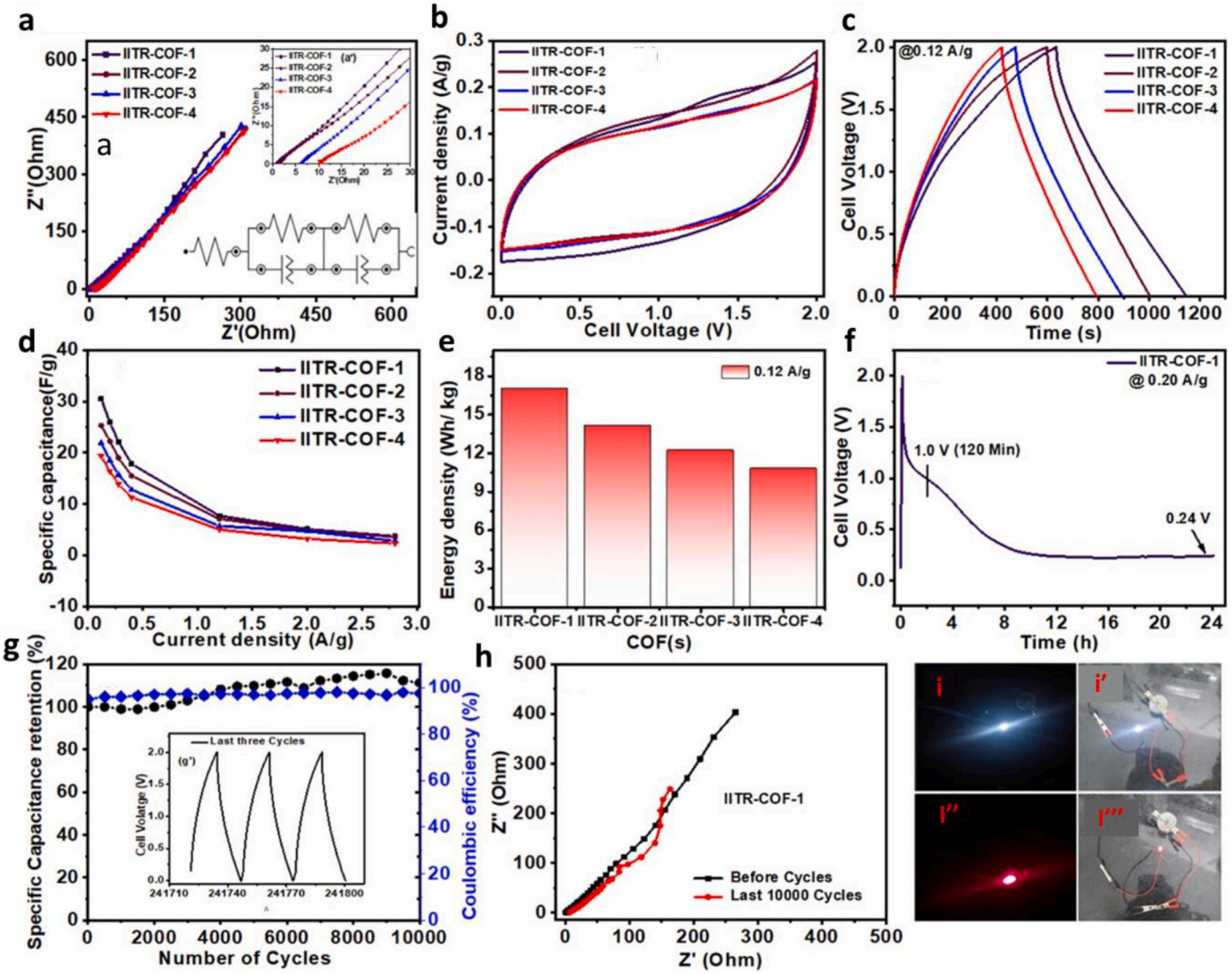


**Fig. 9.** IITR-COF series SCs: EIS (a, a′), CV (b), GCD (c), energy-power density (d, e), stability (g), EIS before and after 10,000 (h), and LED demonstration (i-i‴). Reproduced with permission from Ref. [47] Copyright 2024, American Chemical Society.

3-dihydroxynaphthalene-1,4-dicarbaldehyde (2,3-NADC) and 2,6-dihydroxynaphthalene-1,5-dicarbaldehyde (2,6-NADC) in that order. The incorporation of redox-active 2,3-dihydroxynaphthalene and 2,6-dihydroxynaphthalene units into the COF skeletons imparted electrochemical redox activity to these materials. Electrochemical characterization revealed that the hydroxy-functionalized COFs exhibited a high specific capacitance of 271 F $g^{-1}$ at a current density of 0.5 A $g^{-1}$. Furthermore, after 2000 charge-discharge cycles, these COFs showed remarkable cycling stability, retaining 86.5 % of their initial capacitance [48].

Li et al. reported the design and synthesis of a 2D COF, named DBT-MA-COF, by adopting a carbon-nitrogen coupling reaction between DBT and MA monomers [35]. The researchers constructed an ASC using DBT-MA-COF as one electrode and a carbon-based material (C-CTS) as the counter electrode. At a power density of 800 W $kg^{-1}$, the DBT-MA-COF//C-CTS ASC achieved a high energy density of 32.1 Wh $kg^{-1}$, demonstrating excellent energy storage performance. Notably, after 30,000 continuous GCD cycles, the device retained 83 % of its initial capacitance, highlighting its remarkable cycling stability [35].

Li et al. successfully synthesized a crystalline COF, designated TTT-DHTD, incorporating dithiophenedione moieties in its backbone, and conducted a comparative study with a dimethoxybenzene-dithiophene-based COF (TTT-DMTD) to explore the impact of redox-active dithiophenedione units on capacitance enhancement [49]. Three COFs—TTT-DTDA, TTT-DMTD, and TTT-DHTD—were thoroughly compared, with their chemical structures (Fig. 10a), and electrochemical properties examined (Fig. 10). CV measurements at a 10 mV $s^{-1}$ scan rate demonstrated TTT-DHTD's superior capacitance (163.7 F $g^{-1}$), attributed to its redox-active dithiophenedione units (Fig. 10b). Further CV analysis of TTT-DHTD revealed a proportional increase in current density with scan rate, indicating excellent rate performance (Fig. 10c). GCD measurements showed that TTT-DHTD achieved an impressive specific capacitance of 273.3 F $g^{-1}$ at a current density of 0.5 A $g^{-1}$ (Fig. 10d), highlighting its exceptional charge storage capability. This performance was attributed to its crystalline structure, redox-active components, and high porosity [49].

Ahmad et al. reported the synthesis of a TCOF (TPT@BDA-COF) using 4′,4‴,4‴′′-(1,3,5-triazine-2,4,6-triyl)tris([1,1′-biphenyl]-4-amine) (TPT) and 4,4′-oxydibenzaldehyde (BDA) via a polycondensation process. This synthesis resulted in the fabrication of a well-connected, orderly porous crystalline structure containing redox-active moieties and exhibiting a significantly high nitrogen doping content (~13.6 atomic %). Three-electrode electrochemical studies demonstrated a stable electrochemical potential window of 1.8 V (−0.45 to +1.35 V) in 1 M $NaClO_4$ electrolyte, with the material exhibiting a high specific capacitance of 92.6 mF $cm^{-2}$ and a high energy density of 41.7 Wh $kg^{-1}$. A symmetric SC device constructed using TPT@BDA-COF as both anode and cathode exhibited varying specific capacitances and gravimetric energy densities across different electrolytes: 17.8 F $g^{-1}$ and 3.5 Wh $kg^{-1}$ in 1 M $CH_3COONa$; 36.9 F $g^{-1}$ and 16.6 Wh $kg^{-1}$ in 1 M $Na_2SO_4$; 43.7 F $g^{-1}$ and 13.7 Wh $kg^{-1}$ in 1 M $NaNO_3$; and 47.7 F $g^{-1}$ and 21.6 Wh $kg^{-1}$ in 1 M $NaClO_4$, respectively. The device demonstrated excellent cycling stability (105.2 % capacitance retention) and high Coulombic efficiency (97.5 %) even after 10,000 GCD cycles in 1 M $NaClO_4$ at a current density of 2 A $g^{-1}$. Notably, $ClO_4^-$ anions exhibited superior chaotropic nature (water structure-breaking capability) compared to

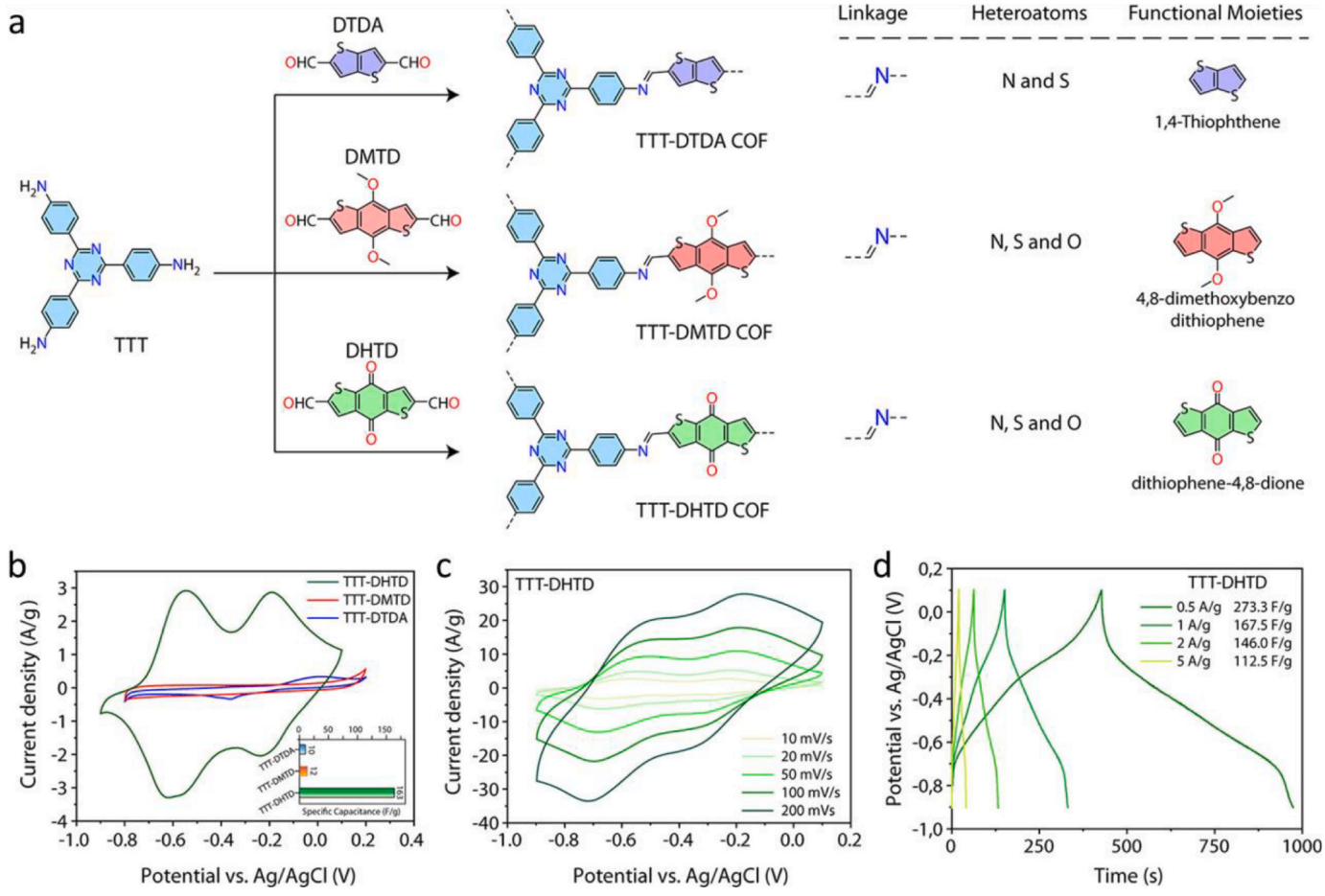


**Fig. 10.** TTT-based COFs: Structures (a), CV comparison (b, c), and TTT-DHTD charge-discharge analysis (d). Reproduced with permission from Ref. [49]. Copyright 2023, American Chemical Society.

$CH_3COO^-$, $SO_4^{2-}$, and $NO_3^-$ anions [50].

Maity et al. utilized a thiafulvalene-based ligand, 2,3,6,7-tetra(4-cyanophenyl)tetrathiafulvalene (TTFCN), for the synthesis of covalent triazine framework (CTF) materials that strategically combine electron-rich thiafulvalene moieties with electron-accepting triazine rings. The researchers employed a trimerization reaction of the nitrile groups in TTFCN to effectively promote the formation of CTF materials, using $ZnCl_2$ as both a Lewis acid catalyst and a solvent (porogen) at 400 °C. By subsequently employing a higher temperature treatment at 700 °C, the CTF materials underwent a transformation into sulfur and nitrogen-containing carbon materials, designated as CTFTTF@2–700. Electrochemical characterization revealed that CTFTTF@2–700 exhibited exceptional performance with a specific capacitance of 943 F $g^{-1}$ at a current density of 1 A $g^{-1}$ and demonstrated excellent electrochemical cycling stability throughout the extended charge-discharge cycling process [51].

Contemporary investigations of TCOFs inadequately elucidate the mechanistic implications of elevated nitrogen content on redox phenomena, particularly concerning electron delocalization pathways and ionic interactions, thereby constraining rational optimization of charge storage mechanisms. The synthetic scalability of nitrogen-enriched TCOFs presents formidable economic and technical barriers to industrial implementation. The anomalous capacitance enhancement during electrochemical cycling, exemplified by IITR-COF-1 (111.3 % retention) and TPT@BDA-COF (105.2 % retention), lacks comprehensive mechanistic rationalization, raising methodological concerns regarding reproducibility and measurement precision. The substantial performance disparities across reported specific capacitances (92.6 mF $cm^{-2}$

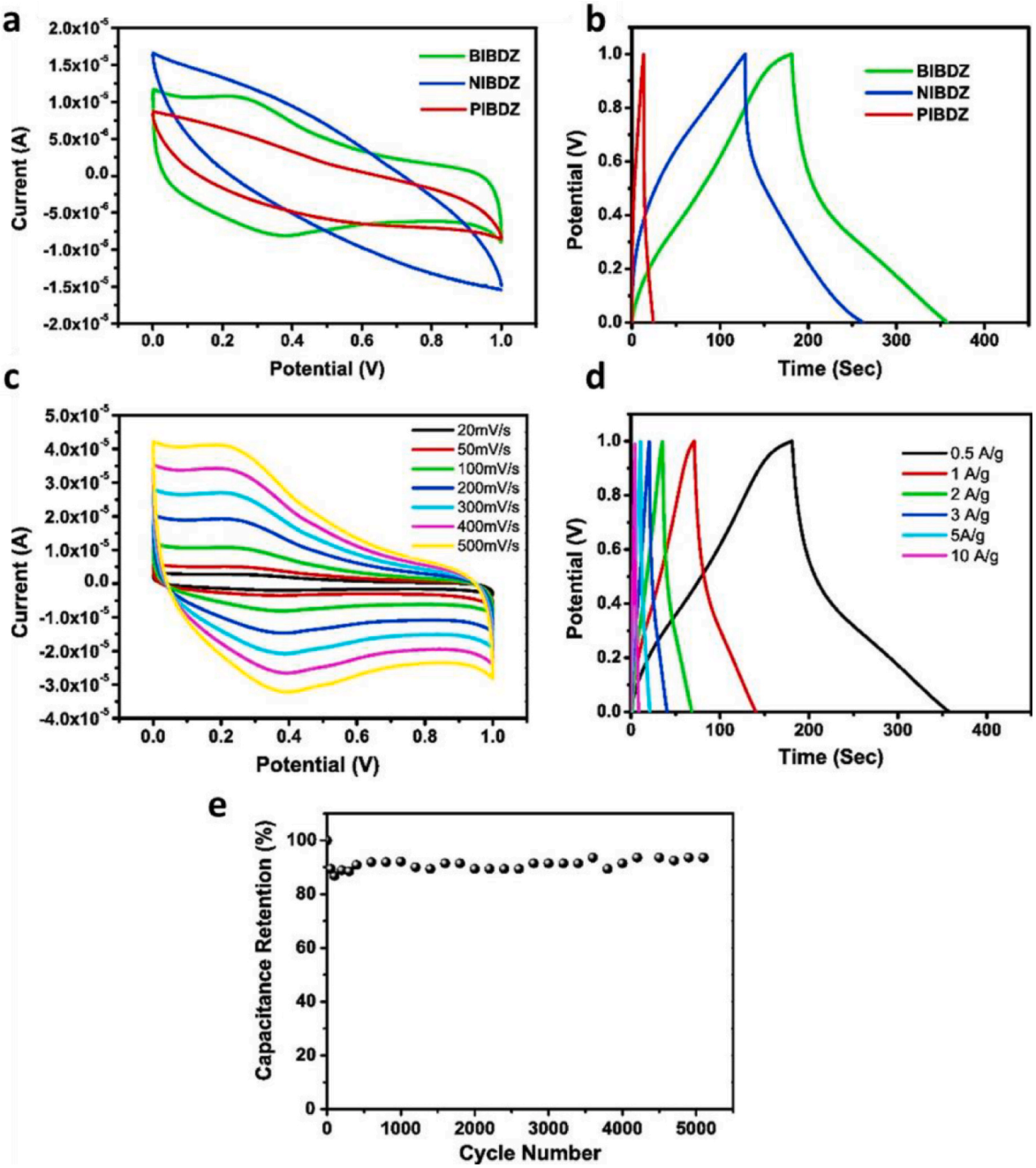


**Fig. 11.** Electrochemical analysis of 3,3′-diaminobenzedene polymers and BIBDZ: (a) CV comparison at 100 mV $s^{-1}$, (b) GCD at 0.5 A/g, (c–d) rate-dependent CV and GCD of BIBDZ, and (e) cycling stability. Reproduced with permission from Ref. [52]. Copyright 2017, Elsevier.

for TPT@BDA-COF versus 943 F $g^{-1}$ for CTFTTF@2–700) introduce significant uncertainties potentially attributable to electrode fabrication heterogeneities, electrolyte interaction variations, or experimental configuration inconsistencies. The mechanistic debate regarding triazine's intrinsic redox activity versus structural porosity contributions to electrochemical performance remains unresolved, with conflicting interpretations emphasizing either pseudocapacitive or EDLC mechanisms.

#### 4.4.3. *Benzimidazole-based COFs for SCs*

Roy et al. synthesized a series of COFs featuring benzimidazole-functionalized arylimide units, incorporating pyromellitic, naphthalene, and perylene-based imides [52]. Among these, the pyromellitic diimide-containing benzimidazole COF (BIBDZ) exhibited outstanding electrochemical performance. When tested in a 1 M $H_3PO_4$ electrolyte solution, BIBDZ achieved a specific capacitance of 88.4 F $g^{-1}$ at a current density of 0.5 A $g^{-1}$. The electrochemical behavior of the BIBDZ COF highlighted its exceptional capacitive performance (Fig. 11). CV measurements (Fig. 11a) revealed distinct redox peaks at 0.23 V and 0.37 V (vs. Ag/AgCl), indicating reversible pseudocapacitive behavior with a small peak separation (ΔEp = 0.14 V). GCD studies (Fig. 11b) in the same electrolyte demonstrated a high specific capacitance of 88.4 F $g^{-1}$ at a current density of 1 A $g^{-1}$. Furthermore, the scan rate dependency analysis (Fig. 11c) showed consistent peak currents, although

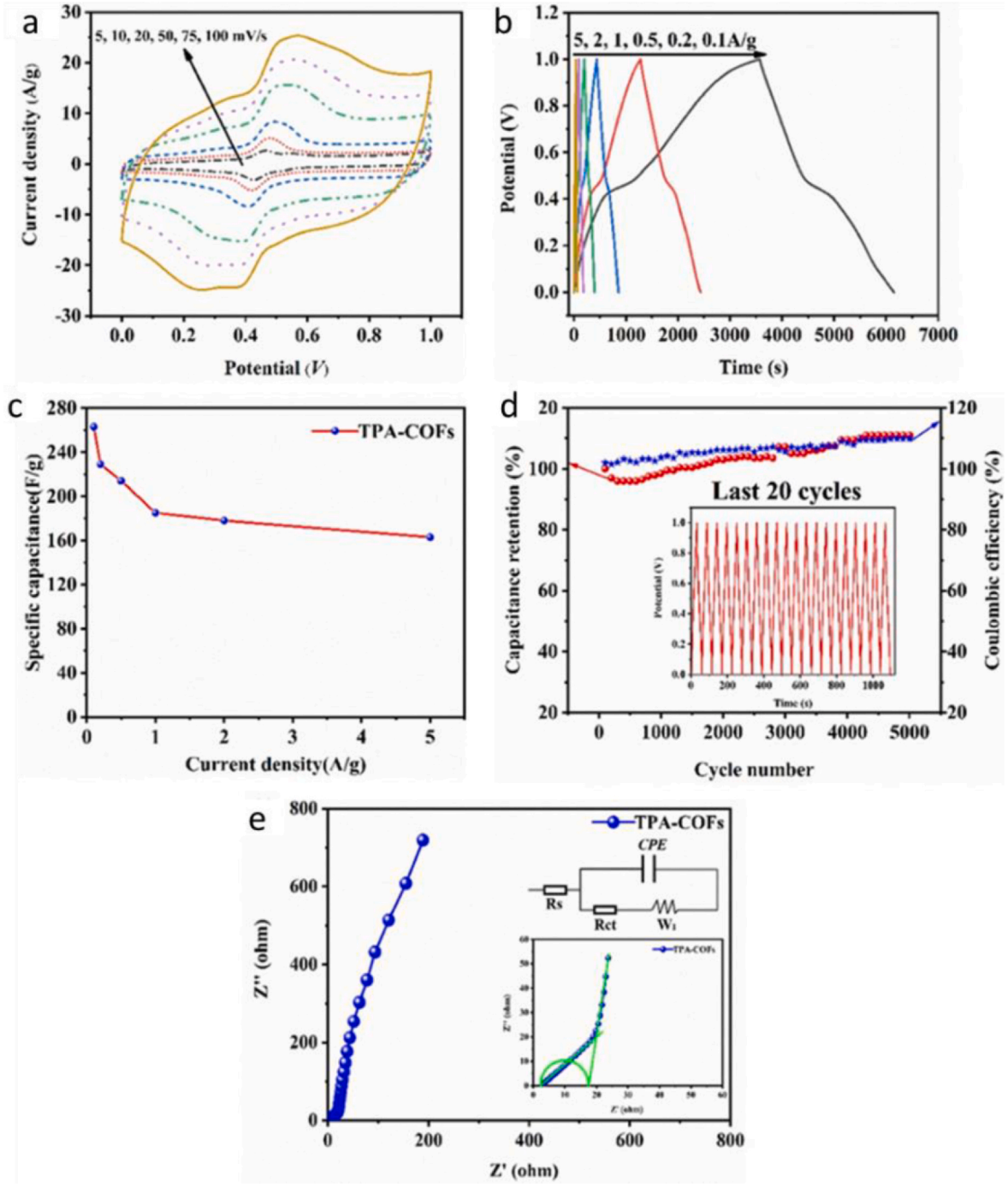


**Fig. 12.** Electrochemical characterization of TPA-COFs: (a) CV curves, (b) GCD profiles, (c) rate performance, (d) cycling stability, and (e) Nyquist plots with high-frequency inset. Reproduced with permission from Ref. [53] Copyright 2022, John Wiley & Sons – Books.

with broader peaks, reflecting pseudocapacitive characteristics. Rate performance analysis (Fig. 11d) revealed that BIBDZ retained 48.6 % of its initial capacitance (43 F $g^{-1}$) at an increased current density of 10 A $g^{-1}$, where diffusion-limited charge transfer becomes dominant. Additionally, BIBDZ demonstrated excellent cycling stability (Fig. 11e), maintaining 93.61 % of its initial capacitance after 5000 consecutive charge-discharge cycles at a current density of 5 A $g^{-1}$ [52].

Despite promising electrochemical performance, benzimidazole-based COFs such as BIBDZ exhibit critical knowledge gaps that limit their optimization and practical implementation in supercapacitor applications. The mechanistic understanding of benzimidazole's redox contributions remains inadequately developed, with insufficient in-situ spectroscopic studies to elucidate electron transfer pathways during charge-discharge cycles. BIBDZ's reported specific capacitance (88.4 F $g^{-1}$ at 0.5 A $g^{-1}$) is notably lower than other redox-active COFs, while the influence of imide unit variations on electrochemical performance remains underexplored. Current solvothermal synthesis methods present significant scalability constraints, imposing economic and technical barriers that limit industrial viability. Although BIBDZ demonstrates cycling stability (93.61 % retention after 5000 cycles), validation across diverse electrolyte systems is lacking, and the impact of electrolyte interactions on long-term performance remains poorly characterized. The relationship between structural parameters and charge storage mechanisms requires systematic quantification, with inconsistent rate performance data (48.6 % capacitance retention at 10 A $g^{-1}$) suggesting methodological variations. Future research should prioritize advanced electrochemical diagnostics, particularly operando X-ray absorption spectroscopy, to clarify benzimidazole's redox mechanisms, alongside exploring mechanochemical synthesis routes and conducting systematic electrolyte studies to resolve performance disparities.

#### 4.4.4. Triphenylamine-based COFs for SCs

Xiong et al. successfully synthesized a triphenylamine-based COF (TPA-COF) using a solvothermal method via a Schiff base condensation reaction between TFPA and tris(4-aminophenyl)amine (TAPA) [53]. The resulting TPA-COF demonstrated outstanding electrochemical properties, achieving a specific capacitance of 263.1 F $g^{-1}$ at 0.1 A $g^{-1}$, along with an impressive specific surface area of 398.59 $m^2$ $g^{-1}$. Detailed electrochemical analyses (Fig. 12), highlighted the material's excellent performance as a SC electrode. The electron-rich triphenylamine structure contributed to well-defined reversible redox peaks observed in the CV analysis (Fig. 12a), indicative of pseudocapacitive behavior. GCD measurements further confirmed the capacitive nature of the material (Fig. 12b). Rate capability tests showed a notable capacitance retention of 62 % when the current density increased from 0.1 A $g^{-1}$ (263 F $g^{-1}$) to 5 A $g^{-1}$ (163 F $g^{-1}$) (Fig. 12c). Remarkably, the TPA-COF exhibited exceptional cycling stability, retaining 111 % of its initial capacitance after 5000 charge-discharge cycles, with a coulombic efficiency of 109 % (Fig. 12d). This suggests enhanced structural stability and potential activation of additional redox sites during cycling. The Nyquist plot revealed excellent ion transport properties, characterized by a low solution resistance (Rs = 2.604 Ω) and charge transfer resistance (Rct = 11.9 Ω) (Fig. 12e) [53].

Triphenylamine-based COFs, exemplified by TPA-COF, demonstrate electrochemical activity in supercapacitor applications; however, fundamental mechanistic understanding remains incomplete. The electron-rich triphenylamine framework's contribution to pseudocapacitive behavior lacks comprehensive characterization through computational modeling and in-situ spectroscopic techniques to elucidate charge delocalization pathways and redox kinetics. While TPA-COF exhibits unusual capacitance enhancement during electrochemical cycling (111 % retention after 5000 cycles), this phenomenon requires mechanistic clarification and independent validation to address reproducibility concerns and potential redox site activation mechanisms. The reported specific capacitance (263.1 F $g^{-1}$ at 0.1 A $g^{-1}$) indicates suboptimal performance relative to other COF architectures, suggesting limitations in pore accessibility or redox site utilization that warrant systematic structural optimization studies. Synthesis scalability remains constrained by solvothermal methodologies, while electrolyte-performance relationships are inadequately explored. Inconsistent rate performance data (62 % retention at 5 A $g^{-1}$) reflects methodological variations in electrode preparation and testing protocols that compromise comparative analysis. Future investigations should employ density functional theory calculations and solid-state NMR spectroscopy to resolve triphenylamine's redox mechanisms, explore mechanochemical synthesis alternatives for scalability, and establish standardized electrochemical protocols to enhance reproducibility and practical implementation potential.

Table 3 demonstrates the diverse electrochemical performance characteristics of nitrogen-rich COFs, primarily attributed to their redox-active pyridine and triazine functionalities. Pyridine-based frameworks exhibit specific capacitances ranging from 102 F $g^{-1}$ (TaPaPy COF) to 546 F $g^{-1}$ (IISERP-COF10), with the latter achieving enhanced redox activity in 1 M $H_2SO_4$ electrolyte while displaying moderate cycling stability (70 % retention after 10,000 cycles). In contrast, TaPa-Py COF, despite lower capacitance values, demonstrates superior long-term stability with 92 % capacitance retention after 6000 cycles, while PFM-COF1 achieves balanced performance with high capacitance (394.28 F $g^{-1}$) and reasonable stability (81 % retention after 2000 cycles). Triazine-based COFs generally exhibit higher capacitance values, exemplified by CTFTTF@2–700 reaching 943 F $g^{-1}$ in 1 M $Na_2SO_4$, with this exceptional performance attributed to thermal treatment-induced conductivity enhancement. DBT-MA-COF achieves 407 F $g^{-1}$ in 6 M KOH, benefiting from triazine unit contributions, while TTT-DHTD COF (273.3 F $g^{-1}$) leverages synergistic effects between triazine and dithiophenedion functionalities. Electrolyte selection significantly influences electrochemical performance, with KOH-based systems (DBT-MA-COF, IITR-COF-1) yielding higher capacitances (271–407 F $g^{-1}$) compared to $NaClO_4$-based systems such as TPT@BDA-COF (2.6 mF $cm^{-2}$) which compensates with a wider 1.8 V potential window. Cycling stability varies considerably across different frameworks, with IITR-COF-1 and TPT@BDA-COF demonstrating exceptional retention (>100 % after 10,000 cycles), possibly due to electrochemical activation phenomena, while other systems maintain 84–92 % retention over 2000–30,000 cycles. The predominantly moderate current density operating ranges (0.3–2 A $g^{-1}$) highlight persistent conductivity limitations inherent to these materials, which may be addressed through thermal treatment strategies and strategic integration of redox-active functionalities.

### 4.5. Thiol-based COFs for SCs

The incorporation of sulfur moieties significantly enhanced the electrochemical performance of the COFs. SH-COF-1, with a higher density of thiol groups per structural unit, demonstrated superior properties, including a larger surface area (227 $m^2$ $g^{-1}$) and improved electrochemical performance [54]. Notably, SH-COF-1 retained over 95 % of its areal capacitance after 1000 charge-discharge cycles, achieving a capacitance of 118 mF $cm^{-2}$. In a two-electrode setup, electrochemical studies revealed that SH-COF-1 outperformed SH-COF-2 (Fig. 13). The CV curves showed capacitive behavior with pseudocapacitive contributions from thiol groups, which were more prominent in SH-COF-1 due to its higher surface area and accessible thiol units (Fig. 13a and b). The GCD curves exhibited distorted triangular shapes, with SH-COF-1 displaying longer discharge times (Fig. 13c and d), indicative of enhanced charge storage capacity. SH-COF-1 demonstrated significantly higher areal capacitance (40 mF $cm^{-2}$ at 0.5 mA $cm^{-2}$) compared to SH-COF-2 (16 mF $cm^{-2}$) (Fig. 13e). EIS analysis further confirmed the superior performance of SH-COF-1, showing lower charge-transfer resistance and faster ion transport (Fig. 13f) [54].

**Table 3**
Capacitance properties of Nitrogen-rich COFs for SCs.

| Materials | Redox group | Electrolyte | Potential window | Specific capacitance | Current density | Capacitance retention | Ref |
|---|---|---|---|---|---|---|---|
| PFM-COF1 | Pyridine | 1 M $H_2SO_4$ | 0 to 0.7 V | 394.28 F $g^{-1}$ | 0.5 A $g^{-1}$ | 81 % after 2000 cycles | [11] |
| TFP-TPP COFs | pyridine | 1 M KOH | −1.0 to 0.0 V | >170 F $g^{-1}$ | 2 A $g^{-1}$ | 88.2 % after 2000 cycles | [31] |
| TaPa-Py COF | pyridine | 1 M $H_2SO_4$ | −0.3 to 0.4 V | 102 F $g^{-1}$ | 0.5 A $g^{-1}$ | 92 % after 6000 cycles | [34] |
| IISERP-COF10 | pyridine | 1 M $H_2SO_4$ | 0 to 0.8 V | 546 F $g^{-1}$ | 0.5 A $g^{-1}$ | 70 % after 10,000 cycles | [46] |
| HM-COF | Triazine | 1 M $H_2SO_4$ | −0.1 to 0.5 V | 145 F $g^{-1}$ | 0.5 A $g^{-1}$ | 84.6 % after 30000 cycles | [21] |
| IITR-COF-1 | Triazine | 0.5 M $K_2SO_4$ | 0 to 2.2 V | 182.6 F $g^{-1}$ | 0.3 A $g^{-1}$ | 111.3 % after 10000 cycles | [47] |
| COFs-TAPT-2,3NA(OH)2 | Triazine | 1 M KOH | −0.8 to 0.2 V | 271 F $g^{-1}$ | 0.5 A $g^{-1}$ | 86.5 % after 2000 cycles | [48] |
| DBT-MA-COF | Triazine | 6 M KOH | 0 to 0.45 V | 407 F $g^{-1}$ | 1.0 A $g^{-1}$ | 85 % after 20000 cycles | [35] |
| TTT-DHTD COF | Triazine, Dithiophenedion | 1 M KOH | −0.2 to 0.8 V | 273.3 F $g^{-1}$ | 0.5 A $g^{-1}$ | _____ | [49] |
| TPT@BDA-COF | Triazine | 1 M $NaClO_4$ | −0.45 to 1.35 V | 2.6 mF $cm^{-2}$ | 2 A $g^{-1}$ | 105.2 % after 10000 cycles | [50] |
| CTFTTF@2-700 | Triazine | 1 M $Na_2SO_4$ | −0.8 to 0 V | 943 F $g^{-1}$ | 1 A $g^{-1}$ | 90 % after 10000 cycles | [51] |

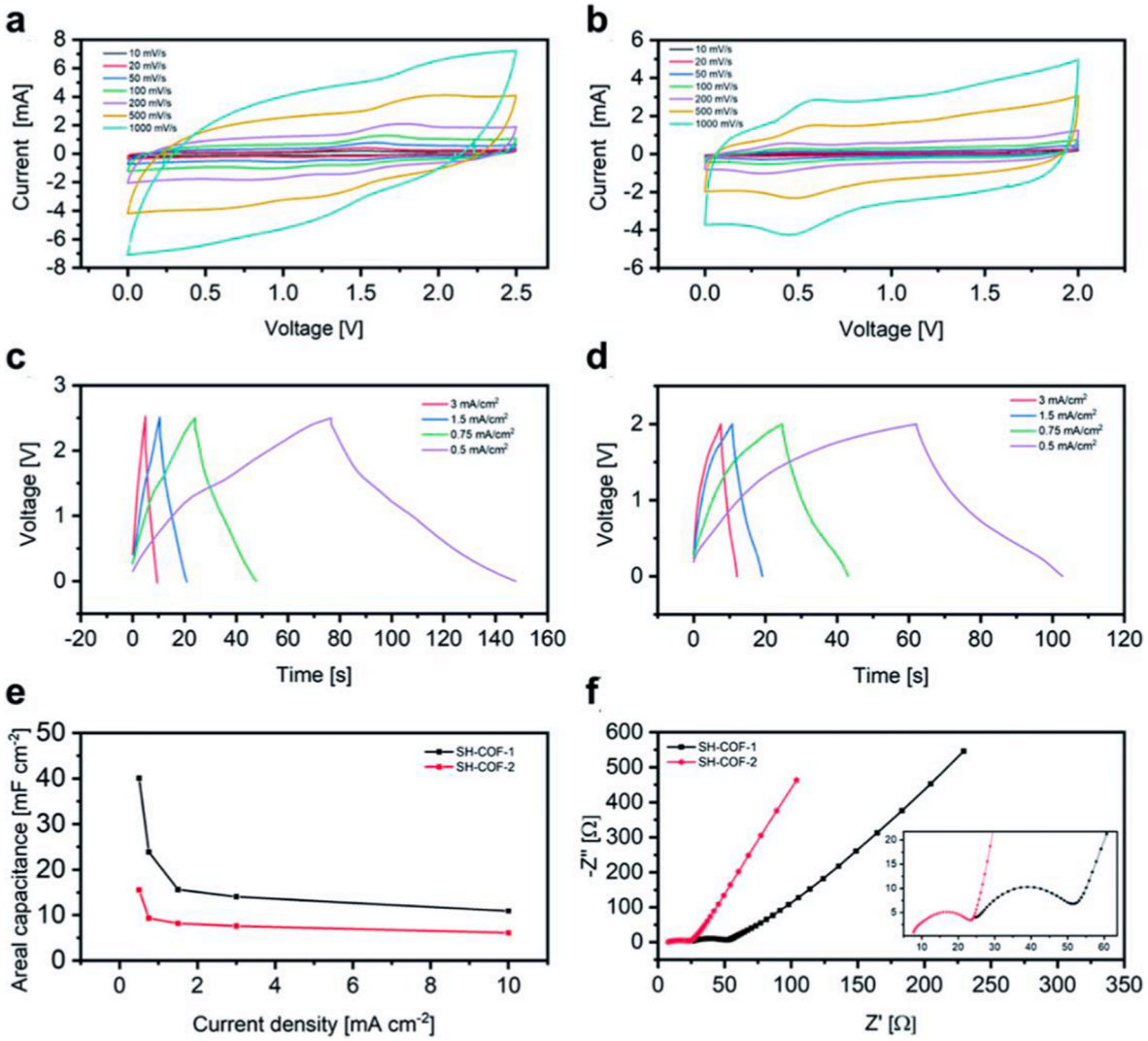


**Fig. 13.** Electrochemical characterization of SH-COFs using a two-electrode setup. CV curves for SH-COF-1 (a and c) and SH-COF-2 (b and d) at varying scan rates and GCD curves at varying current densities. (e) The areal capacitance in relation to the current density, and (f) the EIS spectra of SH-COF-2 (red) and SH-COF-1 (black). Reproduced with permission from Ref. [54]. Copyright 2022, Royal Society of Chemistry. (For interpretation of the references to colour in this figure legend, the reader is referred to the Web version of this article.)

### *4.6. Other*

Zhuang et al. were the first to synthesize an olefin-linked 2D COF by reacting a three-armed aromatic aldehyde with 1,4-phenylene diacetonitrile via a Knoevenagel polycondensation process [55]. Subsequent heating and activation treatments successfully transformed the resulting 2D poly(phenylenevinylene) framework (2DPPV) into porous carbon nanosheets with a high specific surface area of up to 880 $m^2$ $g^{-1}$. These carbon nanosheets exhibited exceptional electrochemical performance when employed as electrocatalysts for the oxygen reduction reaction and as SC electrodes [55].

Patra et al. synthesized a porphyrin-based 2D COF by conducting a Schiff base condensation reaction between 1,1,2,2-tetrakis(4-formyl-(1,1′-biphenyl))ethane (TFBE) and 5,10,15,20-tetrakis(para-

aminophenyl)porphyrin (TAPP) under solvothermal conditions [12]. The resulting porphyrin-tetraphenylethylene COF (PT-COF) exhibited exceptional crystallinity and a high surface area of 1998 $m^2 g^{-1}$. As an electrode material for supercapacitive energy storage, PT-COF demonstrated impressive performance by combining electric double-layer capacitance and pseudocapacitance mechanisms. In a 0.5 M $H_2SO_4$ electrolyte at a current density of 1 A $g^{-1}$, PT-COF achieved a maximum specific capacitance of 1443 F $g^{-1}$, with 91 % capacity retention after 3000 cycles. The excellent redox activity in acidic conditions was attributed to the protonation of the porphyrin unit [$H_2P$] during the cathodic scan, followed by a two-electron reduction to generate a 20π-electronic system [$H_4P$] [12].

Iqbal et al. reported the synthesis of a highly crystalline two-dimensional conjugated COF (250-HADQ COF) under optimized reaction conditions [8]. The resulting material featured 1-nm-wide pores and a high nitrogen content of approximately 37 %. The 250-HADQ COF exhibited remarkable properties, including a high specific surface area of 2443 $m^2 g^{-1}$ and excellent thermal stability up to 1000 °C. When employed in two-electrode double-layer SCs with an ionic liquid electrolyte, the material demonstrated outstanding electrochemical performance. It achieved a high gravimetric capacitance of 516.4 F $g^{-1}$ at 0.5 A $g^{-1}$ and an energy density of 219.4 Wh $kg^{-1}$ at a power density of 437.5 W $kg^{-1}$. Notably, the 250-HADQ COF retained 81 % of its initial capacity after 100,000 charge-discharge cycles at a current density of 2 A $g^{-1}$ [8]. Khojastehnezhad et al. reported the use of two distinct Keggin-type heteropolyacids (HPAs), namely Lewis and Brønsted acids, as catalysts to accelerate the synthesis of 2D and 3D COFs while improving the quality of their constituent components [17]. The designed TAPA-TPT COF exhibited outstanding performance in SC applications. At a current density of 0.5 A $g^{-1}$, this COF achieved an impressive specific capacitance of 205 F $g^{-1}$, making it a highly desirable material for SCs [17].

The excellent pseudocapacitance of the COF, resulting from precise molecular-level control of the redox functionalities within its backbone, likely accounts for its superior specific capacitance. Chandra et al. synthesized and studied two redox-active COFs, TpPa-$(OH)_2$ and TpBD-$(OH)_2$, for SC applications, focusing on the role of their redox-active functional groups in enhancing specific capacitance [33]. Among the two COFs, TpPa-$(OH)_2$ demonstrated superior electrochemical performance. In a three-electrode configuration, it achieved a remarkable specific capacitance of 416 F $g^{-1}$ at a current density of 0.5 A $g^{-1}$. When tested in a two-electrode setup, it exhibited a maximum specific capacitance of 214 F $g^{-1}$ at a current density of 0.2 A $g^{-1}$. TpPa-$(OH)_2$ also displayed excellent cycling stability, retaining 66 % of its initial capacitance after 10,000 cycles in the three-electrode configuration and 88 % in the two-electrode setup. Notably, 43 % of the redox-active hydroquinone ($H_2Q$) moieties were accessible in the three-electrode configuration, significantly contributing to its pseudocapacitive behavior [33].

Diverse COF systems, including olefin-linked, porphyrin-based, and other redox-active architectures, exhibit substantial potential for supercapacitor applications, yet critical research gaps impede their optimization and practical deployment. The mechanistic interplay between pseudocapacitive and electric double-layer capacitance contributions in high-performance materials such as PT-COF (1443 F $g^{-1}$) and 250-HADQ COF (516.4 F $g^{-1}$) remains inadequately characterized, with insufficient operando studies to differentiate redox-driven versus surface-driven charge storage mechanisms. PT-COF's exceptionally high specific capacitance raises reproducibility concerns, as methodological variations in electrode preparation and electrolyte conditions may contribute to reported performance disparities. Scalability of specialized COFs is constrained by complex synthesis routes, including Knoevenagel polycondensation and solvothermal Schiff base reactions, which present significant economic and technical barriers to industrial implementation. The influence of high nitrogen content (37 % in 250-HADQ COF) on electrochemical performance lacks systematic investigation, particularly regarding nitrogen's role in enhancing redox activity versus structural stability. Long-term cycling stability, exemplified by 250-HADQ COF's 81 % retention after 100,000 cycles, requires validation across diverse electrolyte systems to confirm robustness under varied operational conditions. Future investigations should employ advanced in-situ characterization techniques, including synchrotron X-ray diffraction and electrochemical quartz crystal microbalance, to elucidate charge storage mechanisms, while exploring scalable synthesis methods and standardized testing protocols to address performance inconsistencies and facilitate practical applications.

COF architectures demonstrate distinct performance characteristics that dictate their suitability for specific supercapacitor applications. Porphyrin-based COFs (PT-COF, 1443 F $g^{-1}$; 250-HADQ, 516.4 F $g^{-1}$) and triazine-based COFs (CTFTTF@2–700, 943 F $g^{-1}$) exhibit superior specific capacitance attributed to high surface areas (1998–2443 $m^2 g^{-1}$) and abundant redox-active units, making them ideal for high-energy-density applications such as portable electronics, though cycling stability remains moderate (81–91 % retention after 3000–100,000 cycles). Conversely, naphthalene-based COFs (TFPh-NDA, 583 F $g^{-1}$, 100 % retention after 10,000 cycles) and select triazine-based systems (IITR-COF-1, 111.3 % retention) demonstrate exceptional stability suitable for grid storage applications, driven by π-conjugation and nitrogen content (13.6–37 %), albeit with electrolyte-dependent performance variations (943 F $g^{-1}$ in $Na_2SO_4$ versus 47.7 F $g^{-1}$ in $NaClO_4$). DAAQ-based COFs (TpOMe-DAQ, 1600 mF $cm^{-2}$, 169 F $g^{-1}$) offer advantages for flexible, thin-sheet electrodes despite lower gravimetric capacitance, while AZO-based systems (TFPB-AZOCOF, 450 F $g^{-1}$, 8500 W $kg^{-1}$) prioritize power density applications. Pyridine-based (IISERP-COF10, 546 F $g^{-1}$), triphenylamine-based (263.1 F $g^{-1}$), benzimidazole-based (88.4 F $g^{-1}$), and thiol-based (118 mF $cm^{-2}$) COFs exhibit moderate performance limited by surface area constraints or redox site accessibility. Critical research gaps persist, including mechanistic uncertainties regarding pseudocapacitive versus EDLC contributions, solvothermal synthesis scalability limitations, and substantial performance disparities across systems. Future advancement requires operando characterization techniques, standardized testing protocols, and scalable synthesis methods to enhance practical applicability and resolve fundamental mechanistic questions.

## 5. COFs composites in SCs

COFs can be effectively incorporated into composites with conductive materials to improve their overall conductivity, which is crucial for many applications, especially in energy storage. One prominent example of this approach is the growth of COFs on carbon nanotubes (CNTs) or graphene sheets. This strategy creates a synergistic combination of the high surface area and customizable functionality of COFs with the excellent electrical conductivity of CNTs or graphene. As a result, these composites typically demonstrate significantly enhanced conductivity compared to pristine COFs, while retaining the advantages of the COF structure, such as high porosity and tunable chemical functionality. This improved conductivity can lead to superior performance in various applications, including SCs, batteries, and other energy storage devices. The ability to create such COF-based composites highlights the versatility of COFs in materials design and their potential for developing high-performance materials for energy-related applications.

### 5.1. Carbon/COF composites for SCs

CNTs have attracted considerable research attention in the scientific community due to their unique properties. The combination of CNTs with COFs to form CNT/COF composites has emerged as a promising area of study, particularly for energy storage and conversion applications. These composites harness the exceptional electrical conductivity and mechanical strength of CNTs, along with the high surface area, customizable pore structure, and chemical functionality of COFs.

Numerous studies have investigated the potential of CNT/COF composites in various energy-related applications, including SCs, batteries, and electrocatalysis.

The effective synthesis of a CNT-imide COF composite with a unique core-shell structure was reported by Dai et al. [56]. This n-type imide COF was generated in situ on the surface of amine-functionalized CNTs, which served as the substrate. The resulting PAI@40 % CNT composite exhibited enhanced electrical conductivity and high porosity. As a negative electrode material, the PAI@40 % CNT composite demonstrated a specific capacitance of 278 F $g^{-1}$ in the negative potential range of a neutral electrolyte. Notably, even at a high current density of 50 A $g^{-1}$, the composite retained a high specific capacitance of 72 F $g^{-1}$. These exceptional energy-storage capabilities are attributed to the synergistic relationship between the carbon nanotube core and the carbon oxide filler shell. Additionally, $RuO_2$ was used as the positive electrode, and PAI@40 % CNT served as the negative electrode in an ASC device. At a power density of 357.2 W $kg^{-1}$, this $RuO_2$//PAI@40 % CNT ASC device demonstrated a high energy density of 25.9 W h $kg^{-1}$ [56].

Yang et al. reported on COFs enriched with redox-active azo groups, which are capable of undergoing proton-coupled electron transfer reactions, making them promising candidates for pseudocapacitive electrode materials [16]. The researchers developed a novel approach by in situ hybridizing these COFs with CNTs, resulting in a composite material with exceptional electrochemical performance. When evaluated in a three-electrode configuration, the composite exhibited one of the highest specific capacitances reported to date for COF-based SCs, achieving 440 F $g^{-1}$ at a current density of 0.5 A $g^{-1}$. Moreover, the material demonstrated remarkable cycling stability, retaining 90 % of its initial capacitance after 10,000 charge-discharge cycles. This study represents a pioneering effort in the development of high power and energy density pseudocapacitors using Grotthuss proton-conductive organic materials. When assembled into an asymmetric two-electrode SC, the device outperformed all previously reported COF-based devices. Notably, it achieved a maximum energy density of 71 Wh $kg^{-1}$ and a maximum power density of 42 kW $kg^{-1}$, marking a significant milestone in COF-based energy storage technology. The CNT/NKCOF-2/AC ASC has been thoroughly electrochemically characterized, as shown in (Fig. 14). Significant redox peaks are visible in the CV curves (Fig. 14a) over a broad range of scan rates (1–100 mV $s^{-1}$), indicating fast redox kinetics and robust pseudocapacitive behavior. The virtually linear and symmetric profiles of GCD curves (Fig. 14b) at different current densities (1–100 A $g^{-1}$) suggest optimal capacitive behavior with low internal resistance. The Ragone plot (Fig. 14c) highlights the device's remarkable performance, demonstrating a maximum power density of 42 kW $kg^{-1}$ and a high energy density of 71 Wh $kg^{-1}$ [16].

Liu et al. developed a simple one-pot method to synthesize a series of CNT@COF composites using carboxylated multi-walled CNTs. This process involves the in-situ growth of 2D TFA-COFs on the surface of the nanotubes [10]. Among these composites, CNT@TFA-COF-3 exhibited outstanding properties, including a high specific surface area of 1034 $m^2$ $g^{-1}$, uniform pore distribution, strong structural stability, and excellent crystallinity. As a capacitive electrode material, CNT@TFA-COF-3 demonstrated superior electrochemical performance, achieving a specific capacitance of 338 F $g^{-1}$ at a current density of 1.0 A $g^{-1}$. This value is 8.5, 4.9, and 7.5 times higher than that of TFA-COFs,

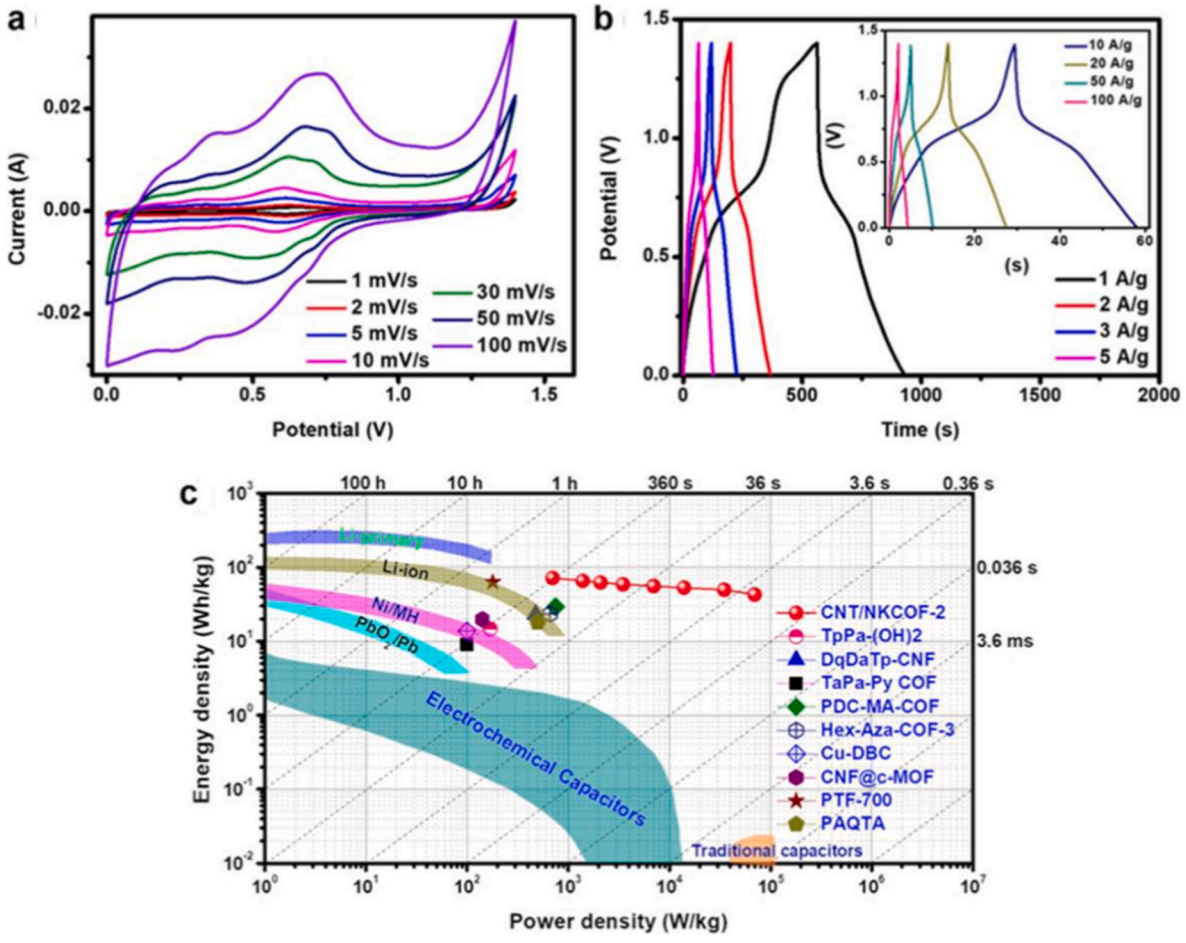


**Fig. 14.** Electrochemical Performance of CNT/NKCOF-2//AC ASC: CV Curves (a), Charge-Discharge (b), and Ragone Plot (c). Reproduced with permission from Ref. [16]. Copyright 2017, American Chemical Society.

CNTs, and the physically mixed CNT/TFA-COF composite, respectively. Furthermore, the CNT@TFA-COF-3-based SC exhibited remarkable long-term cycling stability and exceptional rate performance, maintaining functionality even after 7000 charge-discharge cycles [10].

Yang et al. synthesized SWCNT-COF nanohybrids by integrating redox-active TpPa-COFs with single-walled carbon nanotubes (SWCNTs) through solvothermal in situ polymerization. This method produced a core-shell structure, where TpPa-COFs were uniformly nanocoated onto SWCNTs, enabling precise control over the COF/SWCNT interface at the molecular level compared to mechanical mixing. The nano-hybrid-based electrode exhibited a specific capacitance of 153 F $g^{-1}$ at a current density of 0.5 A/g, along with exceptional long-term cycling stability. These findings underscore the effectiveness of in situ polymerization in developing high-performance COF-based SC materials with enhanced electrochemical properties and durability [57].

Yang et al. developed innovative nanocomposite materials using carbon nanotube fibers (f-CNFs) as templates to synthesize TPTP-COF@f-CNF and TPDA-COF@f-CNF [18]. Their study demonstrated the outstanding electrochemical performance of these materials in SC applications. Electrodes based on TPTP-COF and TPDA-COF exhibited impressive specific capacitances of 577.4 F $g^{-1}$ and 640.4 F $g^{-1}$, respectively, at a scan rate of 5 mV $s^{-1}$. Notably, an inverse relationship was observed between the f-CNF concentration and the specific capacitance of both TPTP-COF@f-CNF and TPDA-COF@f-CNF electrodes. The research team further constructed SSC devices using TPTP-COF and TPDA-COF, achieving maximum specific capacitances of 56.4 F $g^{-1}$ and 70.6 F $g^{-1}$, respectively. Moreover, these devices exhibited remarkable electrochemical stability during prolonged operation. The TPTP-COF-based device retained 78.60 % of its initial capacitance after 10,000 charge-discharge cycles, while the TPDA-COF-based device retained 81.54 % [18].

Dai et al. reported the successful design and synthesis of a polyimide COF (pHANT) composed of imide and hexaazatriphenylene units. Additionally, they constructed a pHANT@10 %CNT composite via in-situ growth of this n-type COF on aminoized multi-walled carbon nanotubes using a simple hydrothermal method. The pHANT@10%CNT composite exhibited exceptional electrochemical performance with a high specific capacitance of 366 F $g^{-1}$ at 0.5 A $g^{-1}$ when operated within a negative potential window in a neutral electrolyte. Moreover, the composite demonstrated excellent cycling stability. Ex-situ XPS analysis of the composite at potentials of −0.2 V, −0.6 V, and −1.0 V revealed the participation of C=O and C=N functional units in energy storage processes, confirming that the polyimide-co-hexaazatriphenylene COF structure provides abundant redox-active sites. When assembled into an ASC device (pHANT@10 %CNT//$RuO_2$), the system delivered a high specific capacitance of 82.8 F $g^{-1}$ at 0.5 A $g^{-1}$ across a wide operating voltage window of 1.4 V, achieving an energy density of 22.54 Wh $kg^{-1}$ at a power density of 350 W $kg^{-1}$ [58].

Kang et al. reported the development of a series of hexaazatriphenylene-based COF exfoliated by carbon nanotubes (CNT@HATN-COF-x) through a mild in situ composite formation and chemical stripping method. The exfoliation process resulted in HATN-COF layers with an approximate thickness of 4.5 nm that were intricately interfaced with the carbon nanotubes. The resulting SC based on CNT@HATN-COF-0.6 demonstrated exceptional electrochemical performance, achieving a high specific capacitance of 436 F $g^{-1}$ and an exceptionally high energy density of 155.3 Wh $kg^{-1}$. Moreover, the SC exhibited outstanding cycling stability, maintaining 100 % of its initial capacitance after 10,000 charge-discharge cycles. This remarkable stability indicates that the incorporation of carbon nanotubes has a negligible effect on the inherently stable molecular structure of the COF, while significantly enhancing its electrochemical performance through improved conductivity and structural support [59].

Graphene, alongside CNTs, has attracted significant interest in science and technology. Numerous studies have reported the development of graphene/COF composites for energy conversion and storage. Xu et al. utilized graphene as a conductive substrate for the in-situ growth of a 2D redox-active COF (TFPDQ-COF) under solvent-free conditions, forming TFPDQ-COF/graphene (TFPDQGO) nanohybrids, and explored their applications in both SCs and hybrid capacitive deionization (HCDI) [60]. By optimizing the hybridization ratio, TFPDQGO achieved a high specific capacitance of 429.0 F $g^{-1}$, attributed to the synergistic effect of the graphene layers' charge transport capabilities and the abundant redox-active centers within the COF skeleton. The assembled TFPDQGO//AC ASC exhibited a high energy output of 59.4 Wh $kg^{-1}$ at a power density of 950 W $kg^{-1}$, along with excellent cycling stability. Additionally, the TFPDQGO-based HCDI system demonstrated a maximum salt adsorption capacity of 58.4 mg $g^{-1}$ and stable regeneration performance [60].

Xu et al. reported the development of a 2D redox-active pyrazine-based COF (BAHC-COF) anchored onto graphene via a solvent-free strategy for heterointerface regulation [61]. The resulting BAHC-COF/graphene (BAHCGO) nanohybrid materials effectively combine the high-speed charge transport capabilities of graphene with enhanced electrolyte ion migration within the BAHC-COF, facilitating efficient ion occupation at storage sites. This synergy led to outstanding performance across multiple applications: the BAHCGO//AC ASC achieved a high energy output of 61.2 Wh $kg^{-1}$ with excellent long-term cycling stability, while the BAHCGO-based hybrid capacitive deionization (HCDI) system exhibited a high salt adsorption capacity of 67.5 mg $g^{-1}$ with remarkable long-term desalination and regeneration stability. Electrochemical characterization further demonstrated the superior performance of the BAHCGO-75//AC hybrid electrode system. CV curves (Fig. 15a) confirmed a combination of electric double-layer capacitance and pseudocapacitive behavior. The Nyquist plot revealed minimal charge-transfer resistance, while symmetrical GCD curves indicated excellent reversibility (Fig. 15b and c). The system achieved a maximum energy density of 61.2 Wh $kg^{-1}$ at a power density of 950 W $kg^{-1}$ and a high specific capacitance of 122.1 F $g^{-1}$ at 1 A $g^{-1}$ (Fig. 15d and e). Notably, after 10,000 charge-discharge cycles, the hybrid retained 89.4 % of its initial capacitance (Fig. 15 f), demonstrating exceptional durability [61].

Ibrahim et al. reported the ex-situ and in-situ (one-pot) synthesis of a triazine COF/graphene oxide (GO) nanocomposite [62]. These components undergo a straightforward carbonization process to form N-doped carbon (N-doped C)/reduced graphene oxide (rGO), which is utilized as an electrode material for SCs. Compared to the ex-situ method, N-doped C/rGO synthesized via the in-situ approach exhibits superior electrochemical performance. At a current density of 0.8 A $g^{-1}$, N-doped C/rGO in-situ achieves a specific capacitance of 234 F $g^{-1}$. A SSC device using N-doped C/rGO electrodes successfully powered a white LED bulb, demonstrating practical applicability. The device exhibited a high specific energy of 14.6 Wh·$kg^{-1}$ and a high specific power of 400 W $kg^{-1}$, with only a 14 % decrease in capacitance after 3500 cycles. Electrochemical characterization (Fig. 16) further validated the device's performance. CV measurements displayed quasi-rectangular curves at various scan rates (Fig. 16a), indicating ideal capacitive behavior, while GCD profiles demonstrated linear and symmetric characteristics across different current densities (Fig. 16b). Ragone plot analysis (Fig. 16c) highlighted an excellent energy-power trade-off, achieving an energy density of 14.3 Wh/kg at 0.5 A/g and sustaining performance up to 4800 W $kg^{-1}$ at 6 A/g. EIS revealed a reduction in equivalent series resistance after cycling, suggesting enhanced conductivity and improved ion transport kinetics (Fig. 16d). Long-term stability tests confirmed the device's durability, with 86 % capacitance retention over 3500 cycles (Fig. 16e). The practical viability of this SC device was further demonstrated by its ability to power a white LED lamp (Fig. 16f) [62].

The inherent conductivity of rGO facilitates electron transfer and ion migration, thereby enhancing electrochemical performance. By optimizing the content ratio of graphene and COF, Hu et al. synthesized two-dimensional COF (TpPa-$(OH)_2$) nanowires anchored on the surface of rGO (TpPa-$(OH)_2$/rGO) using a simple hydrothermal method in an

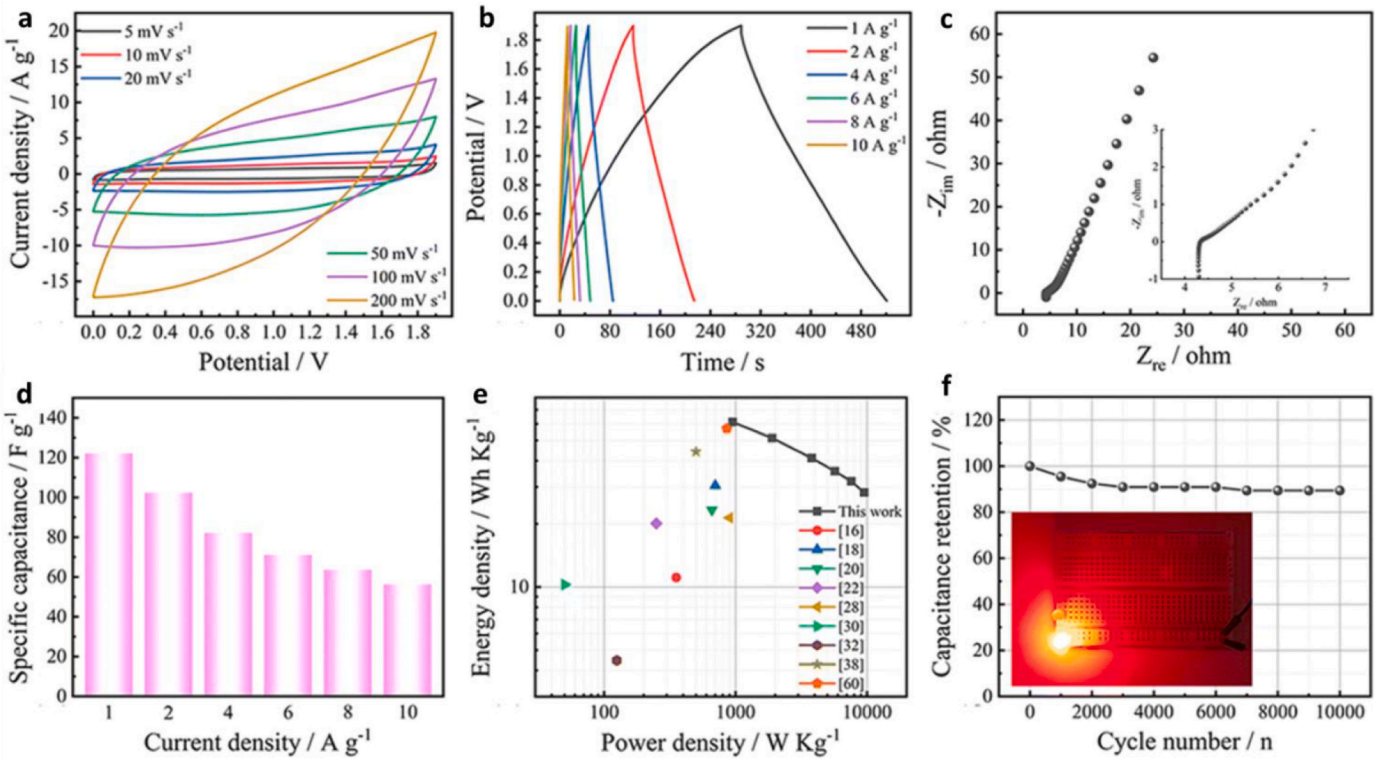


**Fig. 15.** BAHCGO-75//AC Device Performance: CV (a), GCD (b), EIS (c), Capacitance (d), Energy-Power Relations (e), and cycling with LED Test (f). Reproduced with permission from Ref. [61] Copyright 2024, Royal Society of Chemistry.

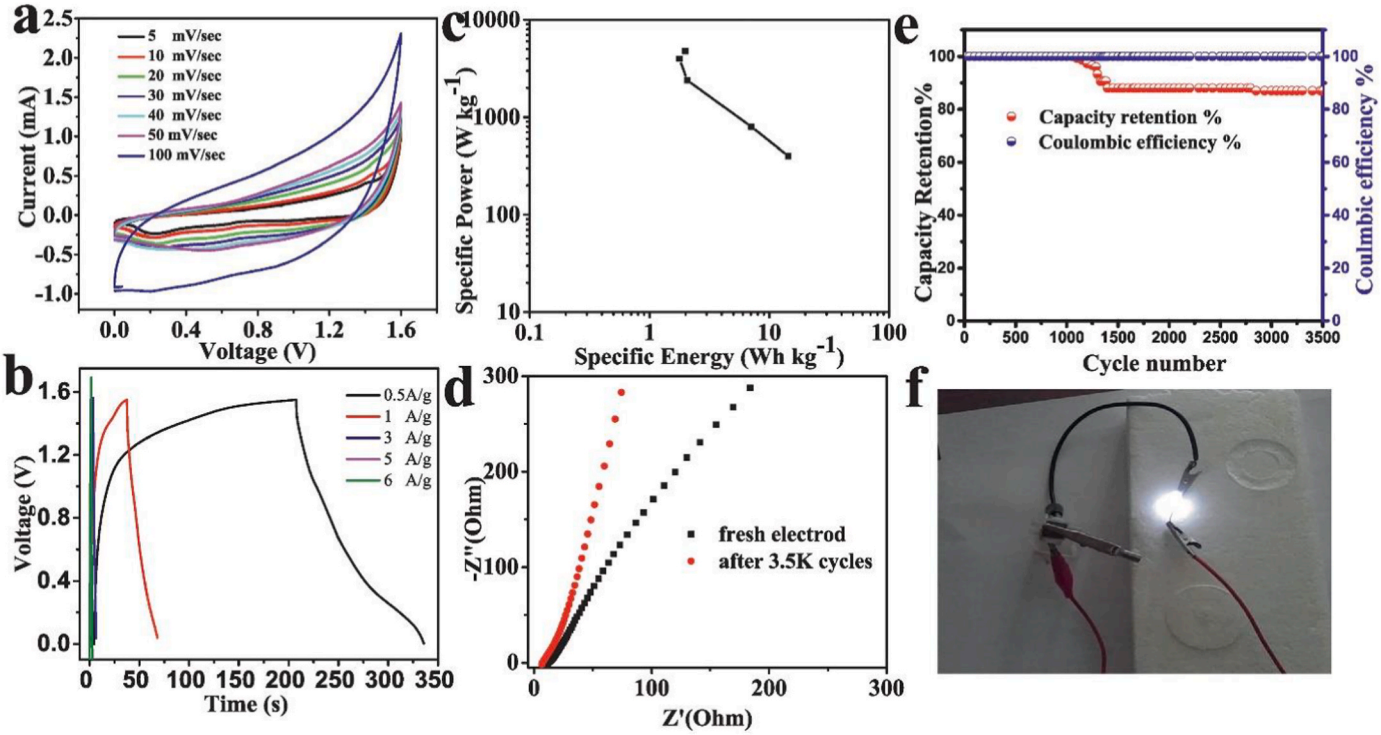


**Fig. 16.** Symmetric Device Performance: CV (a), GCD (b), Energy-Power Relations (c), EIS (d), Cycling Stability (e), and LED Demonstration (f)" Reproduced with permission from Ref. [62]. Copyright 2022, Elsevier.

aqueous solution [63]. The anchored COF nanowires effectively prevent graphene sheets from stacking, improving the electric double-layer capacitance of rGO while introducing additional pseudocapacitance from the redox-active COFs. The optimized TpPa-$(OH)_2$/rGO composite exhibits a well-defined COF nanowire structure anchored on graphene sheets and demonstrates outstanding electrochemical performance, achieving a high specific capacitance of 371.1 F $g^{-1}$ at 0.5 A/g and excellent cycling stability, retaining 93 % of its capacitance after 20,000

cycles at 10 A/g. Furthermore, SSCs assembled with TpPa-$(OH)_2$/rGO-3 achieved a specific capacitance of 197.1 F $g^{-1}$ at 0.2 A/g and delivered a maximum energy density of 16.6 Wh/kg at a power density of 158.7 W $kg^{-1}$ [63].

Sun et al. developed a hybrid nanomaterial featuring ultrathin COF-1 nanosheets oriented perpendicularly to the graphene surface. Benzene-1,4-diboronic acid (DBA) molecules, covalently attached to the GO surface in a vertical orientation, acted as nucleation agents, directing the vertical growth of COF-1 nanosheets. By adjusting the DBA loading, the thickness of the COF-1 nanosheets was precisely controlled, ranging from approximately 3 to 15 nm (spanning several to tens of COF-1 layers). Additionally, it was demonstrated that GO-2D COF hybrids could be converted into boron-doped carbon materials while preserving the unique geometry of their precursor nanostructures. The resulting v-CNS-RGO exhibited exceptional performance as an electrode material for SCs due to its distinctive nanostructure, which facilitated rapid electron transfer from the vertically aligned porous carbon nanosheets to the highly conductive RGO [64].

Yao et al. introduced an innovative strategy to enhance the electrical conductivity of AQ-containing COFs by incorporating rGO nanosheets. The in-situ synthesis of COF along the two-dimensional rGO surfaces facilitated extensive π-π intermolecular interactions within the resulting COF@rGO hybrid films. Notably, the COF matrix effectively prevented rGO nanosheet aggregation, thereby optimizing electrolyte ion transport pathways. The optimized COF@rGO composite film exhibited an outstanding specific capacitance of 451.96 F $g^{-1}$, marking a significant advancement in COF-based electrode materials. The fabricated planar COF@rGO microsupercapacitor (COF@rGO-MSC) demonstrated exceptional electrochemical performance, including a wide operating voltage window (2.5 V), high energy density (44.22 Wh $kg^{-1}$), and excellent structural integrity [65].

Binary and ternary nanocomposites have been successfully explored as electrode materials for energy storage applications. Verma et al. reported the synthesis of a ternary GO/CNT/COF nanocomposite through a simple chemical process, resulting in a novel hybrid material [51]. The effects of varying weight percentages of GO and CNT at a fixed COF ratio were optimized for enhanced electrochemical performance using a central composite design and analyzed via response surface methodology. The optimized ternary GO/CNT/COF electrode (with a composition of 2.4:2.1:1) exhibited excellent electrochemical properties, including a low charge-transfer resistance (Rct) of ~11.34 Ω, a high specific capacitance of 544.91 F $g^{-1}$ at 1 mV $s^{-1}$ and 175.09 F $g^{-1}$ at 1 A/g, as well as outstanding cycling stability, retaining 84.76 % of its capacitance after 8000 cycles. The SSC assembled with this material delivered a specific energy of 24.31 Wh/kg and a specific power of 248.95 W $kg^{-1}$, demonstrating its potential for high-performance energy storage applications [66].

According to Dong et al., a COF/carbon composite foam was meticulously synthesized by directly incorporating COF crystallites onto the surface of a carbon network through the Schiff base reaction, achieving a strong integration of the two phases. The 3D architecture's interconnected carbon skeleton ensures rapid electron transport, enhanced mechanical properties, high compressibility, and excellent fatigue resistance (with almost 100 % retention after 50 cycles at 70 % strain). Moreover, the COF decoration offers abundant active sites and contributes to a more porous structure. The resulting COF/carbon composite foam serves as a self-supported electrode in SC devices, demonstrating superior cycling stability with nearly 100 % capacitance retention after 20,000 cycles at 10 A $g^{-1}$. The material exhibits a high capacitance of 129.2 F $g^{-1}$ at 0.5 A $g^{-1}$ [67].

Redox-active COFs were embedded onto carbon fiber surfaces (AC-COFs) by Yuanyuan He et al. through strong covalent bonding. The strategic integration of DAAQ pillars on the carbon fiber surface enabled precise control over the direction of COF growth [52]. This resulted in a vertically aligned, tentacle-like architecture that facilitated efficient charge transfer while preventing COF aggregation and structural collapse. The synergistic effects of strong covalent coupling and improved accessibility to active sites led to an exceptional areal capacitance of 1034 mF $cm^{-2}$ for the AC-COFs electrode. Notably, the COF-based flexible electrode demonstrated excellent cycling stability, maintaining 98 % of its initial capacitance after 20,000 charge-discharge cycles. A flexible all-solid-state SSC was fabricated using a PVA/$H_2SO_4$ gel electrolyte, achieving an impressive areal capacitance of 715 mF $cm^{-2}$. The performance of the flexible solid-state supercapacitor (FSSC) was validated through extensive electrochemical testing (Fig. 17). The device's mechanical resilience was confirmed by its stable performance under mechanical deformation up to a 180° bending angle (Fig. 17c) and its optimal electrochemical behavior within a 1.4 V potential window (Fig. 17b). Ideal capacitive behavior was demonstrated by the linear and symmetrical characteristics of the GCD curves as shown in (Fig. 17d), which presents the specific capacitance of the AC-COFs//AC-COFs device as a function of current density (0.5–7 mA $cm^{-2}$) in a solid-state configuration with gel electrolyte, with the voltage almost linear with time and the curve close to a symmetrical triangle, indicating relatively ideal specific capacitance characteristics, and specific capacities of 715 mF $cm^{-2}$ at 0.5 mA $cm^{-2}$ and 552 mF $cm^{-2}$ at 7 mA $cm^{-2}$. Long-term stability testing showed 87 % capacitance retention after 20,000 cycles at 5 mA $cm^{-2}$ (Fig. 17f), while rate capability studies detailed in Fig. 17e, demonstrated 77 % retention of areal capacitance when the current density was increased to 7 mA $cm^{-2}$, according to the discharge curves of the AC-COFs//AC-COFs FSSC, with the inset highlighting the cycling stability over 20,000 charge-discharge cycles at 1 mA $cm^{-2}$, retaining 85.3 % of its initial capacitance and including galvanostatic charge-discharge curves at selected cycles to illustrate electrochemical reversibility, indicating rapid charge migration and ion diffusion of the electrodes. The practical utility of the device was demonstrated by successful LED operation in both planar and bent configurations. Additionally, the FSSC exhibited scalable performance when arranged in series and parallel configurations (Fig. 17g–h) [68].

Zhao et al. reported the preparation of COF-templated ordered nanoporous C60 ([C60]XeCOF) for high-performance SCs for the first time [4]. The resulting [C60]X-COFs exhibit excellent electrochemical performance. An ASC device ([C60]0.05-COF//rGO ASC), based on the ordered porous C60, optimizes the operating voltage window to 1.8 V, delivering an impressive energy density of 21.4 Wh/kg at a power density of 900 W $kg^{-1}$ (with a slight decrease in energy density to 16.7 Wh/kg at a power density of 7200 W $kg^{-1}$). The assembled ASC device successfully illuminated a red LED light for 70 s, demonstrating its promising potential for future energy storage applications [4].

Martín-Illán et al. reported an efficient method for monomer exchange from imine to partially β-ketoenamine-linked COFs within the gel phase [53]. The resulting aerogels were successfully converted into electrodes using a compression technique. These flexible electrodes, based on β-ketoenamine-linked COF composites with conductive carbon (Super P), exhibited superior durability and redox activity compared to their imine-based counterparts. In SC assemblies, the β-ketoenamine--linked COF electrodes demonstrated enhanced performance, achieving a higher capacitance of 88 mF $cm^{-2}$ and improved stability at high current densities (2.0 mA $cm^{-2}$) [69].

Sun et al. designed and synthesized a series of functionalized graphene/COF composites via a facile one-pot solvothermal method. The synthesis involved chemical grafting of tetraphenylethylene-based COF (TTPE-COF) with nearly pure carbon framework onto the surface of aniline-functionalized graphene oxide (a-GO), yielding a-rGO@TTPE-COF composites. Comprehensive structural characterization and electrochemical performance evaluation of these composites revealed that a-rGO@TTPE-COF-3 exhibited superior electrochemical properties as capacitive electrode materials. At a current density of 1.0 A $g^{-1}$, a-rGO@TTPE-COF-3 demonstrated a specific capacitance of 139 F $g^{-1}$, representing a 20 % enhancement compared to pristine a-rGO (116 F $g^{-1}$) and significantly outperforming the original TTPE-COF (5.0 F $g^{-1}$). Furthermore, a-rGO@TTPE-COF-3 displayed excellent cycling stability,

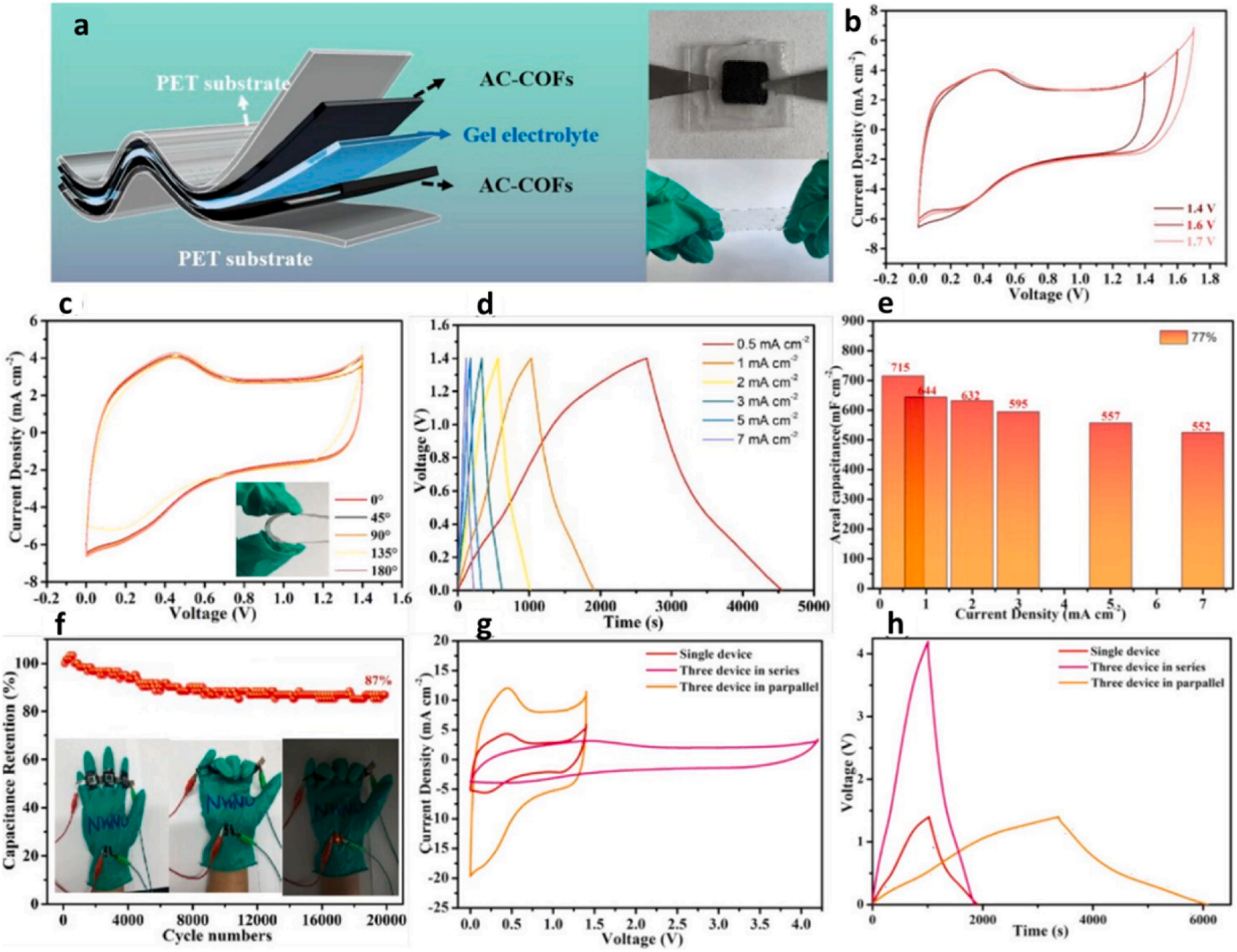


**Fig. 17.** Flexible AC-COF-Based Solid-State SCs: device schematic (a), CV (b), CV curves under bending (c), GCD (d),areal capacitance vs. current density (e), cycling stability with LED demonstration (inset) (f), CV and GCD curves for single vs. series/parallel configurations (g–h). Reproduced with permission from Ref. [68]. Copyright 2022, American Chemical Society.

maintaining 93.0 % of its initial capacitance after 5000 charge-discharge cycles. When assembled into a symmetric SC configuration, a-rGO@TTPE-COF-3 electrodes delivered an energy density of 8.3 Wh $kg^{-1}$ at a power density of 1799.5 W $kg^{-1}$, demonstrating its potential for energy storage applications [70].

Yang et al. reported the synthesis of a composite material combining a COF with reduced graphene oxide (HcDa-COF/rGO). The COF was prepared using hexachlorotriphosphonitrile (HCCP) and DAAQ as monomers, with reduced graphene oxide (rGO) serving as a conductive substrate. The resulting HcDa-COF/rGO composite material exhibited exceptional capacitive performance. the synthesized composite electrode demonstrated a superior specific capacitance of 834.12 F $g^{-1}$ at a current density of 1 A $g^{-1}$. Furthermore, the electrode material retained 58.8 % of its initial specific capacitance when operated at a high current density of 30 A $g^{-1}$, indicating excellent rate capability. The researchers also fabricated an asymmetric SC device using HcDa-COF/rGO as the negative electrode and 2,3-dicarboxylic acid quinoline/N-P-graphene hydrogel (QDC/N-P-GH) as the positive electrode. This asymmetric device delivered a specific capacitance of 70.35 F $g^{-1}$ at 1 A $g^{-1}$ and achieved an energy density of 28.24 Wh $kg^{-1}$ at a power density of 854.32 W $kg^{-1}$ [71].

Khan et al. reported the solvent-free in situ synthesis of a redox-active COF (DAAQ-TFP COF) grown directly on the surface of expanded graphite (EG). The expanded graphite not only enhanced electrical conductivity but also effectively regulated the pore size distribution of the COF. This optimized hierarchical structure proved highly conducive to enhancing the electrochemical performance of the electrode material. Electrochemical characterization showed that the EG@COF-3 composite achieved a specific capacitance of 351 C $g^{-1}$ at a current density of 1 A $g^{-1}$, while maintaining excellent cycling stability with 94.4 % capacitance retention after 10,000 charge-discharge cycles. This exceptional capacitance retention was attributed to the inherently stable molecular backbone of the COF. Additionally, an ASC device fabricated using AC as the negative electrode and EG@COF as the positive electrode delivered an energy density of 16.4 Wh $kg^{-1}$ at a power density of 806.0 W $kg^{-1}$ [72].

Table 4 demonstrates the synergistic enhancement achieved through carbon/COF composite formation, with specific capacitances ranging from 63.1 to 834.12 F $g^{-1}$, significantly surpassing many pure COF materials and highlighting the effectiveness of hybridization strategies for SC electrode optimization. The HcDa-COF/rGO composite exhibited exceptional performance with 834.12 F $g^{-1}$ at 1.0 A $g^{-1}$, demonstrating how the integration of AQ-functionalized COFs with reduced graphene oxide creates an optimal balance between redox activity and electronic conductivity. Carbon nanotube (CNT) incorporation proved particularly effective, with CNT@TFA-COF-3, CNT@HATN-COF-0.6, and various

**Table 4**
Selected properties of Carbon/COF Composites for SCs.

| Materials | Redox group | Electrolyte | Potential window | Specific capacitance | Current density | Capacitance retention | Ref |
|---|---|---|---|---|---|---|---|
| [C60]0.09-COFs | triazole | 1 M $Na_2SO_4$ | 0 to 0.5 V | 63.1 F $g^{-1}$ | 0.7 A $g^{-1}$ | 90.6 % after 5000 cycles | [4] |
| CNT@TFA-COF-3 | triazine | 1 M $H_2SO_4$ | 0 to 0.8 V | 338 F $g^{-1}$ | 1.0 A $g^{-1}$ | after 7000 cycles | [10] |
| NKCOF-8 | azo | 2 M $H_2SO_4$ | 0 to 0.8 V | 440 $Fg^{-1}$ | 0.5 A $g^{-1}$ | 90 % after 10000 cycles. | [16] |
| TPDA-COF | Triazine | 6 M KOH | 0.25 to 0.5 | 640.4 F $g^{-1}$ | 5 mV $s^{-1.}$ | 81.54 % after 10000 cycles. | [18] |
| TPTP-COF | Triazine | 6 M KOH | 0.25 to 0.5 | 577.44 F $g^{-1}$ | 5 mV $s^{-1.}$ | 78.60 % after 10000 cycles. | [18] |
| PAI@40 % CNT | Imide | 1 M $Na_2SO_4$ | −1.0 to 0 V | 278 F $g^{-1}$ | 0.5 A $g^{-1}$ | 96 % after 4400 cycles | [56] |
| SWCNTs-TpPaCOFs | ketoenamine | 1 M $H_2SO_4$ | 0 to 0.5 V | 153 F $g^{-1}$ | 0.5 A $g^{-1}$ | >110 % after 2000 cycles | [57] |
| pHANT@10%CNT | Polyimide | 1 M $Na_2SO_4$ | −1.0 to −0.2 V | 366 F $g^{-1}$ | 0.5 A $g^{-1}$ | 86 % after 5000 cycles | [58] |
| CNT@HATN-COF-0.6 | hexaazatriphenylene | 1 M KOH | −0.8 to 0.2 V | 436 F $g^{-1}$ | 2.0 A $g^{-1}$ | 100 % after 10,000 cycles | [59] |
| TFPDQGO-75 | Anthraquinnone | 1 M NaCl | −1.2 to 0 V | 429.0 F $g^{-1}$ | 2 mV s-1 | 80.6 % after 10000 cycles. | [60] |
| TpPa-(OH)2/rGO | benzoquinone | 1 M $H_2SO_4$ | −0.5 to 0.5 V | 371.1 F $g^{-1}$ | 0.5 A $g^{-1}$ | 93 % after 20,000 cycles | [63] |
| N-doped C/rGO | Triazine | 6 M KOH | 0.2 to 0.6 V | 234 F $g^{-1}$ | 0.8 A $g^{-1}$ | 86 % after 3500 cycles | [62] |
| BAHCGO-75 | Pyrazine | 1 M NaCl | −0.8 to 0.6 V | 380.8 F $g^{-1}$ | 2 mV $s^{-1}$ | 83.2 % after 10000 cycles. | [61] |
| v-CNS-RGO | Boroxine | 6 M KOH | 0 to 1.0 V | >160 F $g^{-1}$ | 2.0 A $g^{-1}$ | 100 % after 3000 cycles | [64] |
| COF@rGO | Anthraquinnone | 1 M $H_2SO_4$ | −0.3 to 0.7 V | 451.96 F $g^{-1}$ | 0.2 A $g^{-1}$ | 94.02 % after 10000 cycles | [65] |
| GO/CNT/COF | $CoFe_2O_4$ | 1 M $H_2SO_4$ | 0 to 0.8 V | 544.91 F $g^{-1}$ | 1 mV $s^{-1}$ | 84.76 % after 8000 cycles | [66] |
| DAB/GCF | Quinone | 1 M $H_2SO_4$ | 0 to 0.8 V | 129.2 F $g^{-1}$ | 0.5 A $g^{-1}$ | 100 % after 20000 cycles | [67] |
| AC-COFs | Anthraquinnone | 1 M $H_2SO_4$ | −0.4 to 0.5 V | 397.7 F $g^{-1}$ | 1 mA $cm^{-2}$ | 98 % after 20000 cycles | [68] |
| ECOF-3 | Ketoenamine | 1M $TBABF_4$ | 0 to 4.6 V | 82 mF $cm^{-2}$ | 2 mA $cm^{-2}$ | 100 % after 10,000 cycles | [69] |
| a-rGO@TTPE-COF-3 | imine bonds | 1 M $H_2SO_4$ | −0.2 to 0.6 V | 139 F $g^{-1}$ | 1.0 A $g^{-1}$ | 92.3 % after 5000 cycles | [70] |
| HcDa-COF/rGO | Anthraquinone | 1 M $H_2SO_4$ | 0 to 0.8 V | 834.12 F $g^{-1}$ | 1.0 A $g^{-1}$ | 88.46 % after 10,000 cycles | [71] |
| EG@COF-3 | Anthraquinone | 6 M KOH | −1 to 0.3 V | 351 C $g^{-1}$ | 1.0A $g^{-1}$ | 94.4 % after 10,000 cycles | [72] |

CNT-based composites achieving capacitances between 338 and 436 F $g^{-1}$, while maintaining good rate capability at current densities up to 2 A $g^{-1}$, addressing the conductivity limitations observed in pure COF systems. The choice of redox-active groups significantly influenced performance, with AQ-based composites (COF@rGO: 451.96 F $g^{-1}$, AC-COFs: 397.7 F $g^{-1}$, TFPDQGO-75: 429.0 F $g^{-1}$) consistently delivering high capacitances due to the reversible quinone/hydroquinone redox chemistry, while triazine-based composites showed moderate to high performance depending on the carbon support structure. Electrolyte compatibility varied across composites, with 6 M KOH enabling the highest capacitances for TPDA-COF (640.4 F $g^{-1}$) and TPTP-COF (577.44 F $g^{-1}$), though these measurements were conducted at low scan rates (5 mV $s^{-1}$), while $H_2SO_4$-based systems demonstrated more consistent performance across different current densities. Cycling stability generally improved compared to pure COFs, with most composites maintaining 80–100 % capacitance retention after extensive cycling (up

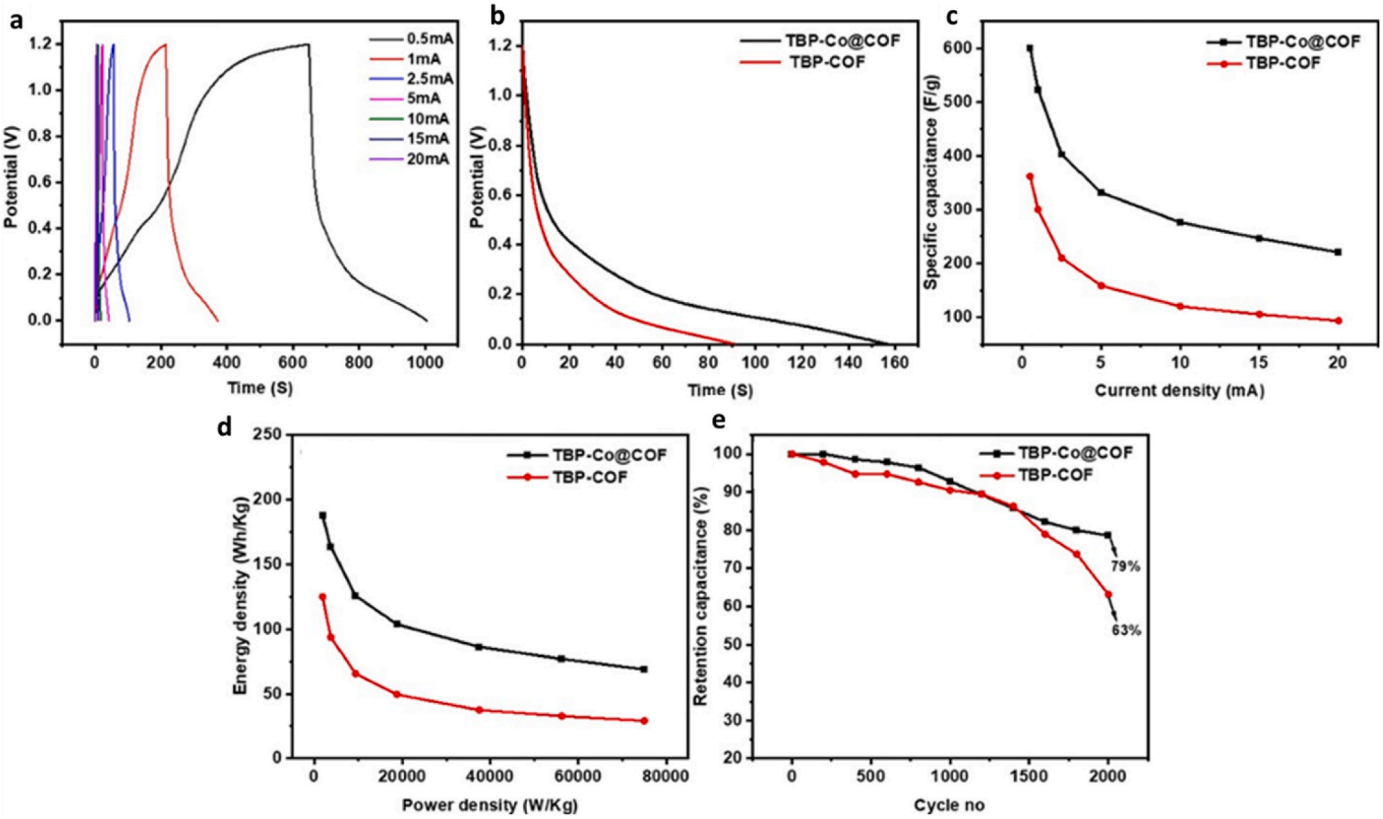


**Fig. 18.** Comparative Performance of TBP-Co@COF vs TBP-COF: GCD curves for TBP-Co@COF (a), discharge curve comparison (b), specific capacitance vs. current density (c), energy/power density comparison (d), and cycling stability over 2000 cycles for TBP-Co@COF and TBP-COF electrodes (e). Reproduced with permission from Ref. [73]. Copyright 2024, Elsevier.

to 20,000 cycles), and several materials (SWCNTs-TpPaCOFs, CNT @HATN-COF-0.6, v-CNS-RGO, DAB/GCF, ECOF-3) showing remarkable stability with ≥100 % retention, indicating potential activation effects during electrochemical cycling.

### 5.2. Metal/COF composites

The selection of stable and efficient electrode materials is critical for developing high-performance SCs. In this regard, inorganic layered structures have emerged as promising candidates for energy storage applications due to their excellent charge mobility and intrinsic bandgap properties. Shanavaz et al. successfully synthesized two-dimensional COFs, specifically TBP-COF and its cobalt-doped derivative (TBP-Co@COF), using a solvothermal method in sealed Pyrex vessels [73]. Electrochemical characterization demonstrated the superior performance of TBP-Co@COF, which achieved a specific capacitance of 975 F $g^{-1}$ at 2 mV $s^{-1}$, significantly surpassing the undoped TBP-COF (827 F $g^{-1}$). The cobalt-doped framework exhibited exceptional energy storage capabilities, delivering an energy density of 69 Wh $kg^{-1}$ alongside an impressive power density of 75,000 W $kg^{-1}$. Long-term stability analysis confirmed 79 % capacitance retention after 2000 charge-discharge cycles. An ASC device fabricated with TBP-COF and TBP-Co@COF electrodes achieved a specific capacitance of 191 F $g^{-1}$ at 2 mV $s^{-1}$. Comprehensive electrochemical characterization (Fig. 18) further confirmed the enhanced performance of TBP-Co@COF compared to its undoped counterpart. The GCD profiles of TBP-Co@COF (Fig. 18a) displayed symmetrical characteristics, indicating reversible charge storage mechanisms and high coulombic efficiency. Comparative discharge analysis (Fig. 18b) revealed longer discharge durations for TBP-Co@COF, supporting its superior capacitive behavior. Rate capability studies (Fig. 18c) consistently showed higher specific capacitance for TBP-Co@COF across all current densities, while both materials exhibited typical rate-dependent capacitance behavior. Additionally, Ragone plot analysis (Fig. 18d) highlighted the favorable energy-power characteristics of TBP-Co@COF for high-performance energy storage applications. Finally, cycling stability assessment (Fig. 18e) confirmed its superior durability, with approximately 79 % of the initial capacitance retained after 2000 cycles [73].

Shanavaz et al. developed a TCOF via Schiff base formation, employing a polycondensation reaction between MA and terephthalaldehyde [6]. To enhance electrochemical performance, they also synthesized a niobium-doped variant (Nb@COF). In a three-electrode system, Nb@COF exhibited a significantly higher specific capacitance of 367 F $g^{-1}$ compared to the pure COF (244 F $g^{-1}$) at 2 mV $s^{-1}$, likely due to increased porosity and interlayer spacing. Both materials demonstrated excellent cycling stability; after 5000 cycles, Nb@COF retained 89 % of its initial capacitance, outperforming the pure COF, which retained 82 %. A coin cell incorporating COF and Nb@COF as electrodes resulted in an ASC device with a specific capacitance of 87 F $g^{-1}$ at 2 mV $s^{-1}$ [6].

Potassium-ion hybrid capacitors (PIHCs) have emerged as a highly promising energy storage system. Li et al. reported the synthesis of a composite material consisting of $Bi_2S_3$ nanoparticles in situ confined within a sulfur-doped COF and combined with graphene ($Bi_2S_3$@SCOF/G). Due to the synergistic effect of COF's structural stability, which buffers large mechanical stresses, and graphene's high electronic conductivity, the $Bi_2S_3$@SCOF/G anode demonstrated a high reversible capacity of 503.8 mAh $g^{-1}$ at 100 mA $g^{-1}$ after 100 cycles. It also exhibited excellent rate performance, maintaining a capacity of 223.9 mAh $g^{-1}$ even at 5000 mA $g^{-1}$ [74].

Liu et al. synthesized $Al_2O_3$@DHTA-COF composites by in situ growing a highly crystalline TCOF (DHTA-COF) on a modified θ-$Al_2O_3$ substrate. These composites exhibited partial retention of crystallinity, structural stability, and a vesicular morphology. Electrochemical characterization demonstrated superior capacitive properties of the 50 % $Al_2O_3$@DHTA-COF composite compared to its precursors, θ-$Al_2O_3$ and DHTA-COF, when evaluated as electrode materials for SCs. In the same experimental setup, the 50 % $Al_2O_3$@DHTA-COF composite achieved a specific capacitance of 261.5 F $g^{-1}$ at 0.5 A $g^{-1}$, which was 6.2 and 9.6 times higher than that of DHTA-COF and δ-$Al_2O_3$–CHO, respectively. Furthermore, after 6000 charge-discharge cycles, the 50 % $Al_2O_3$@DHTA-COF electrode demonstrated remarkable cycling stability [9].

Shanavaz et al. reported the synthesis of an imine-linked COF using 4,4′,4″,4‴-(ethene-1,1,2,2-tetrayl)tetraaniline and terephthalaldehyde as precursors through a solvothermal method, designated as TAT-COF. Additionally, they successfully incorporated cobalt into the imine linkages of TAT-COF to generate Co@TAT-COF. Both TAT-COF and Co@TAT-COF were evaluated for their electrochemical performance in SC applications. Co@TAT-COF exhibited a two-fold higher specific capacitance (637 F $g^{-1}$) compared to pristine TAT-COF (315 F $g^{-1}$) at a scan rate of 5 mV $s^{-1}$. The Co@TAT-COF demonstrated an energy density of 58 Wh $kg^{-1}$ at a power density of 1500 W $kg^{-1}$. The enhanced electrochemical performance of Co@TAT-COF can be attributed to structural confinement, improved conductivity, increased interlayer spacing, and enhanced porosity. Furthermore, Co@TAT-COF was employed as a positive electrode in the fabrication of an asymmetric device (ASD) using a Swagelok cell configuration. The ASD exhibited a specific capacitance of 95 F $g^{-1}$ at a scan rate of 2 mV $s^{-1}$ and demonstrated good cycling stability with 73 % capacitance retention after 5000 charge/discharge cycles [75].

Khatri et al. reported the facile synthesis of hexaminephenylenediamine (HPd) COF and three COF/metal oxide composites—HPd/$MoO_2$, HPd/NiO, and HPd/ZnO—using a one-step hydrothermal method. Electrochemical investigation of these materials revealed specific capacitances of 181.1, 177.4, and 394.3 F $g^{-1}$ for HPd/$MoO_2$, HPd/NiO, and HPd/ZnO, respectively, at a current density of 0.5 A $g^{-1}$. Among the synthesized composites, HPd/ZnO exhibited the highest specific energy of 39.43 Wh $kg^{-1}$ at 0.5 A $g^{-1}$, demonstrating its superior energy storage capabilities [76].

Table 5 presents metal/COF composites as electrode materials for SCs, demonstrating specific capacitances ranging from 261.5 to 975 F $g^{-1}$, with the incorporation of redox-active metals providing additional pseudocapacitive contributions beyond the intrinsic COF redox chemistry. The TBP-Co@COF composite achieved the highest specific capacitance of 975 F $g^{-1}$ at 2 mV $s^{-1}$ in 0.1 M $H_2SO_4$, highlighting the exceptional pseudocapacitive behavior of cobalt species, though this outstanding performance came at the expense of cycling stability with only 79 % retention after 2000 cycles, indicating potential structural degradation or active material dissolution during prolonged electrochemical cycling. Cobalt-based composites consistently showed high capacitances (Co@TAT-COF: 637 F $g^{-1}$), confirming the effectiveness of cobalt's multiple oxidation states for charge storage, while other metal incorporations such as niobium (Nb@COF: 367 F $g^{-1}$) and aluminum oxide (50%$Al_2O_3$@DHTA-COF: 261.5 F $g^{-1}$) provided more moderate enhancements with improved stability profiles. The $Bi_2S_3$@SCOF/G composite represents a unique approach with battery-type behavior, delivering 518.1 mAh $g^{-1}$ over a wide potential window (0.01–3.0 V) in organic electrolyte (1 M $KPF_6$), though the lower cycling stability (80.4 % after 500 cycles) suggests challenges in maintaining structural integrity during the intercalation/deintercalation processes. Cycling stability generally decreased compared to pure COFs and carbon/COF composites, with most materials showing 70–90 % retention, except for the HPd/ZnO composite which demonstrated exceptional stability (98 % after 15,000 cycles) while maintaining reasonable capacitance (394.3 F $g^{-1}$), suggesting that zinc oxide integration provides both pseudocapacitive enhancement and structural reinforcement.

### 5.3. MXenes/COF composite

MXenes are a novel class of two-dimensional layered materials composed of transition metal carbides, nitrides, and carbonitrides.

**Table 5**
Selected properties of Metal/COF Composites for SCs.

| Materials | Redox group | Electrolyte | Potential window | Specific capacitance | Current density | Capacitance retention | Ref |
|---|---|---|---|---|---|---|---|
| Nb@COF | Triazine, Nb | 1 M $H_2SO_4$ | 0.1 to 1.2 V | 367 F $g^{-1}$ | 2 mV $s^{-1}$ | 89 % after 5000 cycles | [6] |
| 50%$Al_2O_3$@DHTA-COF | Triazine, $Al_2O_3$ | 1 M $H_2SO_4$ | 0 to 1.0 V | 261.5 F $g^{-1}$ | 0.5 A $g^{-1}$ | 92 % after 6000 cycles. | [9] |
| TBP-Co@COF | Cobalt | 0.1 M $H_2SO_4$ | 0 to 1.2 V | 975 F $g^{-1}$ | 2 mV $s^{-1}$ | 79 % after 2000 cycles. | [73] |
| $Bi_2S_3$@SCOF/G | $Bi_2S_3$ | 1 M $KPF_6$ | 0.01 to 3.0 V | 518.1 mAh $g^{-1}$ | 100 mA $g^{-1}$ | 80.4 % after 500 cycles | [74] |
| Co@TAT-COF | Cobalt | 1 M $H_2SO_4$ | 0 to 1.2 V | 637 F $g^{-1}$ | 5 mV $s^{-1}$ | 73 % after 5000 cycles | [75] |
| HPd/ZnO | ZnO | 6 M KOH | 0 to 1.5 V | 394.3 F $g^{-1}$ | 0.5 A $g^{-1}$ | 98 % after 15,000 cycles | [76] |

These materials possess exceptional properties, making them highly suitable as platforms or building blocks for fabricating films with engineered microstructures. Their unique combination of high electrical conductivity, hydrophilicity, and diverse surface chemistries enables precise property tailoring for specific applications [77].

An et al. reported the fabrication of flexible carbonyl-containing COF/MXene composite film electrodes (CMFs) using a cation-driven self-assembly approach [20]. Electrostatic interactions between negatively charged 2D MXene nanosheets and protonated DAAQ-COFs facilitated the homogeneous intercalation of porous COFs within the layered MXene structure. The resulting CMF electrode, evaluated in a three-electrode system, exhibited remarkable mechanical strength (withstanding 100 repeated bending cycles), excellent kinetic energy storage characteristics (96.7 % capacitive contribution at 50 mV $s^{-1}$), and outstanding electrochemical performance (390 F $g^{-1}$ at 0.5 A $g^{-1}$). CMFs//CCMP ASCs were further assembled into all-solid-state flexible SCs, demonstrating a maximum power density of 7000 W $kg^{-1}$ at an energy density of 19.7 Wh $kg^{-1}$ and a maximum energy density of 27.5 Wh $kg^{-1}$ at a power density of 350 W $kg^{-1}$. Additionally, the ASC retained an ultrahigh capacitance of 88.9 % after 20,000 charge-discharge cycles, highlighting its strong potential for flexible and wearable energy storage applications [20].

Zhu et al. reported the fabrication of a hierarchically ordered hybrid fiber by integrating interstratified electroactive COF LZU1 (COF-LZU1)

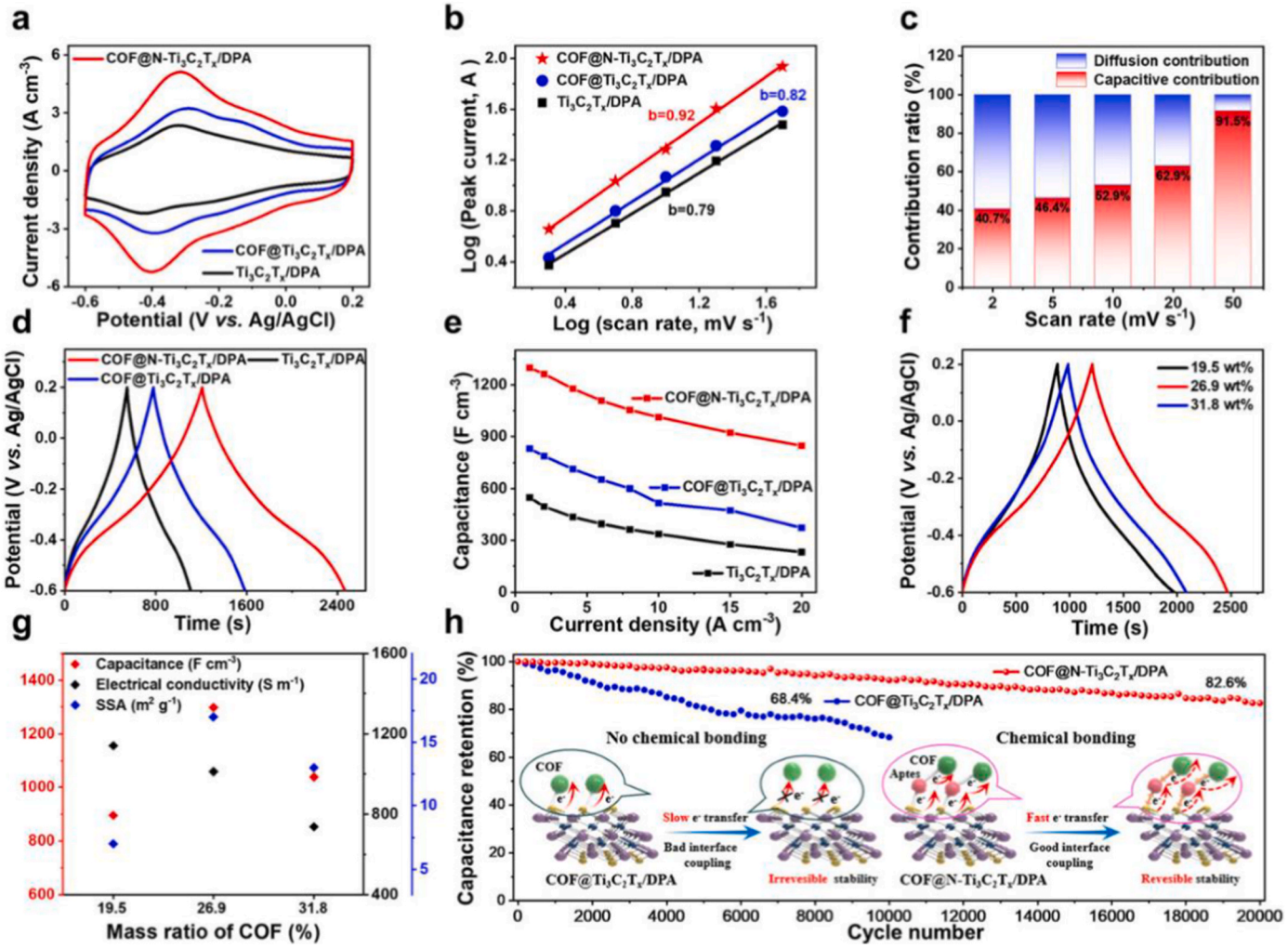


**Fig. 19.** Comparative Electrochemical Analysis of $Ti_3C_2Tx$/DPA Systems: CV (a); Relationship between peak current density and sweep rate (b); Capacitance contributions (c); GCD (d) and Specific capacitances of $Ti_3C_2T_x$/DPA, COF@$Ti_3C_2T_x$/DPA and COF@N-$Ti_3C_2T_x$/DPA (e). f) GCD curves and g) The relationship between mass ratios of COF, capacitance, SSA and electrical conductivity. h) Cycle stability of COF@$Ti_3C_2T_x$/DPA and COF@N-$Ti_3C_2T_x$/DPA at 20 A $cm^{-3}$. Inset: schematic diagram of electron transfer of COF@$Ti_3C_2T_x$/DPA and COF@N-$Ti_3C_2T_x$/DPA. Reproduced with permission from Ref. [79]. Copyright 2023, John Wiley & Sons - Books.

with vertically aligned and conductive $Ti_3C_2T_x$ MXene (VA-$Ti_3C_2T_x$) through a one-step microfluidic synthesis. The resulting VA-$Ti_3C_2T_x$@-COF-LZU1 fibers exhibited an abundance of redox-active sites, vertical channels, and a large accessible surface area across the electrode, contributing to an outstanding gravimetric capacitance of 787 F $g^{-1}$ in a three-electrode system. Furthermore, solid-state asymmetric fiber SCs constructed with these hybrid fibers demonstrated remarkable performance, including an energy density of 27 Wh $kg^{-1}$, a capacitance of 398 F $g^{-1}$, and an extended cycling life of 20,000 cycles [78].

Feng et al. developed high-performance deformable SCs using COF@amino-modified $Ti_3C_2T_x$ deposited on a decorated nylon 6 (DPA) film (COF@N-$Ti_3C_2T_x$/DPA) via a layer-by-layer fabrication process [79]. The hierarchical COF@N-$Ti_3C_2T_x$/DPA structure exhibited excellent specific capacitance, rate performance, and cycling stability in a three-electrode system. These superior characteristics were attributed to enhanced $H^+$ storage properties and efficient interfacial charge transfer, as supported by density functional theory calculations. The solid-state deformable SCs demonstrated outstanding mechanical resilience, retaining 80.7 %, 80.6 %, and 83.4 % of their initial capacitance after 5000 bending cycles, 2000 stretching cycles, and 5000 folding cycles, respectively (Fig. 19). further illustrates the superior electrochemical performance of COF@N-$Ti_3C_2T_x$/DPA electrodes. The CV curves (Fig. 19a) show a larger integral area for this composite compared to $Ti_3C_2T_x$/DPA and COF@$Ti_3C_2T_x$/DPA. The b-value of 0.92 (Fig. 19b) indicates a predominantly capacitive-controlled process, while at high sweep rates, the pseudocapacitance contribution exceeds 90 % (Fig. 19c). The GCD curves (Fig. 19d) demonstrate that COF@N--$Ti_3C_2T_x$/DPA exhibits longer charge-discharge time and more symmetric triangular shape compared to both COF@$Ti_3C_2T_x$/DPA and $Ti_3C_2T_x$/DPA, indicating enhanced capacitive behavior and superior electrochemical reversibility. The composite achieves a peak specific capacitance of 1298.3 F $cm^{-3}$ at 1 A $cm^{-3}$ (Fig. 19e), with the optimal COF content determined to be 26.9 wt% (Fig. 19f). Notably, the electrode retains 81.3 % of its capacitance after 20,000 cycles (Fig. 19h), significantly outperforming COF@$Ti_3C_2T_x$/DPA, which retains only 69.8 %. These results highlight the synergistic effect of COF incorporation and nitrogen doping in $Ti_3C_2T_x$ MXene, enabling superior electrochemical performance and mechanical durability. This combination underscores the potential of these materials for next-generation flexible and wearable energy storage applications [79].

Liu et al. reported the synthesis of two liquid-loaded COF composites (IL-COFs) with remarkable periodic molecular ordering, porosity, and well-defined pores [80]. These composites were created by loading an ionic liquid ([Emim]ESe) into TFPB-TAPT COF and BTA-TAPT COF. Among the synthesized IL-COFs, the [Emim]ESe-TFPB-TAPT COF exhibited outstanding electrochemical performance. It demonstrated excellent rate capability, with an initial specific capacitance of 521 F $g^{-1}$ at a current density of 1 A $g^{-1}$, sustaining 372 F $g^{-1}$ even at a high current density of 4 A $g^{-1}$. Additionally, this material outperformed many previously reported counterparts, retaining 76 % of its initial capacitance (396 F $g^{-1}$) after 5000 charge-discharge cycles [80].

Table 6 demonstrates the emerging potential of MXene/COF composites for SC applications, with these hybrid materials exhibiting exceptional capacitances up to 1298.3 F $cm^{-3}$ and remarkable rate capabilities, leveraging the high electronic conductivity and hydrophilic nature of MXenes combined with the tunable redox chemistry of COFs. The COF@N-$Ti_3C_2T_x$/DPA composite achieved the highest volumetric capacitance of 1298.3 F $cm^{-3}$ at 1 A $cm^{-3}$, demonstrating how nitrogen doping of the $Ti_3C_2T_x$ MXene surface enhances both pseudocapacitive contributions and interfacial interactions with the COF component, though this performance improvement came with reduced cycling stability (82.6 % after 20,000 cycles) compared to the non-doped counterpart. The VA-$Ti_3C_2T_x$@COF LZU1 composite exhibited outstanding rate performance with 787 F $g^{-1}$ maintained at the exceptionally high current density of 20 A $g^{-1}$, highlighting the superior electronic conductivity provided by the MXene framework that effectively addresses the inherent conductivity limitations of organic COF materials. All MXene/COF composites operated within a narrow potential window (−0.6 to 0.2 V or 0–1 V) in 1 M $H_2SO_4$, which is characteristic of MXene-based materials and limits their energy density potential compared to wider potential window systems, though this consistency suggests good electrochemical compatibility between MXene and COF components. Cycling stability presented challenges across most MXene/COF composites, with retention values ranging from 68.4 % to 89 % after 5000–20,000 cycles, indicating that while the integration provides enhanced conductivity and rate capability, the structural stability during prolonged cycling requires further optimization, possibly through improved interfacial bonding or protective coating strategies.

### 5.4. Polymer/COF composite

Growing porous and redox-active COFs on conductive organic polymers presents a promising strategy for developing a novel class of all-organic electrodes for energy storage applications. Wang et al. pioneered the synthesis of all-in-one hollow dioxin-based COF-316 microflowers, featuring interconnected hollow petals with diameters ranging from 5 to 7 μm [81]. This unique structure was achieved through a self-template technique, where inside-out Ostwald ripening, epitaxial growth, and nanoparticle self-assembly collectively governed the growth mechanism. By leveraging both "interior" and "exterior" functionalization, COF-316 seamlessly integrates with polypyrrole (PPy), taking advantage of its inherent porosity and interconnected hollow framework. During charge/discharge cycles, hydrogen bond interactions contribute to enhanced structural stability and charge transfer efficiency. As a result, the COF-316@PPy-based flexible transparent SCs exhibit excellent long-term cycling stability and deliver an areal specific capacitance of 783.6 μF $cm^{-2}$ at a current density of 3 μA $cm^{-2}$ [81].

The post-synthesis modification of COFs with conducting polymers can significantly enhance their electrical conductivity. Dutta et al. demonstrated this approach by synthesizing TCOFs modified with polyaniline (PANI) through in-situ polymerization of aniline within the porous frameworks [82]. The resulting composite materials exhibited remarkable electrical properties at room temperature, with high conductivity ranging from 1.4 to 1.9 × $10^{-2}$ S $cm^{-1}$ (Fig. 20). comprehensively illustrates the superior electrochemical performance of PANI@TCOF composites, particularly PANI@TCOF-2. These PANI-modified COFs demonstrated a specific capacitance approximately 20 times higher than that of the pristine frameworks. CV curves (Fig. 20a–c) reveal a combination of electric double-layer capacitance and pseudocapacitance, with distinct redox peaks corresponding to PANI transitions. GCD experiments (Fig. 20b–d) further confirm the enhanced capacitive behavior of PANI@TCOF-2, attributed to improved

**Table 6**
Selected properties of MXenes/COF Composite for SCs.

| Materials | Redox group | Electrolyte | Potential window | Specific capacitance | Current density | Capacitance retention | Ref |
|---|---|---|---|---|---|---|---|
| COF/MXene | Anthraquinone | 1.0 M $H_2SO_4$ | −0.6 to 0.2 V | 390 F $g^{-1}$ | 0.5 A/g | 88.9 % after 20,000 | [20] |
| VA-$Ti_3C_2Tx$@COF LZU1 | imine | 1.0 M $H_2SO_4$ | −0.6 to 0.2 V | 787 F $g^{-1}$ | 20 A $g^{-1}$ | 89 % after 20000 cycles | [78] |
| COF@N-$Ti_3C_2Tx$/DPA | Nitrogen sites | 1 M $H_2SO_4$ | −0.6 to 0.2 V | 1298.3 F $cm^{-2}$ | 1 A $cm^{-2}$ | 82.6 % after 20000 cycles | [79] |
| COF@$Ti_3C_2Tx$/DPA | Nitrogen sites | 1 M $H_2SO_4$ | −0.6 to 0.2 V | 548.7 F $cm^{-2}$ | 1 A $cm^{-2}$ | 68.4 % after 10000 cycles | [79] |
| [Emim]ESe-TFPB-TAPT COF | imine | 1 M $H_2SO_4$ | 0 to 1.0 V | 521 F $g^{-1}$ | 1 A $g^{-1}$ | 76 % after 5000 cycles | [80] |

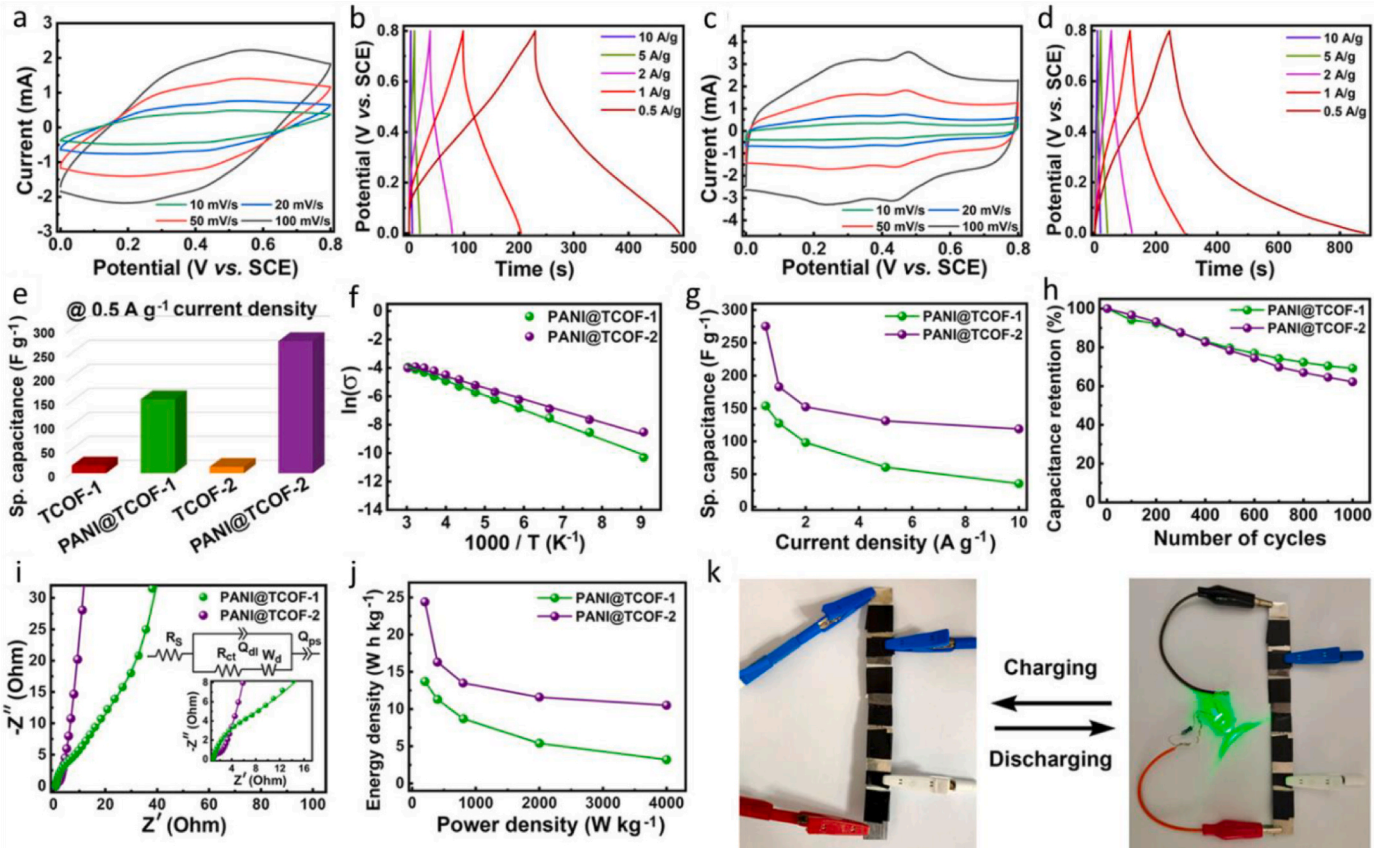


**Fig. 20.** Cyclic voltammograms and charge-discharge curves for PANI@TCOF-1 (a,b) and PANI@TCOF-2 (c,d). Specific capacitance comparison at 0.5 A $g^{-1}$ (e). Temperature-dependent conductivity (f). Rate capability (g). Cycling stability (h). Nyquist plots with equivalent circuit (i). Ragone plot (j). LED demonstration with series-connected devices (k). Reproduced with permission from Ref. [82] Copyright 2021, John Wiley & Sons - Books.

electrical conductivity and ion diffusion. Additionally, the composites exhibited significantly higher conductivity (1.4–1.9 × $10^{-2}$ S/cm) compared to the unmodified TCOFs (Fig. 20e and f). PANI@TCOF-2 demonstrated excellent rate capability, retaining 43 % capacitance at higher current densities and maintaining 62–69 % of its initial capacitance after 1000 cycles (Fig. 20g and h). The Nyquist plot (i) indicates superior charge transfer efficiency for PANI@TCOF-2. Notably, this composite achieved a maximum energy density of 24.4 Wh/kg and a power density of 4000 W $kg^{-1}$ (j), highlighting its potential for high-performance energy storage applications. These substantial improvements in both conductivity and capacitance underscore the effectiveness of post-synthetic modification with conducting polymers in enhancing the electrochemical properties of COFs [82].

Liu et al. successfully developed and synthesized an all-organic composite material, TpPa-COF@PANI, by integrating the highly porous and redox-active TpPa-COF with PANI [83]. This composite was fabricated via solventothermal in-situ polymerization. The TpPa-COF@PANI-based SC exhibited high capacitance, excellent cycling stability, and outstanding rate performance. The electrode achieved a specific capacitance of 95 F $g^{-1}$ at a current density of 0.2 A $g^{-1}$. When the current density was increased to 50 A $g^{-1}$, the specific capacitance decreased to 50 F $g^{-1}$, retaining 53 % of its initial value [83].

Table 7 presents polymer/COF composites for SC applications, demonstrating a limited but diverse range of performance characteristics with specific capacitances varying from 95 to 280 F $g^{-1}$. The COF-316@PPy composite exhibited unique areal capacitance of 783.6 μF $cm^{-2}$ at 3 μA $cm^{-2}$ with exceptional cycling stability (100 % retention after 3400 cycles), suggesting that PPy integration provides both redox enhancement and structural stabilization to the HHTP-TFPN COF framework, though the low current density testing limits assessment of practical rate capability. PANI integration showed contrasting results depending on the COF scaffold, with PANI@TCOF-2 achieving moderate capacitance (280 F $g^{-1}$) but suffering from poor cycling stability (52 % retention after only 1000 cycles), indicating potential structural incompatibility of the polymer-COF interface, while TpPa-COF@PANI demonstrated lower capacitance (95 F $g^{-1}$) but remarkable long-term stability (83 % retention after 30,000 cycles), suggesting that the β-ketoenamine COF framework provides better structural support for the conducting polymer. The narrow potential windows (0.5–0.8 V) employed across all polymer/COF composites reflect the electrochemical limitations of conducting polymers in aqueous acidic electrolytes, constraining the energy density potential of these hybrid systems compared to wider potential window alternatives. The dramatic variation in cycling performance from 52 % to 100 % retention highlights the critical importance of polymer-COF interfacial compatibility and

**Table 7**
Selected properties of Polymer/COF Composite for SCs.

| Materials | Redox group | Electrolyte | Potential window | Specific capacitance | Current density | Retention capability | Ref |
|---|---|---|---|---|---|---|---|
| COF-316@PPy | HHTP, TFPN | 0.5 M $H_2SO_4$ | 0 to 0.5 V | 783.6 μF $cm^{-2}$ | 3 μA $cm^{-2}$ | 100 % after 3400 cycles | [81] |
| PANI@TCOF-2 | triazine | 1 M $H_2SO_4$ | 0 to 0.8 V | 280 F $g^{-1}$ | 0.5 A $g^{-1}$ | 52 % after 1000 cycles | [82] |
| TpPa-COF@PANI | β-Ketoenamine | 1 M $H_2SO_4$ | 0 to 0.8 V | 95 F $g^{-1}$ | 0.2 A $g^{-1}$ | 83 % after 30,000 cycles | [83] |

suggests that successful polymer/COF composite design requires careful matching of polymer properties with COF framework characteristics, electrolyte selection, and operating conditions.

The above results highlight the potential of polymer/COF composites in enhancing conductivity, capacitance, and stability for SC applications. The synergistic effects observed in these composites stem from the complementary properties of conducting polymers and COFs. Conducting polymers enhance electron transport and contributes additional pseudocapacitance, while the porous structure of COFs provides a large surface area for charge storage. Moreover, the integration of COFs with polymers often leads to improved mechanical stability, which is crucial for long-term cycling performance. As this field continues to evolve, advancements in material synthesis and design strategies are expected to further enhance performance metrics, potentially revolutionizing the market for flexible and wearable energy storage devices.

The systematic evaluation of COF composites reveals distinct performance profiles that guide application-specific material selection. MXene/COF composites demonstrate the highest specific capacitances (784 F $g^{-1}$ for $Ti_3C_2T_x$/COF), establishing them as premier candidates for high-energy density applications, while metal/COF systems typically achieve intermediate performance ranges (300–600 F $g^{-1}$) with enhanced pseudocapacitive contributions. Conversely, polymer/COF composites, exemplified by COF-316@PPy achieving 783.6 μF $cm^{-2}$, exhibit remarkable cycling stability with complete retention after 3400 cycles, contrasting sharply with PANI@TCOF-2's moderate 52 % retention after 1000 cycles, highlighting the significant variability within composite categories.

The mechanistic trade-offs across composite types reveal fundamental design considerations for SC optimization. While MXene/COF systems maximize short-term capacitive performance through synergistic EDLC-pseudocapacitive mechanisms, their oxidation susceptibility limits long-term viability. Carbon/COF composites prioritize cycling stability through robust interfacial interactions, accepting moderate capacitance values for enhanced durability. The polymer/COF category demonstrates the broadest performance spectrum, where material selection and processing conditions dramatically influence both capacitance and stability outcomes, as evidenced by the exceptional longevity of TpPa-COF@PANI (83 % retention after 30,000 cycles) despite relatively modest capacitance (95 F $g^{-1}$).

Strategic material selection must therefore balance peak performance against operational longevity, with MXene/COF composites suited for high-power, short-duration applications, while carbon/COF and select polymer/COF systems serve extended-use scenarios where cycling stability outweighs maximum capacitance requirements.

## 6. Effects of COF carbonization on SC performance

Carbonization has proven to be an effective method for preserving the porous structures of COFs during high-temperature treatments, transforming the original COFs into porous carbon materials. Shi et al. reported the synthesis of a COF based on DAAQ and TFP on dialdehyde cellulose fibers, with hyperbranched polyamide-amine (HPAMAM) used as a stabilizing agent [19]. After carbonization, the COF was uniformly and stably supported on conductive carbon fibers (CCFs), facilitating the preparation of a composite paper electrode (CCF-HPAMAM-COF paper). The COF layers' porous structure enabled high utilization of redox-active sites, which shortened the ion diffusion path. As a result, the CCF-HPAMAM-COF paper exhibited excellent electrochemical properties, including a high volumetric specific capacitance of 66.7 F $cm^{-3}$ at 0.5 mA/$cm^2$, excellent rate capability (82 % capacitance retention after a 10-fold increase in current density), and long-term stability (93.7 % charge-discharge stability after 10,000 cycles) [19].

MA and benzene-1,3,5-tricarboxyaldehyde are condensed to synthesize COFs and COF/g-$C_3N_4$ composites, both with and without graphitic carbon nitride (g-$C_3N_4$), as reported by Ibrahim et al. [84]. Following the carbonization of COF and COF/g-$C_3N_4$, N-doped carbon and N-doped carbon/g-$C_3N_4$ materials were obtained. The pre- and post-carbonized materials were evaluated for their potential as SC and lithium-ion battery (LIB) electrode materials. Electrochemical analysis revealed specific capacitances of 211 F $g^{-1}$ for COF, 257.5 F $g^{-1}$ for COF/g-$C_3N_4$, 450 F $g^{-1}$ for N-doped carbon, and 835.2 F $g^{-1}$ for N-doped carbon/g-$C_3N_4$. A SC device based on N-doped carbon/g-$C_3N_4$ exhibited a notable energy density of 45.97 Wh·$kg^{-1}$ and a high-power density of 659.3 W $kg^{-1}$. Furthermore, N-doped carbon/g-$C_3N_4$ demonstrated a discharge capacity of 390 mAh·$g^{-1}$ at a current density of 50 mA $g^{-1}$ when used as an electrode material in LIBs [84].

Umezawa et al. developed a simple method for creating boron-doped porous carbon by directly carbonizing a boron-based PCCOF-5 [85]. The boron oxides produced as byproducts during the carbonization process were easily removed by treating the resulting carbon with water, yielding boron-doped porous carbon. This method effectively incorporated boron atoms into the carbon matrix. SC electrodes fabricated from the boron-doped carbon exhibited a specific capacitance of 15.3 mF $cm^{-2}$ at a current density of 40 mA $g^{-1}$, which is approximately 2.2 times higher than that of conventional AC electrodes (~6.9 mF $cm^{-2}$) under identical current density conditions. The enhanced performance is attributed to the inclusion of boron atoms in the carbon material. After 10,000 charge/discharge cycles, the boron-doped carbon SCs demonstrated excellent cycling stability, retaining 72 % of their initial capacitance. Electrochemical characterization of PCCOF-5 as an SC electrode material showed superior performance compared to conventional AC electrodes (YP50F and MSP20), as demonstrated by various analytical techniques (Fig. 21). CV measurements displayed quasi-rectangular voltammograms, indicating ideal double-layer capacitive behavior and efficient charge accumulation (Fig. 21a). EIS analysis showed Nyquist plots with a near-vertical response in the low-frequency domain, confirming dominant electric double-layer capacitance behavior, while the high-frequency region exhibited a semicircular arc corresponding to interfacial charge transfer resistance (Fig. 21b). GCD profiles demonstrated highly linear and symmetrical characteristics, validating stable capacitive performance (Fig. 21c). Quantitative analysis revealed that PCCOF-5 showed enhanced gravimetric and specific capacitance values across a range of current densities compared to YP50F and MSP20, attributed to its optimized hierarchical pore structure and boron-doped framework (Fig. 21d and e). Long-term stability testing demonstrated a capacity retention of 72 % after 10,000 charge-discharge cycles, indicating robust cyclability. The practical viability of the material was further confirmed by its successful use in a blue LED power demonstration (Fig. 21f) [85].

Table 8 presents carbonized COFs as SC electrode materials, representing a strategic approach to overcome the inherent conductivity limitations of pristine COFs through thermal transformation while potentially retaining beneficial structural features, with specific capacitances ranging from moderate to high values (15.3 mF $cm^{-2}$ to 835.2 F $g^{-1}$) depending on the carbonization strategy and electrolyte system employed. The COF/g-$C_3N_4$ composite achieved the highest capacitance of 835.2 F $g^{-1}$ at 50 mA $g^{-1}$ in 6 M KOH, demonstrating that incorporating g-$C_3N_4$ during the carbonization process can significantly enhance both the pseudocapacitive contributions and structural integrity of the resulting carbon framework, though the relatively low current density testing limits assessment of high-rate performance capabilities. The CCF-HPAMAM-COF material showed impressive performance with 737 F $g^{-1}$ at 1 A $g^{-1}$ and excellent cycling stability (93.7 % retention after 10,000 cycles), indicating that controlled carbonization can produce highly conductive carbon networks while maintaining reasonable electrochemical stability, though the narrow potential window (0.2–0.4 V) suggests limitations in energy density applications. Notably, the carbonization of COF-5 in organic electrolyte (1 M $TEABF_4$) enabled operation over an exceptionally wide potential window (0–2.5 V), achieving 15.3 mF $cm^{-2}$ areal capacitance, though the lower cycling stability (72 % after 10,000 cycles) and modest performance metrics indicate that the carbonization process may have compromised the

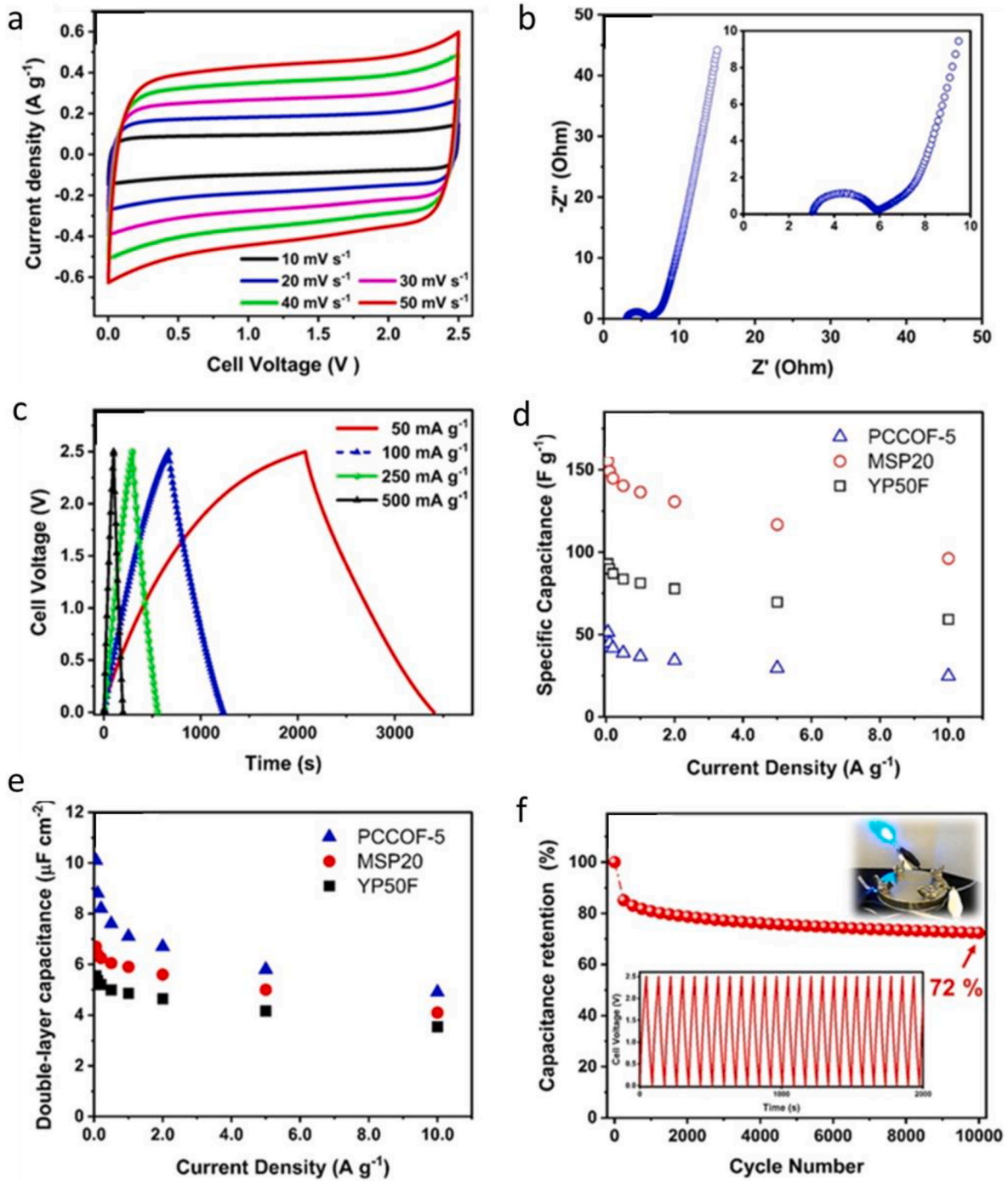


**Fig. 21.** PCCOF-5 electrochemical performance: CV curves at 10–50 mV $s^{-1}$ (a), Nyquist plots (1 MHz-0.1 Hz) (b), GCD curves at 50–500 mA $g^{-1}$ (c), specific and double-layer capacitance comparison with YP50F and MSP20 (d–e), and cycling stability over 10,000 cycles with GCD curves (inset) and LED demonstration (f). Reproduced with permission from Ref. [85]. Copyright 2021, Elsevier.

**Table 8**
Selected properties of Carbonized COFs for SCs.

| Materials | Electrolyte | Potential window | Specific capacitance | Current density | Retention capability | Ref |
|---|---|---|---|---|---|---|
| CCF-HPAMAM-COF | 0.5 M $H_2SO_4$ | 0.2 to 0.4 V | 737 F $g^{-1}$ | 1 A $g^{-1}$ | 93.7 % after 10,000 cycles. | [19] |
| COF/g-$C_3N_4$ | 6 M KOH | 0 to 0.6 V | 835.2 F $g^{-1}$ | 50 mA $g^{-1}$ | 86.5 % after 2000 cycles. | [84] |
| Carbonization of COF-5 | 1 M TEABF | 0 to 2.5 V | 15.3 mF $cm^{-2}$ | 40 mA $g^{-1}$ | 72 % after 10000 cycles | [85] |

original COF's structural advantages without fully realizing the benefits of high-performance carbon materials. The absence of specific redox group listings for carbonized materials reflects the fundamental transformation from discrete organic functional groups to extended carbon networks with delocalized electronic states, where charge storage mechanisms shift from localized redox reactions to electrical double-

layer formation and surface pseudocapacitance.

While carbonization enhances electrical conductivity, the thermodynamic optimization of carbonization temperatures and their mechanistic effects on porosity preservation and heteroatom retention remain inadequately investigated, constraining performance optimization strategies. The substantial diminution of intrinsic COF redox functionality post-carbonization represents a critical limitation, with insufficient systematic studies addressing the trade-off between enhanced conductivity and preserved redox activity. The industrial scalability of carbonization processes presents formidable challenges due to high-temperature facility requirements and associated energy costs. The mechanistic transition from pseudocapacitive behavior in pristine COFs to EDLC-dominated mechanisms in carbonized derivatives remains contentious, with critical debates regarding whether carbonization negates COF-specific electrochemical advantages. Future investigations should prioritize carbonization parameter optimization, explore hybrid carbonization strategies for preserving redox functionality, and develop scalable thermal processing methodologies, employing advanced characterization techniques to definitively elucidate charge storage mechanism transitions in these thermally-modified architectures.

## 7. Challenges and opportunities

### 7.1. Current challenges

The development of COF-based SCs faces several critical challenges that limit their commercial viability. Synthesis scalability remains a primary obstacle, as current methods are confined to laboratory-scale batch processes yielding milligrams to grams rather than the kilograms required for industrial applications [86]. Solvothermal synthesis requires extended reaction times (24–120 h) and expensive organic solvents, making it economically unfavorable. Additionally, batch-to-batch reproducibility issues result in 10–30 % variations in device performance, with inconsistencies in crystallinity, surface area, and pore size distribution commonly observed.

A fundamental challenge is balancing high surface areas with adequate electrical conductivity. While COFs can achieve exceptional surface areas (up to 3000 $m^2/g$), their intrinsic conductivity is poor ($10^{-9}$ to $10^{-6}$ $S/cm^{-1}$), limiting charge transport [87]. Incorporating conductive additives like carbon black improves conductivity by 2-3 orders of magnitude but reduces COF content and theoretical capacitance. This trade-off becomes critical in thick electrodes (>100 μm) where resistive losses significantly impact rate capability.

Long-term stability represents another major barrier encompassing chemical, electrochemical, and mechanical aspects. Many COFs with imine linkages are susceptible to hydrolysis under humid conditions, leading to framework degradation and surface area reduction. Electrochemically, capacity fade of 10–20 % over 5000–10000 cycles is common due to linker oxidation and structural rearrangement [88]. Mechanical stress during electrode swelling/contraction cycles can cause active material delamination and increased internal resistance. Processing challenges include poor COF adhesion to current collectors, requiring binders that may block pores, and difficulties in achieving uniform electrode coatings with consistent electrolyte infiltration.

### 7.2. Opportunities

To overcome these challenges, innovative strategies offer promising pathways for advancing COF-based SCs. Scalable synthesis can be achieved through continuous flow microreactor systems and mechanochemical methods, which enhance yield consistency and reduce solvent use, potentially lowering production costs [89]. Electrical conductivity can be improved by integrating COFs with conductive materials like MXenes or by doping with heteroatoms (e.g., nitrogen, sulfur), boosting charge transport while maintaining high surface area [90].Long-term stability can be enhanced through covalent cross-linking and surface passivation techniques, reducing hydrolysis and extending cycle life beyond 20,000 cycles with >90 % capacity retention. Binder-free electrode fabrication, such as direct COF growth on current collectors, can improve adhesion and electrolyte infiltration. Beyond SCs, COFs show potential as ion-transport membranes in batteries and electrocatalysts for sustainable energy applications, leveraging their tunable porosity and active sites [91].

## 8. Boundaries of this review

This narrative review provides a comprehensive overview of COFs for SC applications, but it is subject to certain limitations. First, the review focuses primarily on COF-based materials for SCs, excluding other energy storage applications such as batteries or fuel cells, which may limit its applicability to broader EES contexts. Second, the literature search was restricted to peer-reviewed articles published in English between January 2010 and March 2025, potentially overlooking relevant studies in other languages or non-peer-reviewed sources, such as conference proceedings or patents. Third, the narrative nature of the review, while allowing for a thematic synthesis of COF classification and electrode types, did not incorporate quantitative meta-analysis due to the heterogeneity of electrochemical performance metrics across studies. Additionally, limited studies were available for certain COF types, such as thiol-based COFs, and long-term stability data for some composite materials were sparse, constraining the depth of analysis in these areas. Future reviews could address these limitations by employing systematic review methodologies, including quantitative synthesis, and expanding the scope to include non-English studies or emerging COF applications in other energy storage systems.

## 9. Conclusion and future perspective in this field

COFs represent a paradigm shift in SC electrode design, offering unprecedented control over porosity, surface chemistry, and structural architecture through their crystalline, designable nature. This comprehensive review systematically examines the rapid evolution of COF-based SC technologies, categorizing materials according to their redox-active mechanisms, including carbonyl/hydroxyl functionalities, heterostructure frameworks, and radical-based systems—while critically evaluating their electrochemical performance characteristics. Strategic integration of COFs with complementary materials, encompassing carbon matrices, metal nanoparticles, MXene nanosheets, and conducting polymers, has yielded synergistic enhancements in conductivity, capacitance, and operational stability.

The electrochemical landscape of COF-based electrodes spans diverse structural motifs, from DAAQ and AZO frameworks to naphthalene-based architectures and nitrogen-enriched systems, each demonstrating distinct advantages in specific capacitance, rate performance, and cycling endurance. Carbonization strategies have emerged as a transformative approach for overcoming intrinsic conductivity limitations, fundamentally altering charge storage mechanisms while preserving beneficial structural features. However, critical challenges persist, including the optimization of porosity-conductivity relationships, mitigation of long-term degradation pathways, and development of scalable synthetic methodologies suitable for industrial implementation.

Despite significant progress in COF-based SCs, several challenges remain to be addressed through targeted research efforts. This section outlines specific research directions that merit investigation to advance the field.

The enhancement of specific capacitance represents a primary focus for future research. For 2D COFs, developing π-electron-rich building blocks with optimized pore sizes (1–2 nm) could maximize accessible surface area while facilitating rapid ion transport. These structures would incorporate strategically positioned functional groups to enhance charge storage capacity. Similarly, 3D COFs could benefit from the

integration of redox-active moieties such as quinone, nitroxide, and phenothiazine groups at precisely calculated positions within the framework to enhance pseudocapacitive behavior. Heteroatom doping strategies involving nitrogen, sulfur, and boron with controlled concentration gradients offer additional opportunities to optimize charge distribution and boost capacitance values beyond current limits.

Improving rate performance constitutes another critical research direction. The design of hierarchical pore structures in COFs combining micropores (<2 nm) for charge storage with mesopores (2–50 nm) for rapid ion diffusion could significantly enhance power density. Development of oriented COF thin films with channels perpendicular to electrode surfaces would minimize ion diffusion paths, thereby improving high-rate performance. Engineering COF-carbon composites with precisely tailored interfaces merits investigation as a means to enhance electrical conductivity without sacrificing surface area. These approaches could collectively address the conductivity limitations that currently restrict high-rate performance in many COF-based systems.

Long-term stability remains crucial for practical applications, necessitating focused research on extending cycle life. Reinforcement of COF frameworks through covalent cross-linking strategies shows promise for resisting structural collapse during cycling. Surface modification approaches to mitigate electrolyte decomposition at COF interfaces could further enhance stability. The establishment of quantitative structure-stability relationships through accelerated aging protocols and in-situ mechanical testing would provide valuable insights for designing more durable COF materials that maintain performance over thousands of cycles.

Translation to industrial applications requires addressing synthesis challenges through scalable methods. Continuous flow microreactor systems optimized for specific COF chemistries, with real-time monitoring of crystallinity and porosity, could enable consistent large-scale production. Mechanochemical approaches for solvent-free COF synthesis merit exploration for their reduced environmental impact and potential scalability. Developing efficient recovery and purification processes remains essential for industrial-scale production with consistent quality and reasonable cost structures.

The unique properties of COFs make them promising candidates for applications beyond SCs. Their integration as selective membranes in next-generation batteries could suppress dendrite formation and enhance safety. COF-based electrocatalysts for hydrogen evolution and oxygen reduction reactions could advance fuel cell technologies by providing precisely engineered active sites. Additionally, COF-based sorbents for carbon capture with efficient regeneration capabilities could contribute to environmental sustainability efforts, leveraging the tunable porosity and functionality of these materials.

Deeper understanding of COF behavior during device operation requires sophisticated characterization techniques. Implementation of operando synchrotron X-ray diffraction could track structural changes during charge-discharge cycles at atomic resolution. Specialized solid-state NMR techniques could probe local electronic environments within charged COFs, revealing charge storage mechanisms. Quantum mechanical simulations that predict and interpret spectroscopic signatures would complement experimental approaches, guiding rational material design. By pursuing these specific research directions, the scientific community can overcome current limitations in COF-based SCs and accelerate their integration into practical energy storage solutions, potentially transforming applications ranging from portable electronics to grid-scale storage systems.

## Declaration of competing interest

The authors declare the following financial interests/personal relationships which may be considered as potential competing interests: Rong-Ho Lee reports financial support was provided by National Chung Cheng University. Rong-Ho Lee reports a relationship with National Chung Hsing University that includes: employment. If there are other authors, they declare that they have no known competing financial interests or personal relationships that could have appeared to influence the work reported in this paper.

## Acknowledgment

The authors thank the National Science and Technology Council (NSTC) of Taiwan (grant no. NSTC 113- 2221-E-005-006) for financial support.

## Data availability

The authors are unable or have chosen not to specify which data has been used.

## References

[1] Li L, Lu F, Xue R, Ma B, Li Q, Wu N, Liu H, Yao W, Guo H, Yang W. Ultrastable triazine-based covalent organic framework with an interlayer hydrogen bonding for supercapacitor applications. ACS Appl Mater Interfaces 2019;11:26355–63. https://doi.org/10.1021/acsami.9b06867.

[2] Yu M, Chandrasekhar N, Raghupathy RKM, Ly KH, Zhang H, Dmitrieva E, Liang C, Lu X, Kühne TD, Mirhosseini H, Weidinger IM, Feng X. A high-rate two-dimensional polyarylimide covalent organic framework anode for aqueous Zn-ion energy storage devices. J Am Chem Soc 2020;142:19570–8. https://doi.org/10.1021/jacs.0c07992.

[3] Anwar M, Cochran EW, Zulfiqar S, Warsi MF, Shakir I, Chaudhary K. In-situ fabricated copper-holmium co-doped cobalt ferrite nanocomposite with cross-linked graphene as novel electrode material for supercapacitor application. J Energy Storage 2023;72:108438. https://doi.org/10.1016/j.est.2023.108438.

[4] Zhao X, Sajjad M, Zheng Y, Zhao M, Li Z, Wu Z, Kang K, Qiu L. Covalent organic framework templated ordered nanoporous $C_{60}$ as stable energy efficient supercapacitor electrode material. Carbon N Y 2021;182:144–54. https://doi.org/10.1016/J.CARBON.2021.05.061.

[5] Peng C, Yang H, Chen S, Wang L. Supercapacitors based on three-dimensional porous carbon/covalent-organic framework/polyaniline array composites. J Energy Storage 2020;32:101786. https://doi.org/10.1016/J.EST.2020.101786.

[6] Shanavaz H, Prasanna BP, Archana S, Prashanth MK, Alharthi FA, Zhou R, Raghu MS, Jeon BH, Kumar KY. Niobium doped triazine based covalent organic frameworks for supercapacitor applications. J Energy Storage 2023;67:107561. https://doi.org/10.1016/j.est.2023.107561.

[7] Ahmadi M, Asadinezhad A. Synthesis and characterization of azodianiline covalent organic frameworks intended for energy storage. J Mol Struct 2023;1286:135647. https://doi.org/10.1016/j.molstruc.2023.135647.

[8] Iqbal R, Majeed MK, Hussain A, Ahmad A, Ahmad M, Jabar B, Akbar AR, Ali S, Rauf S, Saleem A. Boosting the crystallinity of novel two-dimensional hexamine dipyrazino quinoxaline-based covalent organic frameworks for electrical double-layer supercapacitors. Mater Chem Front 2023;7:2464–74. https://doi.org/10.1039/d3qm00169e.

[9] Liu L, Cui D, Zhang S, Xie W, Yao C, Xu N, Xu Y. Triazine covalent organic framework (COF)/θ-$Al_2O_3$ composites for supercapacitor application. Dalton Trans 2023;52:6138–45. https://doi.org/10.1039/d3dt00613a.

[10] Liu L, Cui D, Zhang S, Xie W, Yao C, Xu Y. Integrated carbon nanotube and triazine-based covalent organic framework composites for high capacitance performance. Dalton Trans 2023;52:2762–9. https://doi.org/10.1039/d2dt03910a.

[11] Biradar MR, Rao CRK, Bhosale SV, Bhosale SV. Flame-retardant 3D covalent organic framework for high-performance symmetric supercapacitors. Energy Fuels 2023;37:4671–81. https://doi.org/10.1021/acs.energyfuels.2c04226.

[12] Patra BC, Bhattacharya S. New covalent organic square lattice based on porphyrin and tetraphenyl ethylene building blocks toward high-performance supercapacitive energy storage. Chem Mater 2021;33:8512–23. https://doi.org/10.1021/acs.chemmater.1c02973.

[13] Esser B, Dolhem F, Becuwe M, Poizot P, Vlad A, Brandell D. A perspective on organic electrode materials and technologies for next generation batteries. J Power Sources 2021;482:228814. https://doi.org/10.1016/j.jpowsour.2020.228814.

[14] Panchu SJ, Raju K, Swart HC. Emerging two–dimensional intercalation pseudocapacitive electrodes for supercapacitors. Chemelectrochem 2024;11: e202300810. https://doi.org/10.1002/celc.202300810.

[15] González A, Goikolea E, Barrena JA, Mysyk R. Review on supercapacitors: technologies and materials. Renew Sustain Energy Rev 2016;58:1189–206. https://doi.org/10.1016/j.rser.2015.12.249.

[16] Yang Y, Zhang P, Hao L, Cheng P, Chen Y, Zhang Z. Grotthuss proton-conductive covalent organic frameworks for efficient proton pseudocapacitors. Angewandte Chemie - International Edition 2021;60:21838–45. https://doi.org/10.1002/anie.202105725.

[17] Khojastehnezhad A, Rhili K, Shehab MK, Gamraoui H, Peng Z, Samih ElDouhaibi A, Touzani R, Hammouti B, El-Kaderi HM, Siaj M. Rapid, mild, and catalytic synthesis of 2D and 3D COFs with promising supercapacitor applications. ACS Appl Energy Mater 2023;6:12216–25. https://doi.org/10.1021/acsaem.3c01913.

[18] Yang HC, Chen YY, Suen SY, Lee RH. Triazine-based covalent organic framework/carbon nanotube fiber nanocomposites for high-performance supercapacitor

electrodes. Polymer 2023;273:125853. https://doi.org/10.1016/j.polymer.2023.125853.
[19] Shi Y, Liu Y, Huang X, Qian X. Carbonized paper-supported electrode with covalent organic framework layers on carbonized cellulose fibers for supercapacitor application. Mater Today Chem 2023;31:101617. https://doi.org/10.1016/j.mtchem.2023.101617.
[20] An N, Guo Z, Guo C, Wei M, Sun D, He Y, Li W, Zhou L, Hu Z, Dong X. A novel COF/MXene film electrode with fast redox kinetics for high-performance flexible supercapacitor. Chem Eng J 2023;458:141434. https://doi.org/10.1016/J.CEJ.2023.141434.
[21] Xue R, Zheng YP, Qian DQ, Xu DY, Liu YS, Huang SL, Yang GY. A 2-D microporous covalent organic framework for high-performance supercapacitor electrode. Mater Lett 2022;308:131229. https://doi.org/10.1016/j.matlet.2021.131229.
[22] Yu A, Liu W, Xi W, Mu M, Shi L. Unraveling the rapid proton transport mechanism of covalent organic frameworks. Chem Mater 2024;36:1880–90. https://doi.org/10.1021/acs.chemmater.3c02421.
[23] Li M, Liu J, Li Y, Xing G, Yu X, Peng C, Chen L. Skeleton engineering of isostructural 2D covalent organic frameworks: orthoquinone redox-active sites enhanced energy storage. CCS Chem 2021;3:696–706. https://doi.org/10.31635/ccschem.020.202000257.
[24] Zhang X, Xiao Z, Liu X, Mei P, Yang Y. Redox-active polymers as organic electrode materials for sustainable supercapacitors. Renew Sustain Energy Rev 2021;147. https://doi.org/10.1016/j.rser.2021.111247.
[25] Yuan S, Li X, Zhu J, Zhang G, Van Puyvelde P, Van Der Bruggen B. Covalent organic frameworks for membrane separation. Chem Soc Rev 2019;48:2665–81. https://doi.org/10.1039/c8cs00919h.
[26] Hegazy HH, Sana SS, Ramachandran T, Kumar YA, Kulurumotlakatla DK, Abd-Rabboh HSM, Kim SC. Covalent organic frameworks in supercapacitors: Unraveling the pros and cons for energy storage. J Energy Storage 2023;74:109405. https://doi.org/10.1016/j.est.2023.109405.
[27] Wang Z, Wang C, Chen Y, Wei L. Covalent organic frameworks for capacitive energy storage: recent progress and technological challenges. Adv Mater Technol 2023;8:2201828. https://doi.org/10.1002/admt.202201828.
[28] Li R, Li J, Liu Q, Li T, Lan D, Ma Y. Recent progress on covalent organic frameworks and their composites as electrode materials for supercapacitors. Adv Compos Hybrid Mater 2025;8:86. https://doi.org/10.1007/s42114-024-01177-x.
[29] Deblase CR, Silberstein KE, Truong TT, Abruña HD, Dichtel WR. β-ketoenamine-linked covalent organic frameworks capable of pseudocapacitive energy storage. J Am Chem Soc 2013;135:16821–4. https://doi.org/10.1021/ja409421d.
[30] Halder A, Ghosh M, Khayum AM, Bera S, Addicoat M, Sasmal HS, Karak S, Kurungot S, Banerjee R. Interlayer hydrogen-bonded covalent organic frameworks as high-performance supercapacitors. J Am Chem Soc 2018;140:10941–5. https://doi.org/10.1021/jacs.8b06460.
[31] EL-Mahdy AFM, Hung YH, Mansoure TH, Yu HH, Hsu YS, Wu KCW, Kuo SW. Synthesis of [3 + 3] β-ketoenamine-tethered covalent organic frameworks (COFs) for high-performance supercapacitance and CO2 storage. J Taiwan Inst Chem Eng 2019;103:199–208. https://doi.org/10.1016/j.jtice.2019.07.016.
[32] Deblase CR, Hernández-Burgos K, Silberstein KE, Rodríguez-Calero GG, Bisbey RP, Abruña HD, Dichtel WR. Rapid and efficient redox processes within 2D covalent organic framework thin films. ACS Nano 2015;9:3178–83. https://doi.org/10.1021/acsnano.5b00184.
[33] Chandra S, Roy Chowdhury D, Addicoat M, Heine T, Paul A, Banerjee R. Molecular level control of the capacitance of two-dimensional covalent organic frameworks: role of hydrogen bonding in energy storage materials. Chem Mater 2017;29:2074–80. https://doi.org/10.1021/acs.chemmater.6b04178.
[34] Khattak AM, Ghazi ZA, Liang B, Khan NA, Iqbal A, Li L, Tang Z. A redox-active 2D covalent organic framework with pyridine moieties capable of faradaic energy storage. J Mater Chem A Mater 2016;4:16312–7. https://doi.org/10.1039/c6ta05784e.
[35] Li L, Lu F, Guo H, Yang W. A new two-dimensional covalent organic framework with intralayer hydrogen bonding as supercapacitor electrode material. Microporous Mesoporous Mater 2021;312:110766. https://doi.org/10.1016/j.micromeso.2020.110766.
[36] Peng H, Montes-García V, Raya J, Wang H, Guo H, Richard F, Samorì P, Ciesielski A. Supramolecular engineering of cathode materials for aqueous zinc-ion hybrid supercapacitors: novel thiophene-bridged donor-acceptor sp2 carbon-linked polymers. J Mater Chem A Mater 2023;11:2718–25. https://doi.org/10.1039/d2ta09651j.
[37] Xu F, Xu H, Chen X, Wu D, Wu Y, Liu H, Gu C, Fu R, Jiang D. Radical covalent organic frameworks: a general strategy to immobilize open-accessible polyradicals for high-performance capacitive energy storage. Angew Chem 2015;127:6918–22. https://doi.org/10.1002/ange.201501706.
[38] Wang J, Chen M, Lu Z, Chen Z, Si L. Radical covalent organic frameworks associated with liquid Na-K toward dendrite-free alkali metal anodes. Adv Sci 2022;9:2203058. https://doi.org/10.1002/advs.202203058.
[39] Ambrose B, Nasrin K, Arunkumar M, Kannan A, Sathish M, Kathiresan M. Viologen-based covalent organic polymers: variation of morphology and evaluation of their ultra-long cycle supercapacitor performance. J Energy Storage 2023;61:106714. https://doi.org/10.1016/j.est.2023.106714.
[40] Khayum MA, Vijayakumar V, Karak S, Kandambeth S, Bhadra M, Suresh K, Acharambath N, Kurungot S, Banerjee R. Convergent covalent organic framework thin sheets as flexible supercapacitor electrodes. ACS Appl Mater Interfaces 2018;10:28139–46. https://doi.org/10.1021/acsami.8b10486.
[41] Desai AV, Seymour VR, Ettlinger R, Pramanik A, Manche AG, Rainer DN, Wheatley PS, Griffin JM, Morris RE, Armstrong AR. Azo-functionalised metal-organic framework for charge storage in sodium-ion batteries. Chem Commun 2023;59:1321. https://doi.org/10.17630/e06b0d3a-6dc5-4ea6-b865-0324094d2edd.
[42] Bhanja P, Bhunia K, Das SK, Pradhan D, Kimura R, Hijikata Y, Irle S, Bhaumik A. A new triazine-based covalent organic framework for high-performance capacitive energy storage. ChemSusChem 2017;10:921–9. https://doi.org/10.1002/cssc.201601571.
[43] Das SK, Bhunia K, Mallick A, Pradhan A, Pradhan D, Bhaumik A. A new electrochemically responsive 2D Π-conjugated covalent organic framework as a high performance supercapacitor. Microporous Mesoporous Mater 2018;266:109–16. https://doi.org/10.1016/j.micromeso.2018.02.026.
[44] Ruidas S, Pradhan L, Mohanty B, Dalapati S, Kumar S, Jena BK, Bhaumik A. Imine-linked π-conjugated covalent organic frameworks as an efficient electrode material for pseudocapacitive energy storage. ACS Appl Energy Mater 2024;7:2872–80. https://doi.org/10.1021/acsaem.4c00086.
[45] Weng C, Li X, Yang Z, Long H, Lu C, Dong L, Zhao S, Tan L. A directly linked COF-like conjugated microporous polymer based on naphthalene diimides for high performance supercapacitors. Chem Commun 2022;58:6809–12. https://doi.org/10.1039/d2cc02097a.
[46] Haldar S, Kushwaha R, Maity R, Vaidhyanathan R. Pyridine-rich covalent organic frameworks as high-performance solid-state supercapacitors. ACS Mater Lett 2019;1:490–7. https://doi.org/10.1021/acsmaterialslett.9b00222.
[47] Kumar Y, Ahmad I, Rawat A, Pandey RK, Mohanty P, Pandey R. Flexible linker-based triazine-functionalized 2D covalent organic frameworks for supercapacitor and gas sorption applications. ACS Appl Mater Interfaces 2024;16:11605–16. https://doi.org/10.1021/acsami.4c00126.
[48] Yang TL, Chen JY, Kuo SW, Lo CT, El-Mahdy AFM. Hydroxyl-functionalized covalent organic frameworks as high-performance supercapacitors. Polymers 2022;14:3428. https://doi.org/10.3390/polym14163428.
[49] Li S, Kumbhakar B, Mishra B, Roeser J, Chaoui N, Schmidt J, Thomas A, Pachfule P. Dithiophenedione-based covalent organic frameworks for supercapacitive energy storage. ACS Appl Energy Mater 2023;6:9256–63. https://doi.org/10.1021/acsaem.3c01072.
[50] Ahmad I, Singh O, Ahmed J, Priyanka Alshehri SM, Bharti C. Vidivay. Triazine-functionalized nitrogen-rich covalent organic framework as an electrode material for aqueous symmetric supercapacitor. Chem Asian J 2025;20:e202401149. https://doi.org/10.1002/asia.202401149.
[51] Bhunia A, Janiak C, Maity A, Jana A, Dey SK. Enhanced electrochemical capacitor performance of S,N-containing carbon materials derived from covalent triazine-based frameworks with tetrathiafulvalene core. Mater Adv 2025;6:4337-4344. https://doi.org/10.1039/D5MA00225G.
[52] Roy A, Mondal S, Halder A, Banerjee A, Ghoshal D, Paul A, Malik S. Benzimidazole linked arylimide based covalent organic framework as gas adsorbing and electrode materials for supercapacitor application. Eur Polym J 2017;93:448–57. https://doi.org/10.1016/j.eurpolymj.2017.06.028.
[53] Xiong S, Liu J, Wang Y, Wang X, Chu J, Zhang R, Gong M, Wu B. Solvothermal synthesis of triphenylamine-based covalent organic framework nanofibers with excellent cycle stability for supercapacitor electrodes. J Appl Polym Sci 2022;139:e51510. https://doi.org/10.1002/app.51510.
[54] Pakulski D, Montes-García V, Gorczyński A, Czepa W, Chudziak T, Samorì P, Ciesielski A. Thiol-decorated covalent organic frameworks as multifunctional materials for high-performance supercapacitors and heterogeneous catalysis. J Mater Chem A Mater 2022;10:16685–96. https://doi.org/10.1039/d2ta03867f.
[55] Zhuang X, Zhao W, Zhang F, Cao Y, Liu F, Bi S, Feng X. A two-dimensional conjugated polymer framework with fully sp2-bonded carbon skeleton. Polym Chem 2016;7:4176–81. https://doi.org/10.1039/c6py00561f.
[56] Dai Y, Wang Y, Li X, Cui M, Gao Y, Xu H, Xu X. In situ form core-shell carbon nanotube-imide COF composite for high performance negative electrode of pseudocapacitor. Electrochim Acta 2022;421:140470. https://doi.org/10.1016/j.electacta.2022.140470.
[57] Han Y, Zhang Q, Hu N, Zhang X, Mai Y, Liu J, Hua X, Wei H. Core-shell nanostructure of single-wall carbon nanotubes and covalent organic frameworks for supercapacitors. Chin Chem Lett 2017;28:2269–73. https://doi.org/10.1016/J.CCLET.2017.10.024.
[58] Dai Y, Huang J, Zhao Y, Niu W, Xu X. A novel polyimide-co-hexaazatripheylene covalent organic framework carbon nanotube composite as negative material of pseudocapacitor. J Energy Storage 2025;120:116471. https://doi.org/10.1016/j.est.2025.116471.
[59] Kang K, Tang X, Duan J, Yang B, Hu JY. Carbon nanotubes exfoliated HATN-COF for efficient supercapacitor active materials. Energy Fuels 2025;39:921-927. https://doi.org/10.1021/acs.energyfuels.4c04884.
[60] Xu L, Liu Y, Ding Z, Xu X, Liu X, Gong Z, Li J, Lu T, Pan L. Solvent-free synthesis of covalent organic framework/graphene nanohybrids: high-performance faradaic cathodes for supercapacitors and hybrid capacitive deionization. Small 2024;20:2307843. https://doi.org/10.1002/smll.202307843.
[61] Xu L, Liu Y, Xuan X, Xu X, Li Y, Lu T, Pan L. Heterointerface regulation of covalent organic framework-anchored graphene via a solvent-free strategy for high-performance supercapacitor and hybrid capacitive deionization electrodes. Mater Horiz 2024;11:2974-2985. https://doi.org/10.1039/d4mh00161c.
[62] Ibrahim M, Abdelhamid HN, Abuelftooh AM, Mohamed SG, Wen Z, Sun X. Covalent organic frameworks (COFs)-derived nitrogen-doped carbon/reduced graphene oxide nanocomposite as electrodes materials for supercapacitors. J Energy Storage 2022;55:105375. https://doi.org/10.1016/j.est.2022.105375.
[63] Hu D, Jia Y, Yang S, Lin C, Huang F, Wu R, Guo S, Xie K, Du P. Hierarchical nanocomposites of redox covalent organic frameworks nanowires anchored on graphene sheets for super stability supercapacitor. Chem Eng J 2024;488:151160. https://doi.org/10.1016/j.cej.2024.151160.

[64] Sun J, Klechikov A, Moise C, Prodana M, Enachescu M, Talyzin AV. A molecular pillar approach to grow vertical covalent organic framework nanosheets on graphene: hybrid materials for energy storage. Angew Chem 2018;130:1046–50. https://doi.org/10.1002/ange.201710502.
[65] Yao M, Guo C, Geng Q, Zhang Y, Zhao X, Zhao X, Wang Y. Construction of anthraquinone-containing covalent organic frameworks/graphene hybrid films for a flexible high-performance microsupercapacitor. Ind Eng Chem Res 2022;61:7480–8. https://doi.org/10.1021/acs.iecr.1c04638.
[66] Verma S, Verma B. Synergistic optimization of nanostructured graphene oxide based ternary composite for boosting the performance of supercapacitor electrode material via response surface methodology. Colloids Surf A Physicochem Eng Asp 2024;682:132893. https://doi.org/10.1016/j.colsurfa.2023.132893.
[67] Dong Y, Wang Y, Zhang X, Lai Q, Yang Y. Carbon-based elastic foams supported redox-active covalent organic frameworks for flexible supercapacitors. Chem Eng J 2022;449:137858. https://doi.org/10.1016/j.cej.2022.137858.
[68] He Y, An N, Meng C, Xiao L, Wei Q, Zhou Y, Yang Y, Li Z, Hu Z. COF-based electrodes with vertically supported tentacle array for ultrahigh stability flexible energy storage. ACS Appl Mater Interfaces 2022;14:57328–39. https://doi.org/10.1021/acsami.2c15092.
[69] Martín-Illán J, Sierra L, Guillem-Navajas A, Suárez JA, Royuela S, Rodríguez-San-Miguel D, Maspoch D, Ocón P, Zamora F. β-ketoenamine-linked covalent organic frameworks synthesized via gel-to-gel monomer exchange reaction: from aerogel monoliths to electrodes for supercapacitors. Adv Funct Mater 2024;34:2403567. https://doi.org/10.1002/adfm.202403567.
[70] Sun B, Cui D, Xu X, Liu W, Xie W, Xu Y. Functionalized graphene/tetraphenylethylene-based covalent organic framework composites for enhanced electrochemical energy storage. Colloids Surf A Physicochem Eng Asp 2025;715:136659. https://doi.org/10.1016/j.colsurfa.2025.136659.
[71] Yang Y, Xu D, Sun Q, Li Y, Zhang W, Li Z, Hu Z. Anthraquinone-based covalent organic framework/reduced graphene oxide composites for supercapacitors. J Energy Storage 2025;114:115881. https://doi.org/10.1016/j.est.2025.115881.
[72] Khan J, Ahmed A, Al-Kahtani AA. Enhanced supercapacitor performance using EG@COF: a layered porous composite. RSC Adv 2025;15:11441–50. https://doi.org/10.1039/d5ra01653c.
[73] Shanavaz H, Prasanna BP, Prashanth MK, Alharethy F, Raghu MS, Jeon BH, Yogesh Kumar K. Novel cobalt-incorporated two dimensional covalent organic frameworks for supercapacitor applications. FlatChem 2024;45:100645. https://doi.org/10.1016/j.flatc.2024.100645.
[74] Li W, Zhang Q, Pei Q, Yang Y, Zhao J, Xie S, Huang J. $Bi_2S_3$ confined by covalent organic frameworks enables high-rate high-capacity potassium storage. Adv Funct Mater 2024;34:2404197. https://doi.org/10.1002/adfm.202404197.
[75] Shanavaz H, Prasanna BP, Prashanth MK, Alharethy F, Raghu MS, Jeon BH, Kumar KY. Exploring the potential of metal tailored imine based covalent organic framework for asymmetric supercapacitor applications. J Mol Struct 2025;1321:139983. https://doi.org/10.1016/j.molstruc.2024.139983.
[76] Khatri I, Siwach P, Gaba L, Dahiya S, Punia R, Maan AS, Singh K, Ashraf IM, Shkir M, Ohlan A. Designing of novel hexamine-phenylenediamine covalent organic framework - metal oxide composites as electrode materials for supercapacitors. FlatChem 2025;50:100835. https://doi.org/10.1016/j.flatc.2025.100835.
[77] Wang Y, Wang X, Li X, Li X, Liu Y, Bai Y, Xiao H, Yuan G. A high-performance, tailorable, wearable, and foldable solid-state supercapacitor enabled by arranging pseudocapacitivegroups and MXene slakes on textile electrode surface. Adv Funct Mater 2021;31:2008185. https://doi.org/10.1002/adfm.202008185.
[78] Zhu X, Zhang Y, Man Z, Lu W, Chen W, Xu J, Bao N, Chen W, Wu G. Microfluidic-assembled covalent organic frameworks@$Ti_3C_2Tx$ MXene vertical fibers for high-performance electrochemical supercapacitors. Adv Mater 2023;35:2307186. https://doi.org/10.1002/adma.202307186.
[79] Feng M, Zhang Y, Zhu X, Chen W, Lu W, Wu G. Interface-anchored covalent organic frameworks@amino-modified $Ti_3C_2Tx$ MXene on nylon 6 film for high-performance deformable supercapacitors. Angewandte Chemie - International Edition 2023;62:e202307195. https://doi.org/10.1002/anie.202307195.
[80] Liu X, Yang F, Wu L, Zhou Q, Ren R, Lv YK. Ionic liquid-loaded covalent organic frameworks with favorable electrochemical properties as a potential electrode material. Microporous Mesoporous Mater 2022;336:111906. https://doi.org/10.1016/j.micromeso.2022.111906.
[81] Wang W, Zhao W, Chen T, Bai Y, Xu H, Jiang M, Liu S, Huang W, Zhao Q. All-in-One Hollow flower-like covalent organic frameworks for flexible transparent devices. Adv Funct Mater 2021;31:2010306. https://doi.org/10.1002/adfm.202010306.
[82] Dutta TK, Patra A. Post-synthetic modification of covalent organic frameworks through in situ polymerization of aniline for enhanced capacitive energy storage. Chem Asian J 2021;16:158–64. https://doi.org/10.1002/asia.202001216.
[83] Liu S, Yao L, Lu Y, Hua X, Liu J, Yang Z, Wei H, Mai Y. All-organic covalent organic framework/polyaniline composites as stable electrode for high-performance supercapacitors. Mater Lett 2019;236:354–7. https://doi.org/10.1016/j.matlet.2018.10.131.
[84] Ibrahim M, Fayed MG, Mohamed SG, Wen Z, Sun X, Abdelhamid HN. High-performance lithium-ion battery and supercapacitors using covalent organic frameworks (COFs)/graphitic carbon nitride (g-$C_3N_4$)-derived hierarchical N-doped carbon. ACS Appl Energy Mater 2022;5:12828–36. https://doi.org/10.1021/acsaem.2c02415.
[85] Umezawa S, Douura T, Yoshikawa K, Takashima Y, Yoneda M, Gotoh K, Stolojan V, Silva SRP, Hayashi Y, Tanaka D. Supercapacitor electrode with high charge density based on boron-doped porous carbon derived from covalent organic frameworks. Carbon N Y 2021;184:418–25. https://doi.org/10.1016/j.carbon.2021.08.022.
[86] Geng K, He T, Liu R, Dalapati S, Tan KT, Li Z, Tao S, Gong Y, Jiang Q, Jiang D. Covalent organic frameworks: design, synthesis, and functions. Chem Rev 2020;120:8814–933. https://doi.org/10.1021/acs.chemrev.9b00550.
[87] Yang Y, Börjesson K. Electroactive covalent organic frameworks: a new choice for organic electronics. Trends Chem 2022;4:60–75. https://doi.org/10.1016/j.trechm.2021.10.007.
[88] Chafiq M, Chaouiki A, Ko YG. Advances in COFs for energy storage devices: Harnessing the potential of covalent organic framework materials. Energy Storage Mater 2023;63:103014. https://doi.org/10.1016/j.ensm.2023.103014.
[89] Khalil S, Alazmi A, Gao G, Martínez-Jiménez C, Saxena R, Chen Y, Jiang SY, Li J, Alhashim S, Senftle TP, Martí AA, Verduzco R. Continuous synthesis and processing of covalent organic frameworks in a flow reactor. ACS Appl Mater Interfaces 2024;16:55206–17. https://doi.org/10.1021/acsami.4c09577.
[90] Nabeela K, Deka R, Abbas Z, Kumar P, Saraf M, Mobin SM. Covalent organic frameworks (COFs)/MXenes heterostructures for electrochemical energy storage. Cryst Growth Des 2023;23:3057–78. https://doi.org/10.1021/acs.cgd.3c00206.
[91] Zhao X, Pachfule P, Thomas A. Covalent organic frameworks (COFs) for electrochemical applications. Chem Soc Rev 2021;50:6871–913. https://doi.org/10.1039/d0cs01569e.